NATIONAL AERONAUTICS AND SPACE ADMINISTRATION

Technical Memorandum 33-305

Structural Analysis and Matrix Interpretive System (SAMIS) User Report

Theodore E. Lang

JET PROPULSION LABORATORY

CALIFORNIA INSTITUTE OF TECHNOLOGY

PASADENA, CALIFORNIA

March 1, 1967

NATIONAL AERONAUTICS AND SPACE ADMINISTRATION

Technical Memorandum 33-305

Structural Analysis and Matrix Interpretive System (SAMIS) User Report

Theodore E. Lang

Approved by:

M. E. Alper

M. E. Alper, *Manager*
Applied Mechanics Section

JET PROPULSION LABORATORY
CALIFORNIA INSTITUTE OF TECHNOLOGY
PASADENA, CALIFORNIA

March 1, 1967

Technical Memorandum 33-305

Prepared Under Contract No. NAS 7-100
National Aeronautics & Space Administration

CONTENTS

TABLES

CONTENTS (cont'd)

TABLES (cont'd)

FIGURES

CONTENTS (cont'd)

FIGURES (cont'd)

CONTENTS (cont'd)

FIGURES (cont'd)

ABSTRACT

This report describes the application and user aspects of the Structural Analysis and Matrix Interpretive System (SAMIS) Computer Program. It includes a detailed description of element data preparation, matrix manipulations by use of "pseudo instructions," and solution printout in solving the problem of a shallow spherical shell under thermal and pressure loadings and the calculation of the natural modes and frequencies of the shell. It includes detailed "pseudo instructions" for matrix partitioning and describes structural partitioning and matrix reduction techniques.

The details of the associated computer program and the theoretical basis for the program are contained in two companion reports entitled, "Structural Analysis and Matrix Interpretive System (SAMIS) Program Report," JPL Technical Memorandum No. 33-307, and "Structural Analysis and Matrix Interpretive System (SAMIS Program: Technical Report," JPL Technical Memorandum No. 33-311.

1.0 INTRODUCTION

This document shows the generation and the interpretation of the input and output data of several problems that were used to check out the Structural Analysis and Matrix Interpretative System (SAMIS) computer program. The intent in describing these test problems is to demonstrate the applicability and versatility of the SAMIS program and to provide sample problems that the user can refer to during setup of his problems.

The SAMIS program is based upon the direct stiffness method. The program may be used to compute the deflections, stress resultants, reaction forces and/or dynamic characteristics of rod, beam, shell or composite beam-shell structures. The structures may be loaded by applied external forces, gravity loads, pressure loads or temperature-induced loads.

Consistent with the techniques of the direct stiffness method, the continuous surfaces of shell structures are approximated by an array of flat triangular elements called "facets." Adjoining rod or beam structures or shell-stiffening members are represented by the line element or shear beam element. The triangular plate element has three apexes which are designated "gridpoints" or nodes. Correspondingly, the line element has two nodes. This procedure of structural approximation is used extensively in analysis of complex structures, with versatility in idealization limited only by the availability of suitable elements.

The intent in development of the SAMIS program was to provide structurally oriented analysis capability with extreme versatility in application and relative ease in modification and improvement of the program. For this reason the SAMIS program was developed as a "chain" system in FORTRAN II, with each major function of matrix generation and manipulation an individual link of the program. Detailed definition of the system for the program is contained in the SAMIS Program Document (Ref. 1). The SAMIS Technical Document (Ref. 2) contains detailed data and equations that define the theoretical basis of the program.

The technical material in this report is presented in four sections. Sections 2.0 and 3.0 present the formulation of the input data and the interpretation of the output data for the static and dynamic analysis of a shallow spherical shell. In Section 4.0, sample input data for the line element is presented and defined. Finally, in Section 5.0, two special topics are discussed: (1) the concept of matrix partitioning

which is required to apply SAMIS to structural analysis of large order systems and (2) the treatment of gridpoint discontinuities (in displacement or slope) at joints.

The user of the SAMIS program is advised that in many problems system capability can be extended and/or structural idealizations can be improved by ingenuity and deduction. This has already been demonstrated by users of the program at JPL and several NASA centers. By learning the functions and options of the manipulative routines, the engineer can apply the program to a wide spectrum of problem types and sizes. For example, through understanding of the subprogram for matrix multiplication (MULT) the user can recode a matrix. Or by selective use of certain subprograms of the SAMIS, a nonsymmetric matrix can be inverted by Choleski Decomposition (CHOL), which in SAMIS is intended to operate only with symmetric matrices. Adaptability of the program to handle these and other unusual problem circumstances is considered one of the principal advantages of the program, which can only be appreciated and applied after acquiring some knowledge of its inner workings.

To aid the user in this endeavor this document presents discussion of some of the test problems used to check out the SAMIS program. Note, however, that the totality of problems presented here by no means tests every feature of the program, which required the generation of many small problems to accomplish.

2.0 SHALLOW SPHERICAL SHELL, STATIC RESPONSE PREDICTION

The problem considered in this section was formulated to test the static solution capability of the SAMIS. The structure is a thin shallow spherical shell, assumed material isotropic, that is restrained at its outer edge. Considered in detail are the boundary conditions of the problem, definition of the input and output data, and comparison of computed results with results from classical shell theory.

2.1 Description of This Problem

The shell configuration selected for this test problem is a thin, shallow, spherical segment having a principal radius of 28.5 in., a thickness of 0.075 in., and a chord diameter of 21.2 in. (Fig. 2.1). The material is AL 2014-T6 with Poisson's ratio 1/3, Young's modulus 10.5×10^{6} psi, and coefficient of thermal expansion 12.5×10^{-6} in./in./°F. The weight density of the material is 0.101 lb/in^3.

The shell is clamped along its outer edge and is subjected to two separate loading states. One state is a uniform pressure of 50 psi applied to the concave side of the shell. The other state is a uniform temperature rise of 125°F over the zero stress temperature of the shell (70°F), plus a uniform linear gradient of 50°F through the shell thickness. Due to the clamped edge constraint, the 125°F rise in temperature as well as the temperature gradient induce stresses in the shell. The two loading states are shown in Fig. 2.2.

For ease of computation the shell is assumed to be of uniform thickness and material isotropic. Hence, because both loading states are symmetric with respect to the principal axis of the shell, the deformation along any circumferential arc is constant. For this reason only a sector of the total shell is needed for the idealization. However, if only a sector is used, boundary conditions must be imposed not only at the outer edge for the clamped constraint, but also along the radial edges of the sector to account for the circumferential symmetry.

The shell sector selected is a 20 deg slice oriented with respect to an overall Cartesian coordinate system as shown in Fig. 2.3. Fig. 2.3 also defines the force and deflection variables required to represent the load and deformation state of a triangle. The Cartesian coordinates X, Y, Z are the system coordinates to which each gridpoint location is referenced.

Four requirements influenced the selection of the test problem outlined above. First, it was necessary to verify that the computer-generated pressure and

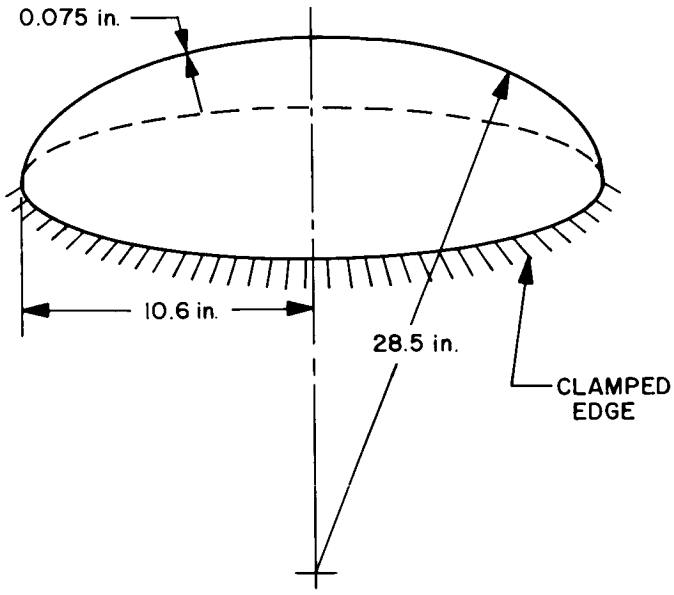

Fig. 2.1. Shell dimensions and support

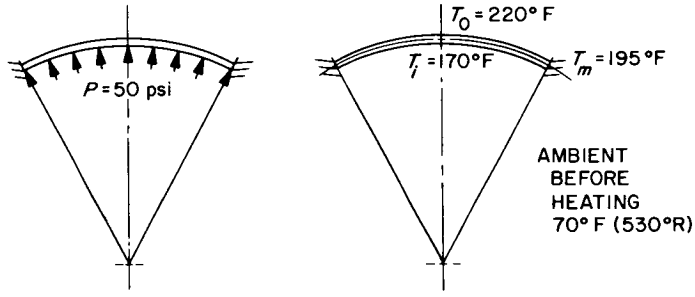

Fig. 2.2. Shell loading conditions

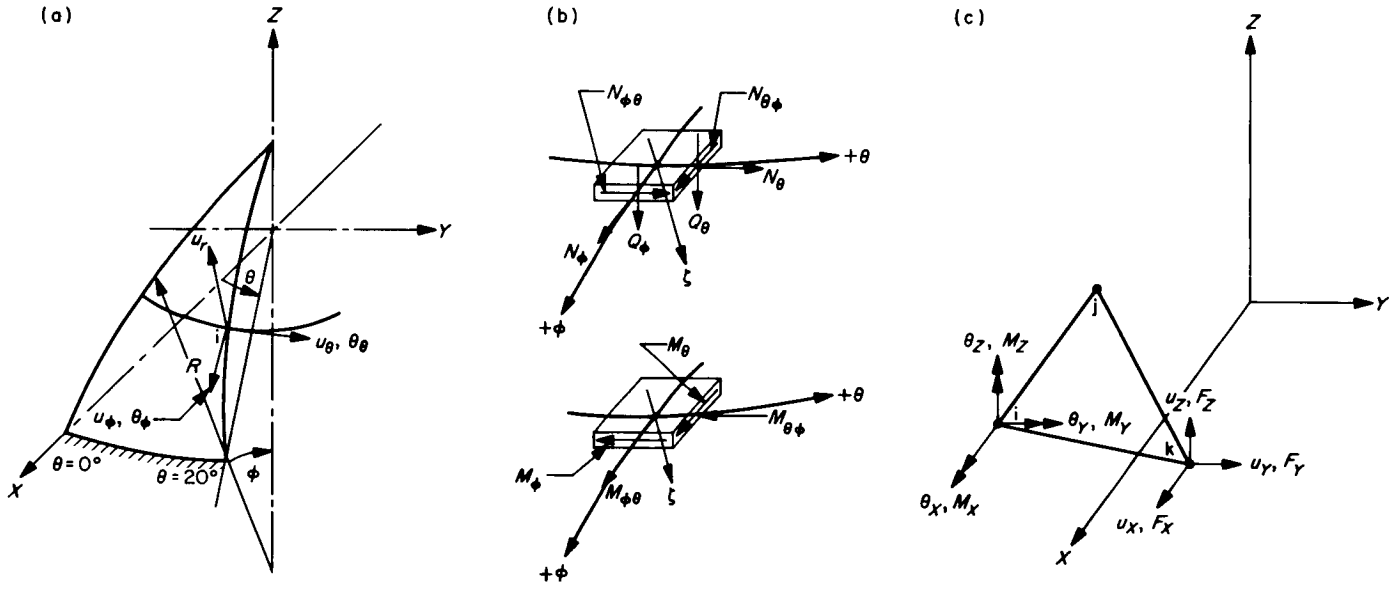

Fig. 2.3. Shell coordinates and force and displacement variables

temperature loading vectors were correct. Second, it was necessary to determine that the computed stresses and deflections compared favorably with corresponding values obtained from shell theory. Third, the shell geometry was selected so that mode shapes and frequencies could also be computed and compared with shell theory values (Section 3.0). Fourth, the static test case was selected to test those subroutines that are meant to operate with matrices larger than core.

To assure the generation of a stiffness matrix which is larger than the computer's core storage, the shell sector was idealized by the triangular array shown in Fig. 2.4. In the vicinity of the clamped edge, the breakdown of triangular elements is greater than near the shell apex. The reason for this refinement is to more accurately predict the stress resultants that vary rapidly near the boundary due to the clamped edge condition.

These stresses reduce in value rapidly with distance from the edge. At a distance defined by $(Rh)\frac{1}{2}$, where R is the shell radius and h is the shell thickness, the stresses due to edge effects are essentially zero. Beyond this distance the stresses are predominantly membrane. In the present case, $(Rh)\frac{1}{2} = 1.5$ in., and it was decided to obtain six values of stress within this distance; so the arrangement of triangles shown in Fig. 2.4 was selected. In computing stresses for a triangular element, the values obtained are referenced to the centroid of the triangle. Thus, the stress computed for, say, triangles 88 and 89 will be different because the distance from the shell apex to the respective triangle centroids is different.

With respect to the coordinate system X, Y, Z, the coordinate distances to each of the 70 gridpoints is given in Table 2-1. This information is needed in the writeup of input data for the problem.

2.2 Boundary Conditions

For the shell all matrices are referenced to the system coordinates X, Y, Z; hence the boundary conditions must be referenced to the same set. This poses no complication except along the meridianal line defined by $\theta = 20$ deg. Along this edge the boundary conditions referenced to polar coordinates ζ, θ, ϕ (Fig. 2.4) are as follows.

ARC LENGTH s, in.	CORD RADIUS r, in.	ARC ANGLE ϕ
1.36	1.36	2° 44'
2.86	2.86	5° 45'
4.37	4.34	8° 46'
5.85	5.82	11° 47'
6.87	6.80	13° 48'
7.85	7.76	15° 48'
8.36	8.24	16° 49'
8.87	8.72	17° 49'
9.38	9.19	18° 49'
9.86	9.66	19° 49'
10.37	10.1	20° 50'
10.86	10.6	21° 50'

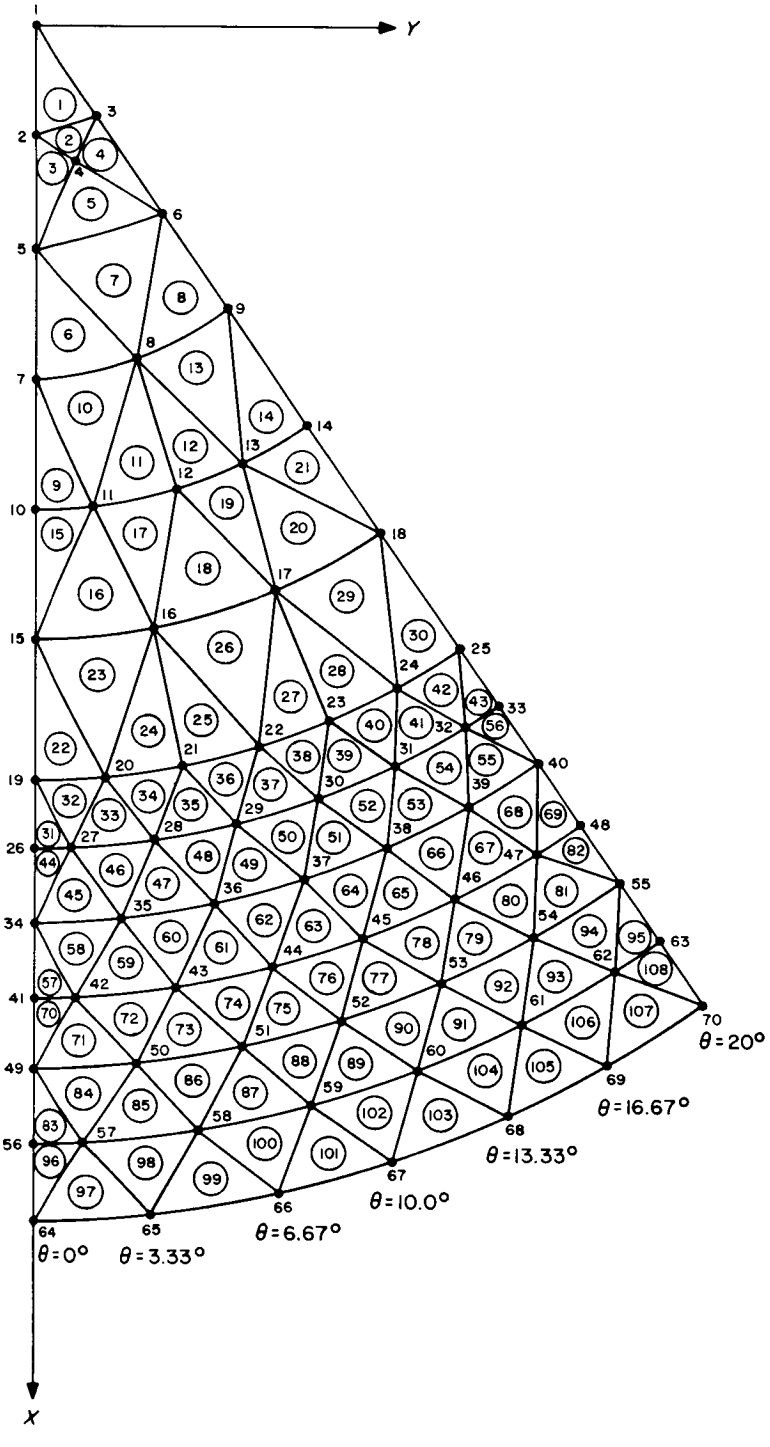

Fig. 2.4. Facet geometry and gridpoint numbering

Table 2-1. Gridpoint coordinate distances (in inches)

Node	x	y	z	Node	x	y	z
1	0	0	28.5	32	7.8268	2.5935	27.281
2	1.3592	0	28.468	33	7.7480	2.8201	27.281
3	1.2772	0.46487	28.468	34	8.7201	0	27.133
4	1.9254	0.33950	28.433	35	8.7054	0.50699	27.133
5	2.8554	0	28.357	36	8.6612	1.0123	27.133
6	2.6832	0.97660	28.357	37	8.5876	1.5142	27.133
7	4.3437	0	28.167	38	8.4850	2.0110	27.133
8	4.2777	0.75428	28.167	39	8.3538	2.5009	27.133
9	4.0817	1.4856	28.167	40	8.1942	2.9824	27.133
10	5.8200	0	27.900	41	9.1924	0	26.977
11	5.7978	0.50727	27.900	42	9.1901	0.26736	26.977
12	5.7316	1.0106	27.900	43	9.1590	0.80135	26.977
13	5.6217	1.5063	27.900	44	9.0969	1.3325	26.977
14	5.4690	1.9906	27.900	45	9.0041	1.8592	26.977
15	6.7981	0	27.677	46	8.8808	2.3796	26.977
16	6.7521	0.78919	27.677	47	8.7273	2.8919	26.977
17	6.6148	1.5678	27.677	48	8.6380	3.1440	26.977
18	6.3881	2.3251	27.677	49	9.6618	0	26.812
19	7.7600	0	27.423	50	9.6455	0.56174	26.812
20	7.7469	0.45117	27.423	51	9.5965	1.1216	26.812
21	7.7075	0.90086	27.423	52	9.5150	1.6778	26.812
22	7.6421	1.3475	27.423	53	9.4013	2.2282	26.812
23	7.5508	1.7896	27.423	54	9.2559	2.7710	26.812
24	7.4340	2.2256	27.423	55	9.0791	3.3045	26.812
25	7.2920	2.6541	27.423	56	10.136	0	26.637
26	8.2453	0	27.281	57	10.132	0.29475	26.637
27	8.2418	0.23977	27.281	58	10.097	0.88345	26.637
28	8.2139	0.71866	27.281	59	10.029	1.4690	26.637
29	8.1582	1.1950	27.281	60	9.9266	2.0497	26.637
30	8.0750	1.6674	27.281	61	9.7907	2.6234	26.637
31	7.9644	2.1340	27.281	62	9.6215	3.1882	26.637

Table 2-1 (Cont'd)

Node	x	y	z	Node	x	y	z
63	9.5247	3.4667	26.637	67	10.439	1.8407	26.456
64	10.600	0	26.456	68	10.314	2.4446	26.456
65	10.582	0.61628	26.456	69	10.155	3.0401	26.456
66	10.528	1.2306	26.456	70	9.9607	3.6254	26.456

$$
\begin{aligned}
u_{\theta_i} &= 0 \\
\theta_{\zeta_i} &= 0 \text{ (not defined in classical shell theory)} \\
\theta_{\phi_i} &= 0 \\
N_{\zeta_i} &= -P_i \text{ (not defined in classical shell theory)} \\
N_{\phi_i} &= 0 \\
M_{\theta_i} &= 0
\end{aligned}
\tag{2.1}
$$

where P_i is the fraction of the total pressure load lumped at gridpoint i. This pressure load is lumped at the gridpoints automatically in the BILD link of SAMIS and need not be considered as input, but is included here in order to specify completely

the boundary conditions. The conditions of Eq. (2.1) transformed to the X, Y, Z system of coordinates using the equations derived in Appendix A result in

$$u_{X_i} \sin 20° - u_{Y_i} \cos 20° = 0$$

$$\theta_{X_i} \cos 20° + \theta_{Y_i} \sin 20° = 0$$

$$\theta_{Z_i} = 0$$

$$\left.\begin{aligned} F_{X_i} \cos 20° + F_{Y_i} \sin 20° &= P_i \sin \phi_i \\ F_{Z_i} &= P_i \cos \phi_i \end{aligned}\right\} \text{Right-hand side component pressure loads are generated internal to SAMIS}$$

$$M_{X_i} \sin 20° - M_{Y_i} \cos 20° = 0 \qquad (2.2)$$

where the stress resultants referenced to the X, Y, Z coordinate system are defined in Ref. 1, Table 5-3. These boundary conditions apply to gridpoints 3, 6, 9, 14, 18, 25, 33, 40, 48, 55, 63 and 70. To impose these boundary conditions a coordinate transformation is required, which is derived in this section.

Along the meridianal edge defined by $\theta = 0$ deg, the boundary conditions referenced to the system Cartesian coordinates are:

$$u_{Y_i} = 0$$

$$\theta_{X_i} = 0$$

$$\theta_{Z_i} = 0 \qquad (2.3)$$

$$F_{X_i} = P_i \sin \phi_i$$

$$F_{Z_i} = P_i \cos \phi_i$$

$$M_{X_i} = 0 \qquad (2.3)\ (\text{Cont'd})$$

These conditions apply at gridpoints 2, 5, 7, 10, 15, 19, 26, 34, 41, 49, 56 and 64.

Remaining boundary and symmetry conditions must be imposed at the clamped outer edge and the apex of the sector. At the clamped edge

$$u_{X_i} = 0$$

$$u_{Y_i} = 0$$

$$u_{Z_i} = 0$$

$$\theta_{X_i} = 0$$

$$\theta_{Y_i} = 0$$

$$\theta_{Z_i} = 0 \qquad (2.4)$$

which are imposed at gridpoints 64, 65, 66, 67, 68, 69 and 70.

Finally, based upon symmetry conditions, the boundary conditions at gridpoint 1 (apex) are:

$$u_{X_1} = 0$$

$$u_{Y_1} = 0$$

$$\theta_{X_1} = 0$$

$$\theta_{Y_1} = 0$$

$$\theta_{Z_1} = 0 \qquad (2.5)$$

The zero-valued boundary and symmetry conditions at the apex, side $\theta = 0$ deg, and clamped outer edge are summarized in Table 2-2.

The boundary conditions for gridpoints along the side of the sector at $\theta = 20$ deg are defined by Eq. (2.2). To apply these it is necessary first to transform the displacement variables from

$$\begin{Bmatrix} u_{X_i} \\ u_{Y_i} \\ u_{Z_i} \\ \theta_{X_i} \\ \theta_{Y_i} \\ \theta_{Z_i} \end{Bmatrix} \quad \text{to} \quad \begin{Bmatrix} u_{X_i} \cos 20° + u_{Y_i} \sin 20° \\ -u_{X_i} \sin 20° + u_{Y_i} \cos 20° \\ u_{Z_i} \\ \theta_{X_i} \cos 20° + \theta_{Y_i} \sin 20° \\ -\theta_{X_i} \sin 20° + \theta_{Y_i} \cos 20° \\ \theta_{Z_i} \end{Bmatrix}$$

Table 2-2. Zero-valued gridpoint boundary conditions

Node No. i	u_{X_i}	u_{Y_i}	u_{Z_i}	θ_{X_i}	θ_{Y_i}	θ_{Z_i}
1	0	0	u_{Z_1}	0	0	0
2	u_{X_2}	0	u_{Z_2}	0	θ_{Y_2}	0
5	u_{X_5}	0	u_{Z_5}	0	θ_{Y_5}	0
7	u_{X_7}	0	u_{Z_7}	0	θ_{Y_7}	0
10	$u_{X_{10}}$	0	$u_{Z_{10}}$	0	$\theta_{Y_{10}}$	0
15	$u_{X_{15}}$	0	$u_{Z_{15}}$	0	$\theta_{Y_{15}}$	0
19	$u_{X_{19}}$	0	$u_{Z_{19}}$	0	$\theta_{Y_{19}}$	0
26	$u_{X_{26}}$	0	$u_{Z_{26}}$	0	$\theta_{Y_{26}}$	0
34	$u_{X_{34}}$	0	$u_{Z_{34}}$	0	$\theta_{Y_{34}}$	0
41	$u_{X_{41}}$	0	$u_{Z_{41}}$	0	$\theta_{Y_{41}}$	0
49	$u_{X_{49}}$	0	$u_{Z_{49}}$	0	$\theta_{Y_{49}}$	0
56	$u_{X_{56}}$	0	$u_{Z_{56}}$	0	$\theta_{Y_{56}}$	0
64	0	0	0	0	0	0
65	0	0	0	0	0	0
66	0	0	0	0	0	0
67	0	0	0	0	0	0
68	0	0	0	0	0	0
69	0	0	0	0	0	0
70	0	0	0	0	0	0

and similarly the force variables from

$$\begin{Bmatrix} F_{X_i} \\ F_{Y_i} \\ F_{Z_i} \\ M_{X_i} \\ M_{Y_i} \\ M_{Z_i} \end{Bmatrix} \text{ to } \begin{Bmatrix} F_{X_i} \cos 20° + F_{Y_i} \sin 20° \\ -F_{X_i} \sin 20° + F_{Y_i} \cos 20° \\ F_{Z_i} \\ M_{X_i} \cos 20° + M_{Y_i} \sin 20° \\ -M_{X_i} \sin 20° + M_{Y_i} \cos 20° \\ M_{Z_i} \end{Bmatrix}$$

A single transformation matrix will accomplish this task. Stated another way, what is wanted is a matrix that does the following:

$$\begin{Bmatrix} u_{X_i} \\ u_{Y_i} \\ u_{Z_i} \\ \theta_{X_i} \\ \theta_{Y_i} \\ \theta_{Z_i} \end{Bmatrix} = \begin{bmatrix} a_{11} & a_{12} & a_{13} & a_{14} & a_{15} & a_{16} \\ a_{21} & \cdot & \cdot & \cdot & \cdot & \cdot \\ a_{31} & \cdot & \cdot & \cdot & \cdot & \cdot \\ a_{41} & \cdot & \cdot & \cdot & \cdot & \cdot \\ a_{51} & \cdot & \cdot & \cdot & \cdot & \cdot \\ a_{61} & \cdot & \cdot & \cdot & \cdot & \cdot \end{bmatrix} \begin{Bmatrix} u_{X_i} \cos 20° + u_{Y_i} \sin 20° \\ -u_{X_i} \sin 20° + u_{Y_i} \cos 20° \\ u_{Z_i} \\ \theta_{X_i} \cos 20° + \theta_{Y_i} \sin 20° \\ -\theta_{X_i} \sin 20° + \theta_{Y_i} \cos 20° \\ \theta_{Z_i} \end{Bmatrix} \tag{2.6}$$

The a_{ij} can be found by writing the individual equations of the above matrix equation and solving the coefficient equations of the variables.

The result is:

$a_{11} = \cos 20°$ $\quad a_{33} = 1.0$ $\quad a_{44} = \cos 20°$

$a_{12} = -\sin 20°$ $\quad a_{66} = 1.0$ $\quad a_{45} = -\sin 20°$

$a_{21} = \sin 20°$ $\quad a_{54} = \sin 20°$

$a_{22} = \cos 20°$ $\quad a_{55} = \cos 20°$

Therefore, the transformation matrix is

$$\left[a_{ij}\right] = \begin{bmatrix} 0.940 & -0.342 & 0 & 0 & 0 & 0 \\ 0.342 & 0.940 & 0 & 0 & 0 & 0 \\ 0 & 0 & 1.0 & 0 & 0 & 0 \\ 0 & 0 & 0 & 0.940 & -0.342 & 0 \\ 0 & 0 & 0 & 0.342 & 0.940 & 0 \\ 0 & 0 & 0 & 0 & 0 & 1.0 \end{bmatrix} \tag{2.7}$$

which must be applied to the variables of gridpoints 3, 6, 9, 14, 18, 25, 33, 40, 48, 55 and 63.

This redefines the variables, so that the boundary conditions at the above gridpoints become those shown in Table 2-3.

2.3 Procedure for the Calculation of Deflections, Stresses, and Reaction Forces

The physical and geometrical data that pertains to idealization of the structure having been defined, this data is assembled in a format required by the SAMIS program.

Additional input is required to direct the computer in performing operations of the structural analysis. This direction is provided by a set of "pseudo instructions," or command instructions, that call for the subprograms of the SAMIS program needed to manipulate the data in the required sequence to solve the problem. The set needed for the statics problem is listed in Table 2-4. The manipulation that each instruction performs is explained below, each instruction being considered in the order that it appears in Table 2-4.

Instructions 1 through 3 represent the generation phase of this set of pseudo instructions. Explicit interpretation of these instructions is:

1.0 BILD: Generate the element stiffness matrices (KAR001 through KAR108), element stress matrices (SSR001 through SSR108), and element temperature and pressure loading vectors (TLC001 through TLC108) for the 108 elements for which input data has been provided. Each stiffness matrix is stored on tape 9 (locations 09001 through 09108), each stress matrix on tape 10 (locations 10001 through 10108), and each loading vector on tape 11 (locations 11001 through 11108).

Table 2-3. Transformed gridpoint boundary conditions

Node	u_{X_i} cos 20° + u_{Y_i} sin 20°	- u_{X_i} sin 20° + u_{Y_i} cos 20°	u_{Z_i}	θ_{X_i} cos 20° + θ_{Y_i} sin 20°	- θ_{X_i} sin 20° + θ_{Y_i} cos 20°	θ_{Z_i}
3	1.0	0.0	1.0	0.0	1.0	0.0
6	1.0	0.0	1.0	0.0	1.0	0.0
9	1.0	0.0	1.0	0.0	1.0	0.0
14	1.0	0.0	1.0	0.0	1.0	0.0
18	1.0	0.0	1.0	0.0	1.0	0.0
25	1.0	0.0	1.0	0.0	1.0	0.0
33	1.0	0.0	1.0	0.0	1.0	0.0
40	1.0	0.0	1.0	0.0	1.0	0.0
48	1.0	0.0	1.0	0.0	1.0	0.0
55	1.0	0.0	1.0	0.0	1.0	0.0
63	1.0	0.0	1.0	0.0	1.0	0.0

Table 2-4. Pseudo instruction program for static response prediction

Pseudo instruction number	Field A		Field B		Field D	Field C		Field E	Comments
	Tape designation	Matrix name	Tape designation	Matrix name	Pseudo instruction name	Tape designation	Matrix name	Control numbers	
1.0	09001	KAR001	10001	SSR001	BILD	11001	TLC001	10800	Generation of stiffness, stress and loading matrices
2.0	09001	KAR001			ADDS	13001	KKR001	10800	
3.0	11001	TLC001			ADDS	13002	TSC001	10800	
4.0	09001	VTC001			READ				
5.0	09001	VTC001			FLIP	11001	VFR001		Transformation of displacement coordinates and imposition of displacement and force boundary conditions
6.0	11001	VFR001	13002	TSC001	MULT	09002	LTC001		
7.0	13001	KKR001	09001	VTC001	MULT	12001	KPR001		
8.0	12001	KPR001			COLS	09003	KPC001		
9.0	11001	VFR001	9003	KPC001	MULT	12001	KKC001		
10.0	12001	KKC001			ROWS	13001	KKR001		
11.0	9002	LTC001			COLS	13002	TSC001		
12.0		WAR001			READ				Calculation of displacements and inverse transformation of same
13.0		WAR001	13001	KKR001	WASH	11001	KWR001		
14.0	11001	KWR001	13002	TSC001	CHOL	12001	DIC001		
15.0	09001	VTC001			ROWS		VTR001		
16.0		VTR001	12001	DIC001	MULT	09004	DAC001		
17.0	09004	DAC001			COLS	12001	DIC001		
18.0	12001	DIC001			INKS			1	Displacements printout
19.0	13001	KKR001	12001	DIC001	MULT	11001	RFC001		Determination of reaction forces
20.0	11001	RFC001			INKS			1	
21.0		ATC001			READ				Computation of element stresses and printout
22.0		ATC001	12001	DIC001	ADDS		DTC001		
23.0	10001	SSR001		DTC001	MULT	11001	SAC001	10800	
24.0	11001	SAC001			INKS			10801	
25.0					HALT				Halt operations

Note that the symbols used in defining the alphanumeric title of each matrix are arbitrary. In the listing in Table 2-4, the last letter indicates the listing of the matrix, where R = row listed and C = column listed. This convention is for user convenience and in no way controls the actual listing of the matrix.

2.0 ADDS: Add the 108 element stiffness matrices. Title the summed matrix KKR001 and store it on tape 13, location 1.

3.0 ADDS: Add the 108 loading matrices. Title the summed matrix TSC001 and store it on tape 13, location 2.

Instructions 4 through 12 effect transformation of the generalized displacements and impose force and displacement boundary conditions.

4.0 READ: Transfer the variable transformation matrix VTC001 from the data input tape to tape 09, location 001.

5.0 FLIP: Transpose the matrix VTC001. Matrix VTC001 is column-listed so the transpose will be row-listed. The transposed matrix VFR001 is stored on tape 11, location 001.

6.0 MULT
7.0 MULT
8.0 COLS
9.0 MULT
10.0 ROWS
11.0 COLS

Transform the loading vector and stiffness matrix in a manner consistent with the following mathematical interpretation:

The outputs of the generation phase $[K]$ and $\{P_i\}$ are related by:

$$[K] \quad \{\delta_i\} = \{P_i\}$$

where

$$[K] \equiv [KKR001]$$

(Instructions 2 and 3)

$$\{P_i\} \equiv [TSC001]$$

The function of the VTC001 matrix is to impose the constraint conditions along the outer edge of the shell and along the edges of the shell sector defined by $\theta = 0$ deg and $\theta = 20$ deg. The transformation is shown to be of the form (see Eq. 2.6):

$$\{\delta_i\} = [T] \{\bar{\delta}_i\}$$

where δ_i are the displacements of the unconstrained system, $\bar{\delta}_i$ are those of the constrained system, and $[T]$ is the transformation matrix. Substituting, we obtain

$$[K] [T] \{\bar{\delta}_i\} = \{P_i\}$$

then

$$[T]^T [K] [T] \{\bar{\delta}_i\} = [T]^T \{P_i\}$$

or

$$[\bar{K}] \{\bar{\delta}_i\} = \{\bar{P}_i\}$$

where this equation represents the transposed force-displacement equation. In the pseudo instruction program:

$$\left.\begin{aligned} [\bar{K}] &\equiv [\text{KKR001}] \\ \{\bar{P}_i\} &\equiv [\text{TSC001}] \end{aligned}\right\} \text{ From Instructions 10 and 11}$$

The matrix triple product $[T]^T [K] [T] = [\bar{K}]$ assures that if $[K]$ is symmetric $[\bar{K}]$ will also be symmetric.

12.0 READ: Transfer the matrix WAR001 to core from the data input tape.

13.0 WASH: Pre- and post-multiply the stiffness matrix KKR001 by the matrix WAR001, which is a diagonal matrix. Mathematically, this equation is identical to the transformation already described in that a matrix triple product is formed. The only difference is that the WASH matrix (WAR001) must be diagonal, hence rows and columns of KKR001 can only be scaled or deleted.

This operation imposes the boundary conditions defined in Table 2-3, and results in reduction of order of the stiffness matrix. The output matrix KWR001 is the compacted stiffness matrix. It is row-listed and is stored on tape 11, location 001.

The transformation performed by instructions 6.0 through 9.0 partly resulted in imposition of certain zero-valued displacement conditions on the structure. It should be noted that this same operation can be performed by inserting appropriate gridpoint continuity numbers in the element input data. In many problems, if this is done, no other transformation is required. However, this is not the case with this statics problem because of the skewed direction of the one meridianal edge with respect to the coordinate axes X, Y, Z.

Instructions 14 through 17 direct the computation of the structural displacements due to loading conditions defined by matrix TSC001.

14.0 CHOL: Solve through matrix decomposition for the displacements. Mathematically, the following operation is performed:

Starting with $[K^*]$ $\{\delta_i^*\}$ = $\{\bar{P}_i\}$, where $[K^*]$ is post-washed and $\{\delta_i^*\}$ are the remaining nonzero displacements, this instruction yields

$$\{\delta_i^*\} = [K^*]^{-1} \{\bar{P}_i\}$$

The quantity $\{\bar{P}_i\}$ is represented above as a column vector. Actually, it consists of two columns, one column of equivalent gridpoint forces due to pressure loading (designated column 04), and one column of fixed-node thermal forces

designated column 05). The quantity $\{\delta_i^*\}$ is also a two-column array. The user of the program should be alert to the fact that, when CHOL is used, the loading vector or B field entry can actually be up to 500 columns of different loading conditions.

15.0 ROWS: Row-list VTC001 and leave the output VTR001 in core.

16.0 MULT: Multiply matrices VTR001 and DIC001 together to obtain DAC001, which is stored on tape 09, location 004. The displacements DAC001 are transformed values defined by

$$\{\delta_i\} = [T]\{\delta_i^*\}$$

However, here the $\{\delta_i\}$ do not include those displacements that were removed by instruction 13.0

17.0 COLS: Column-list DAC001. Title the resulting matrix DIC001 and store it on tape 12, location 001. Note that DAC001 is already column-listed. (The purpose of this instruction is to retitle the displacement vector and relocate it on tape.) This is an extra instruction inserted to include the problem type in which a variable transformation is not required. For that case, instructions 4 through 10 and 15 through 17 would be omitted. However, as this option stands, it is assumed that zero boundary conditions are imposed by a WASH operation rather than by an insertion in the element data.

18.0 INKS: Transfer the displacement vectors DIC001 to the data printout tape from tape 12, location 001. The matrix is also identified by a single title card as specified in the E field. This data will be part of the final printout from the computer.

Instructions 19 and 20 direct the computation of the reaction forces at the restrained gridpoints.

19.0 MULT: Multiply the structure stiffness matrix KKR001 by the nodal displacements DIC001 to obtain the nodal reaction forces RFC001. The reaction forces along the

meridianal edge of the shell defined by $\theta = 20$ deg are referenced to this edge rather than the X, Y, Z coordinate system. Specific interpretation of these forces is contained in the definition of the transformation matrix (see Eq. 2.6).

20.0 INKS: Transfer the reaction force matrix RFC001 to the data printout tape from tape 11, location 001. This matrix will be headed by one title card as specified in the E field.

Note: If reaction forces are not needed, instructions 19 and 20 should be omitted.

21.0 READ: Transfer the matrix ATC001 to core from the data input tape. This matrix is used in the calculation of the thermal stresses, as outlined in Appendix B.

22.0 ADDS: Add the ATC001 matrix to the displacement vectors DIC001. Designate the sum DTC001 and leave it in core.

23.0 MULT: Serial multiply each stress matrix starting with SSR001 with the displacement vectors to obtain values for the stresses for the two loading conditions. Each stress matrix is stored on tape 11 in consecutive order, the last matrix being SAC108.

24.0 INKS: Transfer the 108 stress matrices to the data printout tape in consecutive order. One title card is supplied to label each of these matrices.

25.0 HALT: Halt operation on this program.

2.4 Description of Input Data

The input data for any problem must be listed sequentially as it is used in the pseudo instruction program. If the pseudo instruction program begins with a BILD instruction, then the input data following the list of pseudo instructions must start with a material table followed by element data. If the first pseudo instruction is a READ instruction, then the input data following the pseudo instructions must begin with the matrices being read into the program in sequential order. The only other method of starting the program is with an operation pseudo instruction in which data on specific tapes must be supplied. This option is generally used in program recovery from a noncorrective error stop of a previous run.

In the present case the pseudo instruction program is headed by a generation phase (BILD); thus, the order of listing of the pseudo instructions and other input data is the following:

a. List of pseudo instructions
b. Material tables
c. Zero card
d. List of element data
e. Matrix data and title cards

The complete listing of the element and matrix data is given in Appendix D. Comments regarding each of these as applied to the present problem are given below:

a. Pseudo instructions: The listing of the pseudo instructions is given in Table 2-4. The format for the pseudo instructions is defined in the description of the MAKER subprogram in Ref. 1.

b. Material table: The format of the material table is given in Ref. 1, Table 7-1. For the shell the material is 2014-T6 aluminum alloy, which is assumed isotropic. This material is not particularly sensitive to temperature changes in the range considered in this problem. Therefore, the material is defined for room temperature (70°F or 530°R) and is assumed to remain constant with temperature change. Alternately, a material table for each of several temperatures could be provided, in which case linearly interpolated or extrapolated material coefficients would be computed by the program to match any specified temperature. In this problem, one material table is used.

c. Zero card: This card flags the end of the material data and the start of the element data.

d. Element data: The element data format and identification is described in detail in Ref. 1, Tables 7-5 and 7-6. Therefore, only the information for a typical element of this problem will be identified. The three cards of input data for the element in Fig. 2.4 having gridpoints 1, 2, 3 are shown in Fig. 2.5. The numbers in each data field are identified as parameters of the shell statics problem.

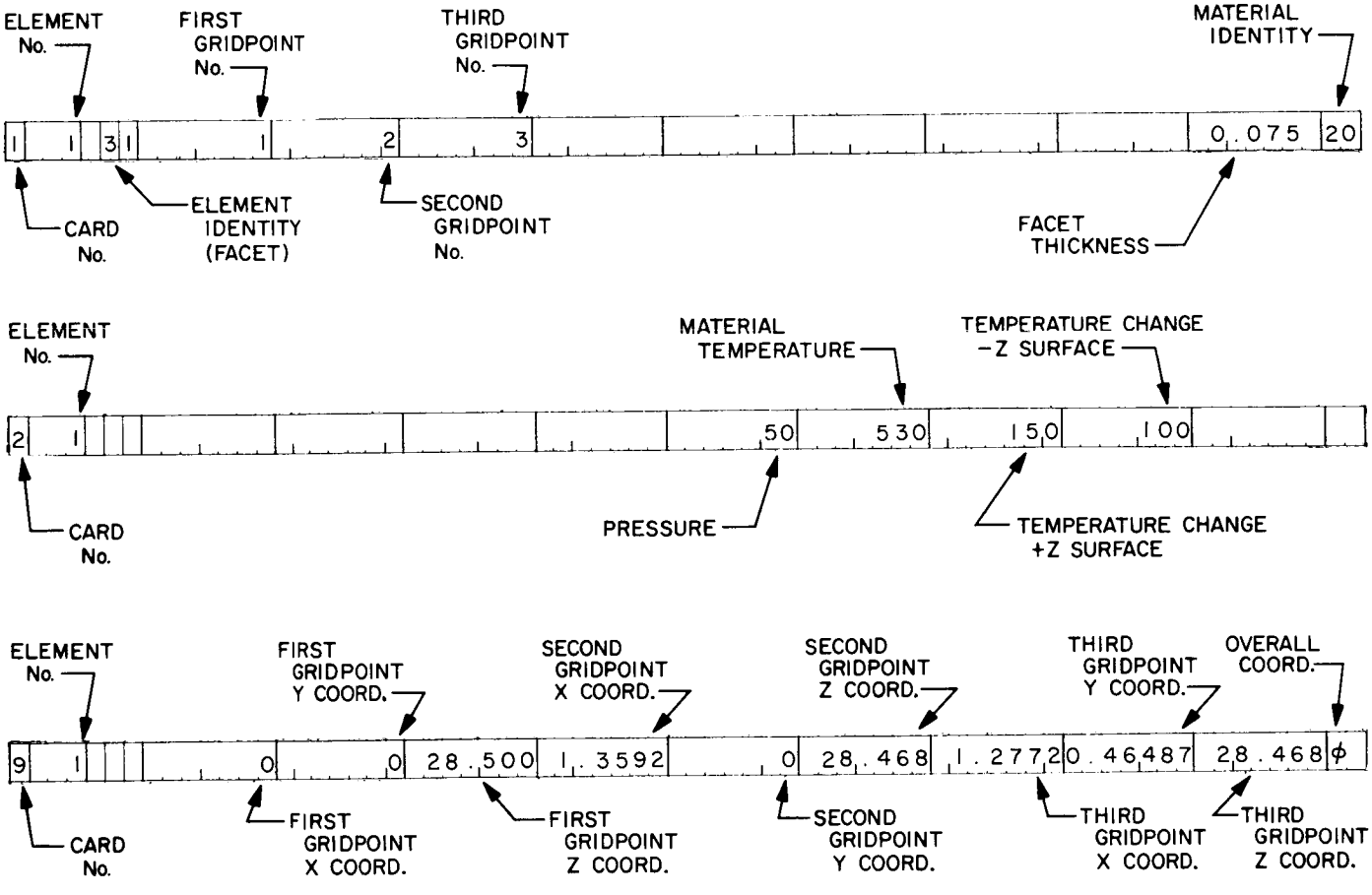

Figure 2.5. Element data for Element 1 of shell statics problem

e. Matrix data and identification cards: The first matrix that is required by the pseudo instruction program is the variable transformation matrix VTC001. The transformation is given by Eq. (2.7), and must be imposed at all gridpoints along the 20 deg meridianal edge of the shell. All other gridpoint variables must be retained, so diagonal unit values must be supplied to preserve these rows and columns during the multiplication sequence. Furthermore, since the matrix is listed in coded format, only nonzero element values need be listed.

The identification card for each matrix has a format defined in Ref. 1 in the READ subprogram description. For the matrix VTC001 the identification card is shown in Fig. 2.6.

The second card of the VTC001 listing is the first data card, the format of which is also detailed in the READ description in Ref. 1. The matrix is in coded format and is column-listed. Information on the first data card applies to gridpoint 1 (see Fig. 2.7). The component numbers depend upon the type of element used, so are defined in each element write-up. Since the "facet" element is used here, the component definition is given in Table 5-1 of Ref. 1.

The second matrix that is required is the row-column elimination matrix WAR001. The variables that need to be eliminated are defined in Tables 2-2 and 2-3. This matrix is row-listed and requires 38 cards to list. In the pseudo instruction the E field is blank, so the first option of WASH is used which retains rows and columns <u>not</u> listed in WAR001.

The next input is the title card called for by the 18th pseudo instruction. The matrix printed out by this INKS instruction is given the title "GRIDPOINT DISPLACEMENTS."

The third matrix that is input is ATC001 by pseudo instruction 21. This matrix is used in computing the stresses due to thermal effects. The function of this matrix is described in Appendix B.

The last input is the title card "ELEMENT STRESSES," which is used in pseudo instruction 24 (INKS).

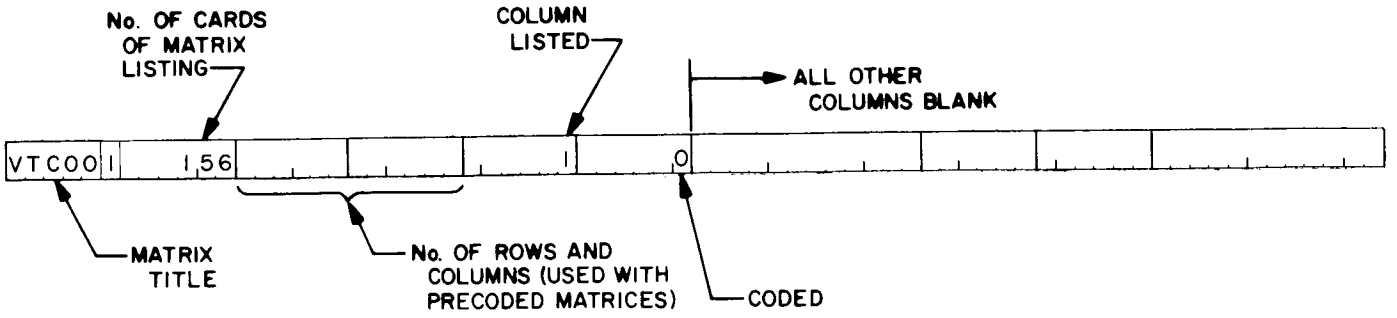

Figure 2.6. Matrix identification card

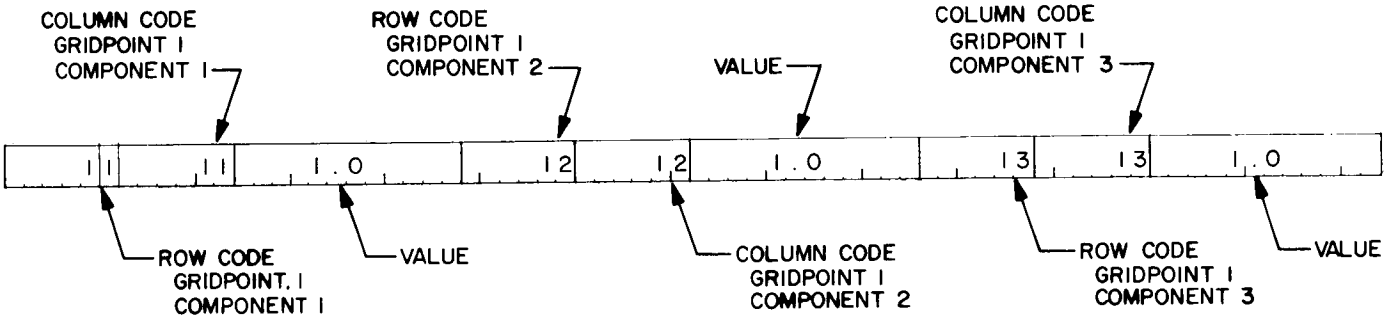

Figure 2.7. Matrix data card

Table 2-5. Program printout of material table and element data

MATERIAL TABLE

FIELD

1	2	3	4	5	6	7	8	9
2014T6	0.5300E 03	0.1250E-04	0.1600E 08	0.8000E 07	0.1600E 08	0.	0.	0.4000E 07
	0.8000E 07	0.8000E 07	-0.	0.1600E 08	0.4000E 07	-0.	0.4000E 07	

ELEMENT DATA

FIELD

1	2	3	4	5	6	7	8	9	10	11	12	13
1	1	31	0.2000E 01	0.3000E 01	0.1000E 01	-0.	-0.	-0.	-0.	-0.	0.7500E-01	20
2	-0	-0	-0.	-0.	-0.	-0.	0.5000E 02	0.5300E 03	0.1500E 03	0.1000E 03	-0.	
9	1	-0	0.1359E 01	-0.	0.2847E 02	0.1277E 01	0.4649E-00	0.2847E 02	-0.	-0.	0.2850E 02	0
1	2	31	0.3000E 01	0.2000E 01	0.4000E 01	-0.	-0.	-0.	-0.	-0.	0.7500E-01	20
2	-0	-0	-0.	-0.	-0.	-0.	0.5000E 02	0.5300E 03	0.1500E 03	0.1000E 03	-0.	
9	2	-0	0.1277E 01	0.4649E-00	0.2847E 02	0.1359E 01	-0.	0.2847E 02	0.1925E 01	0.3395E-00	0.2843E 02	0
1	3	31	0.2000E 01	0.5000E 01	0.4000E 01	-0.	-0.	-0.	-0.	-0.	0.7500E-01	20
2	-0	-0	-0.	-0.	-0.	-0.	0.5000E 02	0.5300E 03	0.1500E 03	0.1000E 03	-0.	
9	3	-0	0.1359E 01	-0.	0.2847E 02	0.2855E 01	-0.	0.2836E 02	0.1925E 01	0.3395E-00	0.2843E 02	0
1	4	31	0.3000E 01	0.4000E 01	0.6000E 01	-0.	-0.	-0.	-0.	-0.	0.7500E-01	20
2	-0	-0	-0.	-0.	-0.	-0.	0.5000E 02	0.5300E 03	0.1500E 03	0.1000E 03	-0.	
9	4	-0	0.1277E 01	0.4649E-00	0.2847E 02	0.1925E 01	0.3395E-00	0.2843E 02	0.2683E 01	0.9766E 00	0.2836E 02	0
1	5	31	0.5000E 01	0.6000E 01	0.4000E 01	-0.	-0.	-0.	-0.	-0.	0.7500E-01	20
2	-0	-0	-0.	-0.	-0.	-0.	0.5000E 02	0.5300E 03	0.1500E 03	0.1000E 03	-0.	
9	5	-0	0.2855E 01	-0.	0.2836E 02	0.2683E 01	0.9766E 00	0.2836E 02	0.1925E 01	0.3395E-00	0.2843E 02	0

2.5 Program Printout of Input Data and Program Status Statements

Upon command by insertion of a negative sign in the E field of BILD, the program prints out the material tables and element data as interpreted from the program input data. The material table printout for 2014-T6 aluminum alloy and the first and second sets of element input data for the shell statics problem are shown in Table 2-5. Comparison of these data with the prepared input data listed in Appendix D shows exact numerical agreement and similar formats.

It should be noted that the material identification is 2014-T6 in the material table (Table 2-5), but in the element data (Fig. 2.5) the identity is 20. That is, material identification is by the first and second characters of the six-character word appearing in the material table. Thus, if several entries of the same material are listed in the material table (say, for specification of different properties at different temperatures), the identification must be distinct for each entry. Numeric or alphabetic characters may be used to vary the identification.

The structural element data is printed out by the program by user option. However, a second set of statements that define core status before and after execution of each pseudo instruction is automatically recorded and printed out by the program. A sample of this printout from the JPL computer is presented in Table 2-6 for pseudo instructions 1 and 2 in Table 2-4. Observing the printout in Table 2-6, it should be noted that a time reference is given at the start and finish of each pseudo instruction. Also, the core status of the matrix data regions corresponding to the A, B, and C fields of each pseudo instruction is provided. For example, chain link 16 (BILD) was transferred from the program library tape to core at 6 hr, 00 min, 40 sec. The status of the final stiffness (KAR108), stress (SSR108), and loading (TLC108) matrices is given after the statement "CORE STATUS AT COMPLETION." Considering the stiffness matrix KAR108, it is 5 blocks long (120 words per block), is row-listed (-1), is coded (0), and, besides being in core in ID location 1, is stored on tape 9 entry 108.

The listing of program status was originally generated to aid in checkout of the program. It has proven to be very useful in locating user as well as program errors, and for this reason is retained as part of the standard output of the SAMIS. The user is cautioned that in some cases one or more of the matrices are stored on scratch tape as the calculation is performed. In the event this happens, the printout of core status may not include all matrices involved in the calculation.

Table 2-6. Printout of program core status

CORE STATUS PRIOR TO EXECUTING 1.0 9001 KAR 1 10001 SSR 1 BILD 11001 TLC 1 10800

MATRIX NAME	BLOCKS	ROWS	COLUMNS	LISTING	FORMAT	TAPE GROUP	CORE LOCATION	ID LOCATION
000 0	0	0	0	0	0	0	-1	1
000 0	0	0	0	0	0	0	-1	11
000 0	0	0	0	0	0	0	-1	21

CHAIN LINK CALLED WAS 16 AT TIME 006004

CORE STATUS ON COMPLETION

MATRIX NAME	BLOCKS	ROWS	COLUMNS	LISTING	FORMAT	TAPE GROUP	CORE LOCATION	ID LOCATION
KAR108	-5	0	0	-1	0	9108	-1	1
SSR108	-1	0	0	-1	0	10108	-1	11
TLC108	-1	0	0	1	0	11108	-1	21

CORE STATUS PRIOR TO EXECUTING 2.0 9001 KAR 1 -0 -0 ADDS 13001 KKR 1 10800

MATRIX NAME	BLOCKS	ROWS	COLUMNS	LISTING	FORMAT	TAPE GROUP	CORE LOCATION	ID LOCATION
000 0	0	0	0	0	0	0	-1	1
000 0	0	0	0	0	0	0	0	11
000 0	0	0	0	0	0	0	-1	21

CHAIN LINK CALLED WAS 8 AT TIME 006035

CORE STATUS ON COMPLETION

MATRIX NAME	BLOCKS	ROWS	COLUMNS	LISTING	FORMAT	TAPE GROUP	CORE LOCATION	ID LOCATION
KAR108	-5	0	0	-1	0	9108	0	1
000 0	0	0	0	0	0	0	0	11
KKR 1	-253	0	0	-1	0	13001	-1	21

2.6 Interpretation of Output Data

Transfer of data to the printout tape of the program as the pseudo instructions are executed can be accomplished by the following options:

a. If the number appearing in the E field of BILD is negative, then the material tables and element input data are written on the output tape.

b. If the number appearing in the E field of READ is negative, then all card data read will also be transferred to the program data-output tape.

c. If the number in the E field of ROOT is negative, then that number of eigenvalues will be transferred to the program output tape. Corresponding eigenvectors must be handled by a separate instruction (INKS).

d. If a number is placed in the E field of the HALT instruction, the program version of the pseudo instruction program is written on the printout tape.

e. Options a through d above apply to transfer of particular data. To transfer general computed data the INKS instruction is used. Most output data such as displacements, stresses, forces, etc., are written on the printout tape by INKS instructions.

Analogous to the ordering of input data as it is required in the pseudo instruction program, the printout data will be in the order that it is written on the printout tape. Labelling of the output is user-controlled by the number and content of title cards supplied to the program (see INKS subprogram description in Ref. 1).

In the present problem the output consists of the gridpoint displacements (DIC001), reaction forces (RFC001), and member stresses (SAC001). Complete listing of these data will not be included in this report, but samples of each will be identified.

a. Gridpoint displacements: Two sets of deflections were computed in this problem. First, the deflections due to the pressure loading identified by a column number 04*, second, the deflections due to the thermal environment identified by a column number 05*. Part

*See Table 5-2 of Ref. 1.

of the displacement listing obtained from the computer is shown in Fig. 2.8 with pertinent identification information.

b. Reaction forces: The reaction forces consist of two sets and have the same type of listing as the displacements. Interpretation of component numbers is analogous to that for displacements. Correspondence is indicated in paragraph 2.2 and may be summarized as follows:

$$u_x \Longrightarrow F_x \qquad \theta_x \Longrightarrow M_x$$

$$u_y \Longrightarrow F_y \qquad \theta_y \Longrightarrow M_y$$

$$u_z \Longrightarrow F_z \qquad \theta_z \Longrightarrow M_z$$

c. Element stresses: The interpretation of the stress resultants is more complicated than of displacements. The stress components are given in Table 5-3 of Ref. 1 in terms of numerical subscripts. The relation between these subscripts and the local x and y directions depends upon the definition of the local coordinate system assigned to each element. Since all input for this problem was in the overall coordinate system, the local coordinate system was generated internally by the program for each element. In this case the local x-y directions are defined by the first and second gridpoint numbers listed in the input data. Observing element 75 in Fig. 2.4 and checking its element data in Appendix D, it is known that the local x-y plane is that shown in Fig. 2.9.

Note: The local x coordinate lies along the line joining the first two gridpoints introduced in the element data, unless the local coordinates axes are defined explicitly by the analyst.

Therefore, consistent with the definition of the force variables as shown in Fig. 2.3, we can make the following equivalences:

$$N_{11} \equiv N_\theta \qquad M_{11} \equiv -M_\theta$$

$$N_{22} \equiv -N_\phi \qquad M_{22} \equiv -M_\phi$$

$$N_{12} \equiv -N_{\theta\phi} \qquad M_{12} \equiv M_{\theta\phi}$$

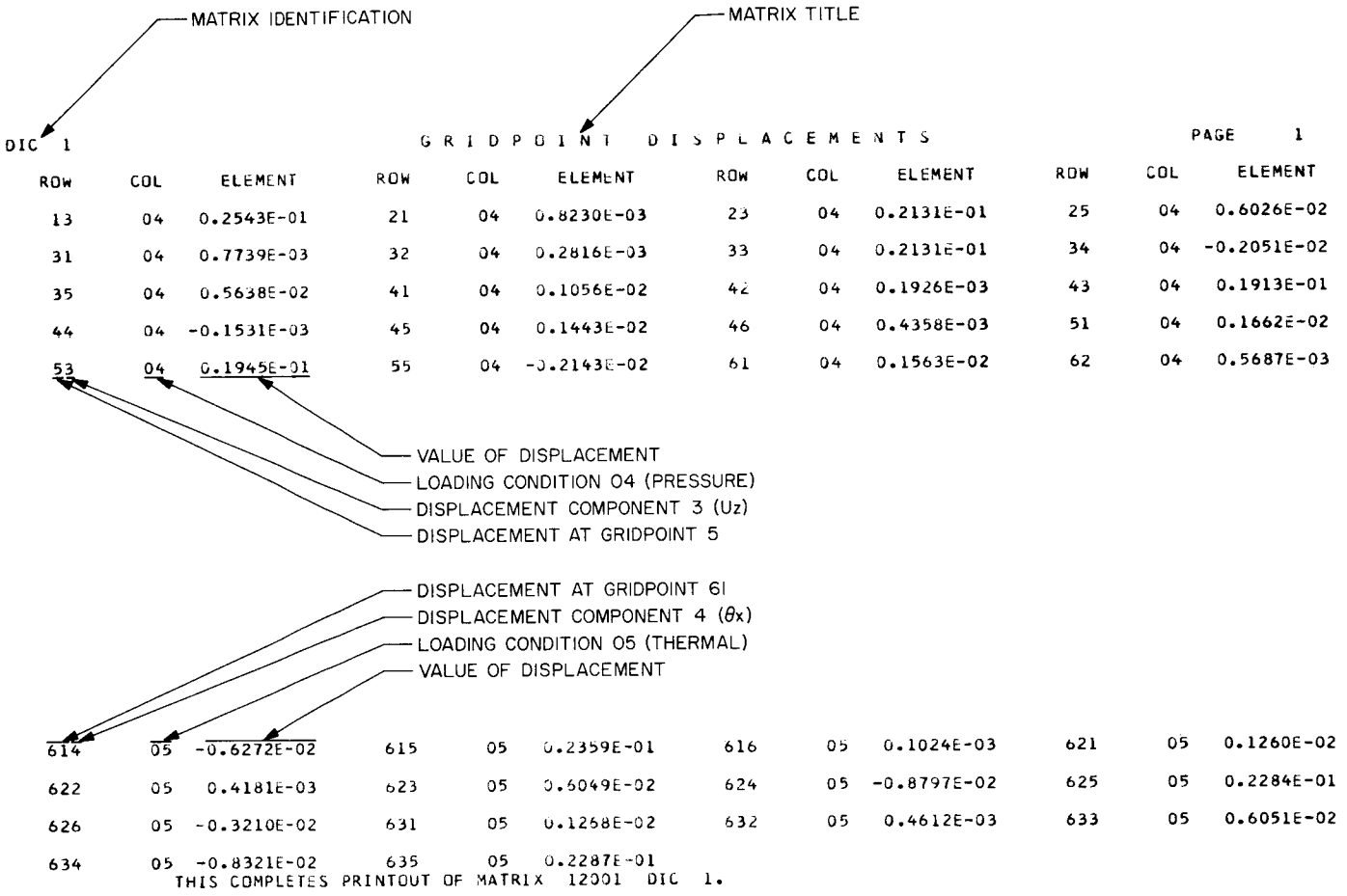

Fig. 2.8. Listing of gridpoint displacements

This information is sufficient to define the component numbers in Fig. 2.10 and interpret the element stress resultants. It should be noted that all elements oriented as element 75 (circumferential edge farthest from shell origin) have been defined in the element data to have the same relative local coordinates as element 75. Three other local coordinate types occur in this problem: those for elements ③ and ④ and a type typical of element ②.

2.7 Summary and Discussion of Computed Results

The displacements and stress resultants due to the pressure loading and temperature-induced loads were computed by three methods. Solution of the governing differential equations in closed form based upon shallow shell theory provided one set of data (see Appendix C). Solution of the differential equations by a finite difference technique provided a second set of data (for details of the method see Ref. 4)*. Third, solutions are obtained by use of the SAMIS, which is a finite element solution.

Since the structure geometry and boundary conditions are axisymmetric, data need only be compared along a meridian of the shell. Furthermore, since variables change rapidly only near the clamped edge of the shell, plotted results are expanded to show this region in greater detail.

Results for the two loading cases are shown in Figs. 2.11 through 2.16. For the pressurized shell, the maximum values of displacements, slopes, and stress resultants are comparable within good engineering accuracy ($< \pm 5\%$). Similar results for the temperature-induced loading case exhibit greater scatter in the membrane stresses (Fig. 2.15) because they are obtained from the differences of large numbers (Appendix B). In addition, the computed bending moments are systematically shifted from the finite difference values for reasons that have not been determined (Fig. 2.16).

As indicated in Fig. 2.10, the stress resultants are referenced only to the triangle, not to any particular location within the triangle. However, it has been shown that the optimum placement of the stress reference point is at the centroid of each triangle (Ref. 5). This procedure was used in locating the finite element values in Figs. 2.12, 2.13, 2.15, and 2.16.

*In computing results by the finite difference approach, constant increments in arc length of 0.01 in. were used.

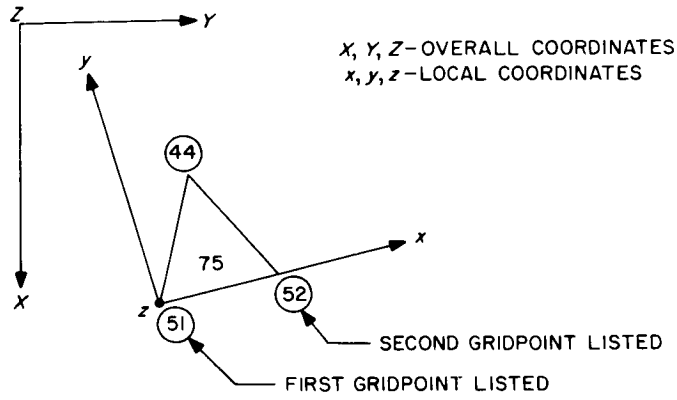

Fig. 2.9 Element 75 orientation and coordinates

MATRIX IDENTIFICATION NUMBER (ELEMENT 75)

MATRIX TITLE

SAC 75 ELEMENT STRESSES PAGE 1

ROW	COL	ELEMENT	ROW	COL	ELEMENT	ROW	COL	ELEMENT	ROW	COL	ELEMENT
751	04	0.3963E 03	752	04	0.7054E 03	753	04	-0.2813E-00	754	04	0.9349E 00
755	04	0.1627E 01	756	04	-0.6199E-02	751	05	0.2921E 04	752	05	0.3730E 04
753	05	-0.6624E 00	754	05	-0.2093E 01	755	05	-0.1549E-00	756	05	-0.4140E-02

THIS COMPLETES PRINTOUT OF MATRIX 11075 SAC 75.

VALUE OF STRESS RESULTANT
LOADING CONDITION 05 (THERMAL)
STRESS COMPONENT 3 (N_{12})
STRESS RESULTANT FOR ELEMENT 75

Fig. 2.10. Listing of typical element stress resultants

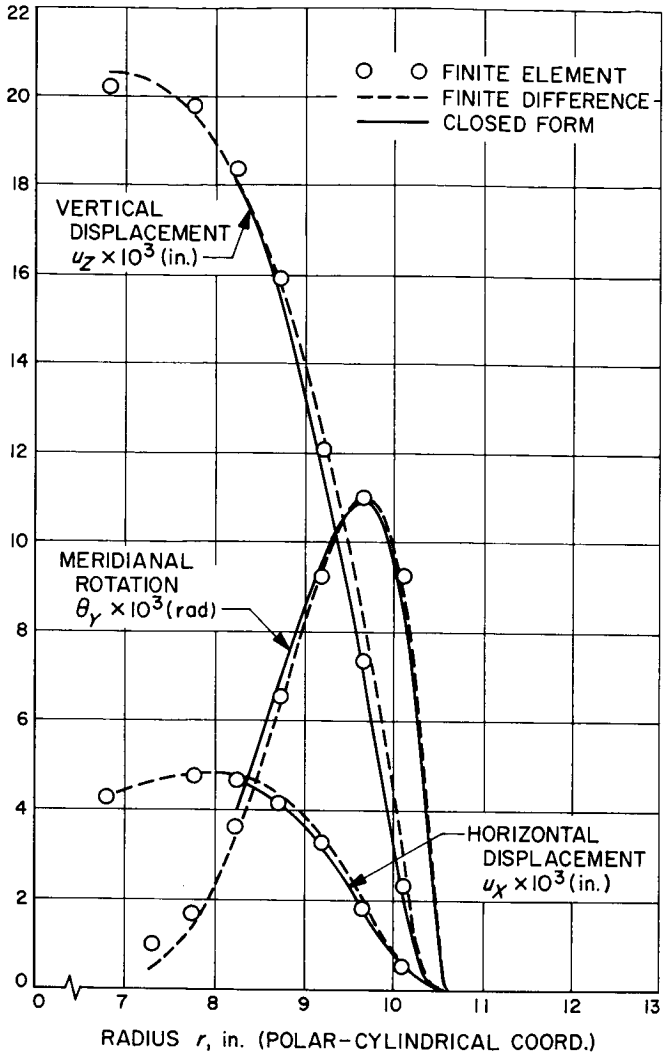

Fig. 2.11. Deformations, pressure loading

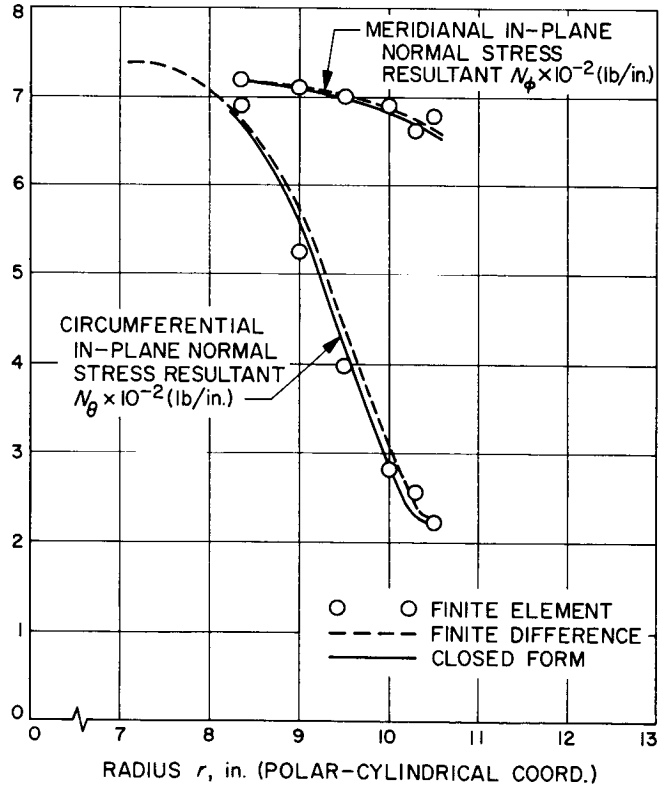

Fig. 2.12. Membrane stress resultants pressure loading

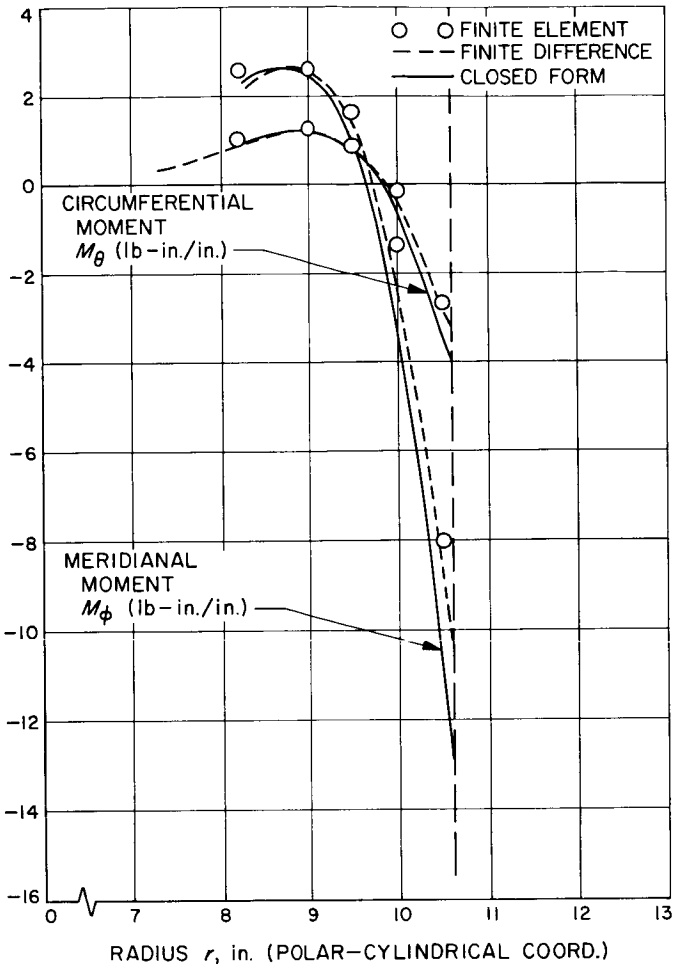

Fig. 2.13. Bending moments, pressure loading

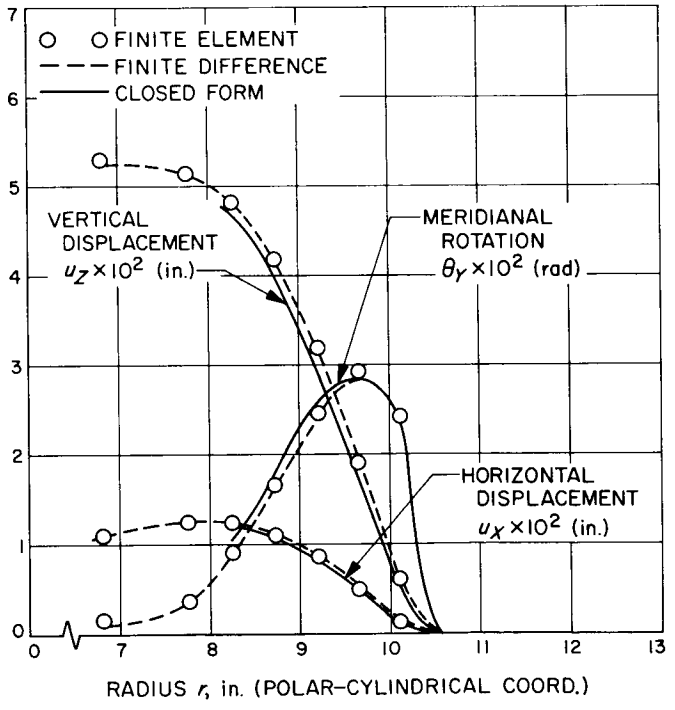

Fig. 2.14. Deformations, temperature induced loading

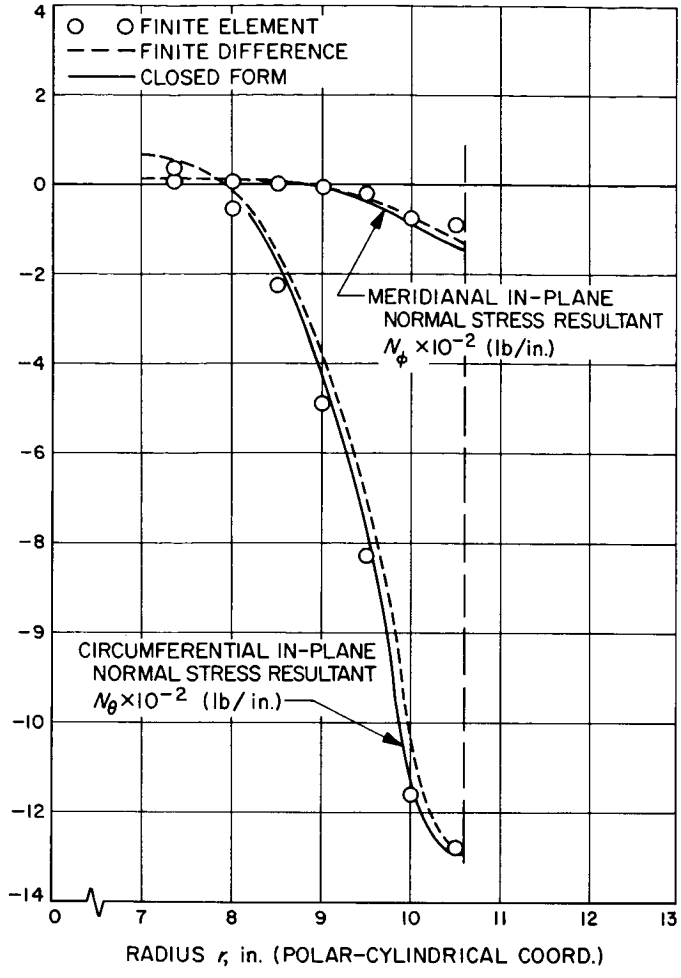

Fig. 2.15. Membrane stress resultants, temperature induced loading

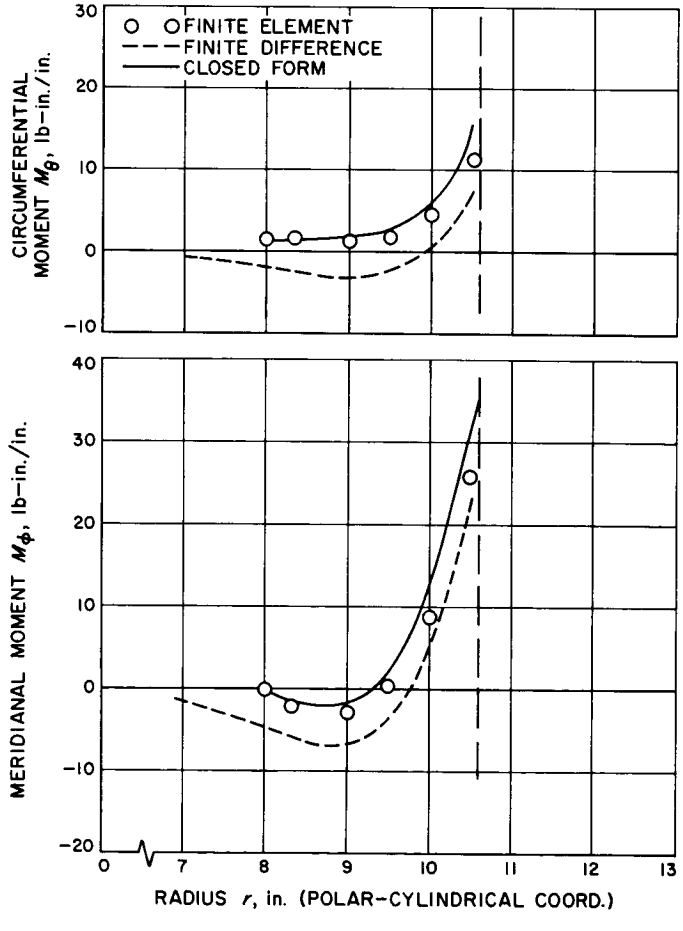

Fig. 2.16. Bending moments, temperature induced loading

Two conditions contribute to the variation in stress values observed in Figs. 2.13 and 2.16. First, a general characteristic in deflection analysis of plates and shells is that stresses are computed with less accuracy than are displacements. The reason is that derivatives (or differences) of the displacements must be computed in determining stresses, and this process inherently results in decreased accuracy. Second, with specific reference to the finite element method, only average stresses are computed for each element. These stresses are referenced to the centroid of each triangle. They may be either less or greater than the exact values at these locations. Thus, it is to be expected that in a deflection analysis the deflections are computed with greatest accuracy and the transverse shear resultants with least accuracy. Values for the slopes and moment resultants fall within these extremes.

With regard to the calculation of transverse shears, in attempting to extract one higher derivative than that for moments, inadequate accuracy was observed. The approach has been to determine shear stresses only from information within each triangle, in the same manner as that in which moments are computed. This modularizing approach, although successful for the calculation of the moment resultant, has not proven accurate in the calculation of transverse shears. For this reason the routine for calculating shear stresses has been omitted from the program.

Normally, transverse shear effects are small for thin shells, and calculation of values is not required. However, in sandwich construction this may not be true. Presently, accurate values of the shear stresses can be computed by a least squares technique. However, this requires the use of data from a number of adjacent elements. Should it be necessary to establish values for the shears, the least squares scheme is recommended (Ref. 5). It is planned that the calculation of transverse shears by the least squares technique will be programmed for the SAMIS.

2.8 Improved Stress Prediction

Degradation in the accuracy of stresses compared to displacements may lead to results in which deflections are sufficiently accurate but stresses are not. Several options are available to the analyst if this situation arises. The most straightforward approach is to refine the element grid array and rerun the problem. If a total of three grid arrays is used, then it is possible to extrapolate values of stresses by plotting or fitting an analytic curve to the data points. However, this approach is not entirely attractive in most problems because of the amount of work

involved in defining and preparing input for three grid arrays. Also, in order for this method to apply, the grid refinement should involve further subdivision of the element pattern of the coarser grid, rather than a redefinition of a new pattern with just a few additional elements. Thus, unless the coarse grid is planned carefully, one grid refinement can involve a large increase in the number of elements in order to maintain a more or less uniform triangular grid size. In some problems there is no alternative to this approach.

In regions where the stresses are not sufficiently accurate, if the gridpoint displacements are plotted and curvature changes are observed between gridpoints, then refinement of the stress prediction is possible without complete reidealization of the entire structure. In this approach, the local region of the structure where stresses vary significantly is reidealized with a finer grid. For example, in the present problem assume that the stresses near the outer clamped edge of the shell are not sufficiently accurate. To improve the stress prediction, a region such as that defined by gridpoints 19, 20, 64, and 65 can be treated separately. This region is further subdivided as depicted by the dashed lines defined by Fig. 2.17. From the results obtained using the coarser grid array, deflections are known at the circled gridpoints. These results are plotted, and interpolated deflections are assigned to all other gridpoints. Element data is then prepared for the new array of triangles for use in the program to generate the element stress matrices $[S_i]$. The original and interpolated deflections are column-listed $\{\delta\}$, and the matrix product $[S_i]\{\delta\}$ is programmed to compute new values for the stresses. It should be noted that if the deflections vary linearily, no improvement in stresses will be obtained by use of this method.

This method is very simple to apply to improve the prediction of stresses. Note, however, that improvement of the stresses for the shell statics problem should not be expected to be large because the displacements appear to be sufficiently accurate.

A second approach to improving the stress prediction is to subdivide a local region as shown in Fig. 2.17. Then only the displacements at the new gridpoints on the boundary are interpolated from previous results by linear or higher-order interpolation procedures. This data defines a set of displacement boundary conditions for the modified local structures. The problem is then rerun with appropriate external loads applied at the interior gridpoints to obtain a new displacement vector for the local region. From this data, element stresses are recomputed to complete

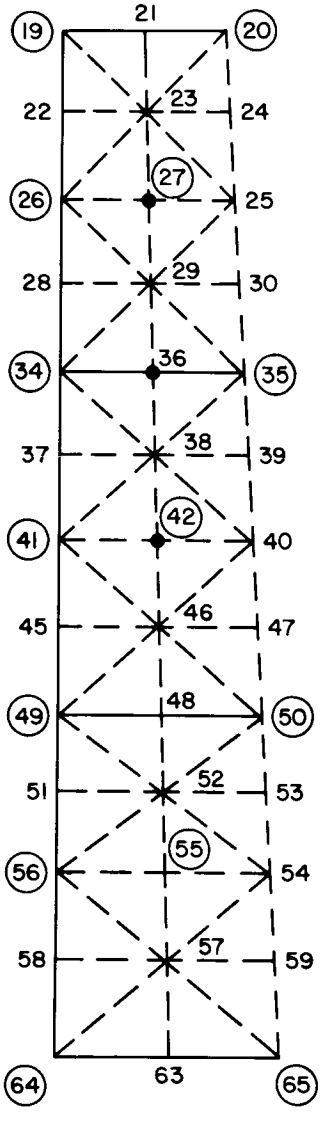

Fig. 2.17. Grid refinement for stress calculation

the procedure. This method requires more setup and computer running time than the previous method, but should yield greater improvement in the stress prediction. The use of either method is recommended as a first step in improving the stress prediction because of the ease of setting up the problem, compared to alternate methods.

2.9 Representation of Sandwich Structure

The most general stress-strain law that can be used with the triangular shell element in the SAMIS program is one having 13 independent elastic constants. The general expression is:

$$\begin{Bmatrix} \sigma_{xx} \\ \sigma_{yy} \\ \sigma_{zz} \\ \sigma_{xy} \\ \sigma_{xz} \\ \sigma_{yz} \end{Bmatrix} = \begin{bmatrix} D_{11} & D_{12} & D_{13} & D_{14} & 0 & 0 \\ & D_{22} & D_{23} & D_{24} & 0 & 0 \\ & & D_{33} & D_{34} & 0 & 0 \\ & & & D_{44} & 0 & 0 \\ & \underline{\text{SYM}} & & & D_{55} & D_{56} \\ & & & & & D_{66} \end{bmatrix} \begin{Bmatrix} \epsilon_{xx} \\ \epsilon_{yy} \\ \epsilon_{zz} \\ \epsilon_{xy} \\ \epsilon_{xz} \\ \epsilon_{yz} \end{Bmatrix} \tag{2.8}$$

For some configurations of sandwich structure these elastic constants can be modified to account for the different cross-sectional geometry. The particular idealization is from a sandwich structure in which the two outer skins are equal in thickness to an equivalent homogenous plate of thickness h. The two structures are shown in Fig. 2.18.

The procedure is to determine the properties of the equivalent plate such that the axial, bending and shear rigidities of the two systems are equal. Consider first the axial and bending rigidities of the two structures.

$$2t\, D_{ij}^{(S)} = h\, D_{ij}^{(P)} \qquad \text{(Axial)}$$

$$2t\left(\frac{r}{2}\right)^2 D_{ij}^{(S)} = \frac{h^3}{12} D_{ij}^{(P)} \qquad \text{(Bending)}$$

Solving for $D_{ij}^{(P)}$ and h, we obtain

$$h = \sqrt{3}r$$

$$D_{ij}^{(P)} = \frac{2t}{\sqrt{3}r} D_{ij}^{(S)} = \alpha D_{ij}^{(S)}$$

The modified thickness h is the value that should appear in the element input data. The elastic constants that relate to axial and bending stresses in Eq. (8) should be scaled by the factor α.

The final assumption made in idealization of the sandwich structure is that the core carries all of the transverse shear stresses. This assumption is generally valid if the thickness of the outer skins is small compared to the thickness of the core and/or the core is very flexible in bending. With this assumption, equating the shear rigidities, we obtain

$$r\, D_{ij}^{(S)} = h\, D_{ij}^{(P)}$$

but $h = \sqrt{3}r$, so

$$D_{ij}^{(P)} = \frac{1}{\sqrt{3}} D_{ij}^{(S)} = \beta D_{ij}^{(S)}$$

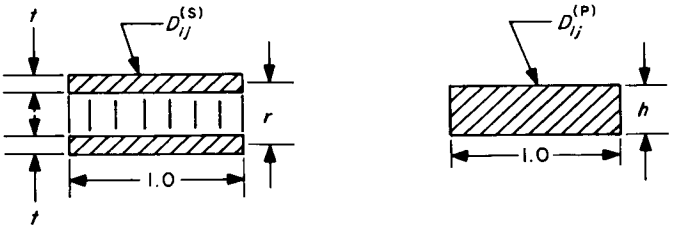

a. SANDWICH STRUCTURE b. EQUIVALENT PLATE

Fig. 2.18. Plate geometry

Therefore, the equivalent stress-strain law that can be used, if the sandwich structure satisfies the assumption that has been made, is:

$$\begin{Bmatrix} \sigma_{xx} \\ \sigma_{yy} \\ \sigma_{zz} \\ \sigma_{xy} \\ \sigma_{xz} \\ \sigma_{yz} \end{Bmatrix} = \begin{bmatrix} \alpha D_{11} & \alpha D_{12} & \alpha D_{13} & \alpha D_{14} & 0 & 0 \\ & \alpha D_{22} & \alpha D_{23} & \alpha D_{24} & 0 & 0 \\ & & \alpha D_{33} & \alpha D_{34} & 0 & 0 \\ & & & \alpha D_{44} & 0 & 0 \\ & \underline{\text{SYM}} & & & \beta D_{55} & \beta D_{56} \\ & & & & & \beta D_{66} \end{bmatrix} \begin{Bmatrix} \epsilon_{xx} \\ \epsilon_{yy} \\ \epsilon_{zz} \\ \epsilon_{xy} \\ \epsilon_{xz} \\ \epsilon_{yz} \end{Bmatrix} \quad (2.9)$$

where $\alpha = 2t/\sqrt{3}r$ and $\beta = 1/\sqrt{3}$. With this modeling, a different material table must be generated for each thickness of sandwich structure. If the structure happens to be uniform there is no problem; however, for nonuniform sandwich structure a number of material tables must be generated. This job is eased if shear deformation is negligibly small, in which case the values of the coefficient preceded by β in Eq. (2.9) are not important. Hence, α may be extracted from Eq. (2.9) and used as a scaling factor for the remaining basic material tables. This scaling may be accomplished by interpolation and extrapolation simulating α as temperature. For this case the form of the constitutive equations becomes

$$\begin{Bmatrix} \sigma_{xx} \\ \sigma_{yy} \\ \sigma_{zz} \\ \sigma_{xy} \\ \sigma_{xz} \\ \sigma_{yz} \end{Bmatrix} \simeq \alpha \begin{bmatrix} D_{11} & D_{12} & D_{13} & D_{14} & 0 & 0 \\ & D_{22} & D_{23} & D_{24} & 0 & 0 \\ & & D_{33} & D_{34} & 0 & 0 \\ & & & D_{44} & 0 & 0 \\ & & & & D_{55} & D_{56} \\ & \underline{\text{SYM}} & & & & D_{66} \end{bmatrix} \begin{Bmatrix} \epsilon_{xx} \\ \epsilon_{yy} \\ \epsilon_{zz} \\ \epsilon_{xy} \\ \epsilon_{xz} \\ \epsilon_{yz} \end{Bmatrix}$$

This equation is a good approximation if ϵ_{xy} and ϵ_{yz} are negligibly small compared to ϵ_{xx}, ϵ_{yy}, ϵ_{zz}, or ϵ_{xy}.

2.10 Solution Variation with Triangle Geometry

As discussed in Ref. 2 the equilateral triangle will provide the most accurate representation of plate-type structure. To appraise this concept, the shallow spherical shell was subdivided into a uniform grid of triangles as shown in Fig. 2.19. Successive solutions were obtained for different values of θ, notably $\theta = 20$, 60, 70 and 90 deg. For the case $\theta = 60$ deg, all triangles were approximately equilateral. The shell curvature perturbing the triangle shapes slightly from equilateral. Transverse displacements at selected gridpoints on the shell, notably gridpoints (1), (16), and (56) are plotted vs the sector angle θ in Fig. 2.20. These results indicate that the most accurate prediction of displacements is for a sector angle of approximately 60 deg. These results are by no means conclusive, because the effects of curvature, shear deflection, and gridpoint load lumping may influence the results. However, we can conclude from these results that use of triangles that have a height-to-base ratio of order unity appears to be better suited for structure idealization than triangles with very large or very small aspect ratios. This condition is used in Section III of this report in idealization of the shallow shell for determination of mode shapes and frequencies.

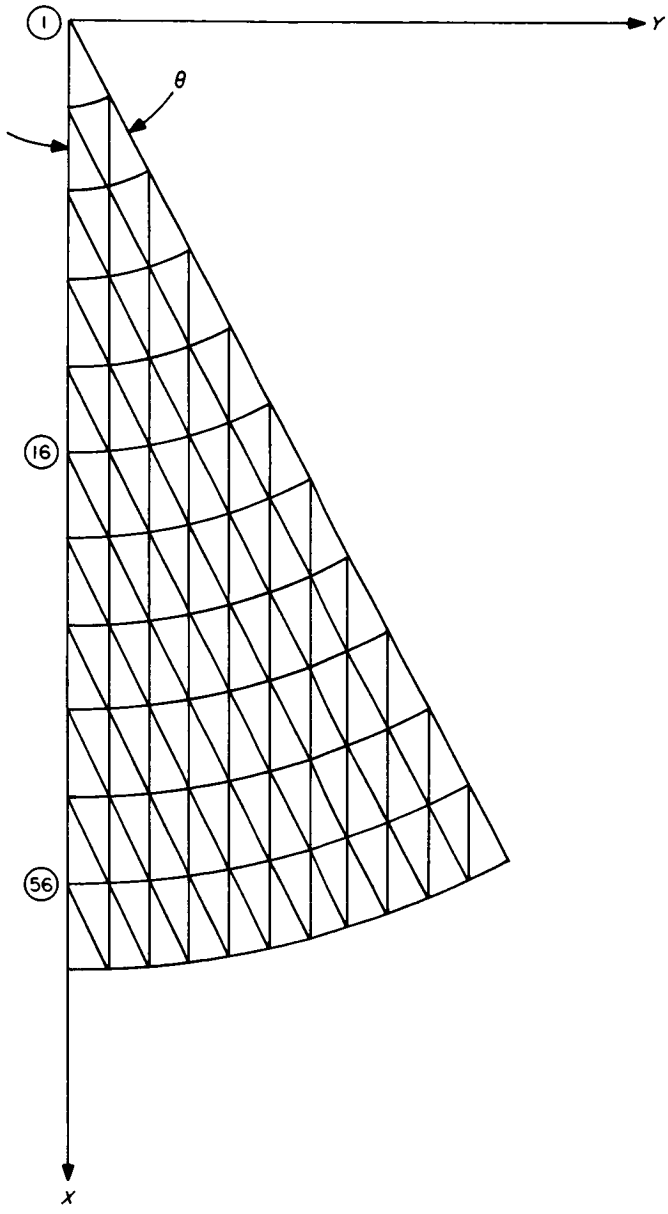

Fig. 2.19. Uniform grid representation of the shallow shell

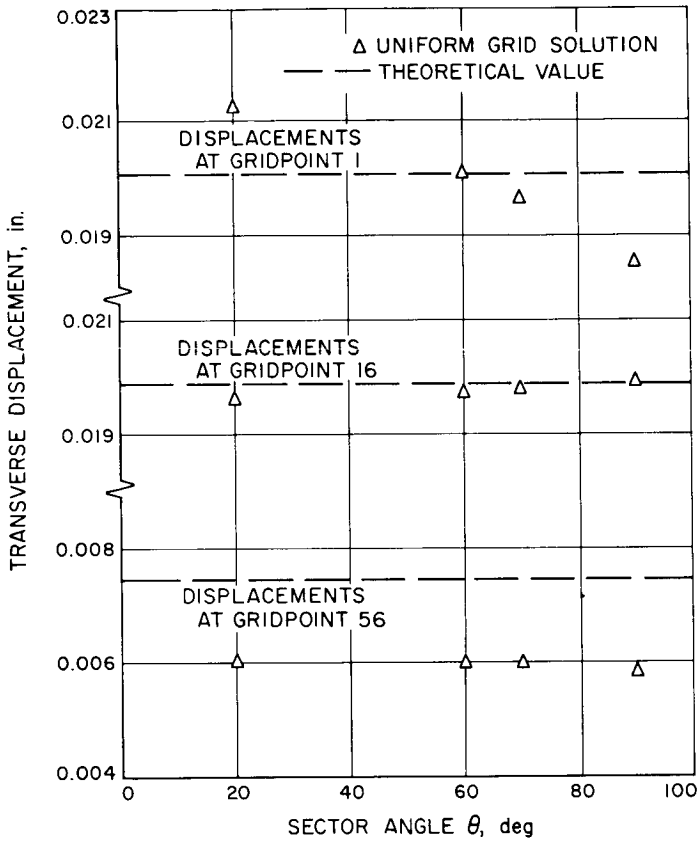

Fig. 2.20. Variation in displacement prediction with triangle geometry

3.0 SHALLOW SPHERICAL SHELL, DYNAMIC RESONANCE PREDICTION

The problem considered in this section is computation of the low-frequency flexural mode shapes of a free shallow spherical shell. Described are the shell geometry and constraint conditions, the input and output data formats, the comparison of computed results with other solutions, and other related dynamics problem topics pertinent to the use of SAMIS.

3.1 Description of Shell

The shell configuration used in the static analyses will be used also to demonstrate the method of computing the low-frequency mode shapes and frequencies using the SAMIS computer program. One change is that the outer edge of the shell will be assumed free rather than clamped as in the static analysis. Overall geometry, material properties, and weight distribution are the same as defined in Section 2.0.

3.2 Boundary Conditions for the Flexural Modes

A shallow spherical shell has low-frequency mode shapes similar to those of a plate. The modal patterns for the lower symmetric flexural modes are shown in Fig. 3.1. The plus and minus signs indicate relative direction of the transverse displacement. The nodal patterns of the lower asymmetric flexural modes are shown in Fig. 3.2. The symmetry of the nodes about the centerline of the shell determines whether the mode shapes are classified symmetric or asymmetric.

Observing the characteristics of the mode shapes in Figs. 3.1 and 3.2, it is noted that a sector of 90-deg arc can be selected for the symmetric modes to have nodal lines at each of its radial boundaries. For the asymmetric modes, the same sector would have a nodal line at one boundary and an antinodal line at the other boundary. This arrangement of nodal lines will be identical for all modes, although there will be additional nodal lines within the 90-deg sector for higher-frequency modes.

The reason for analyzing a sector rather than the entire shell is that fewer triangular elements are needed, thereby reducing the order of the various matrices of the problem. However, the boundary conditions are more difficult to formulate than if the entire shell were analyzed. Modeling only a quadrant of the shell is valid only if the shell is uniform in the circumferential direction. If it has nonuniform properties, then it is necessary to analyze the complete shell.

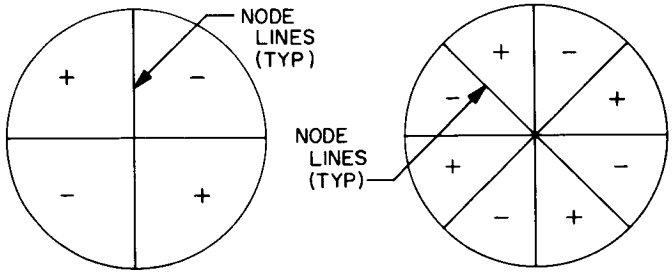

Fig. 3.1. Nodal patterns of the symmetric flexural modes

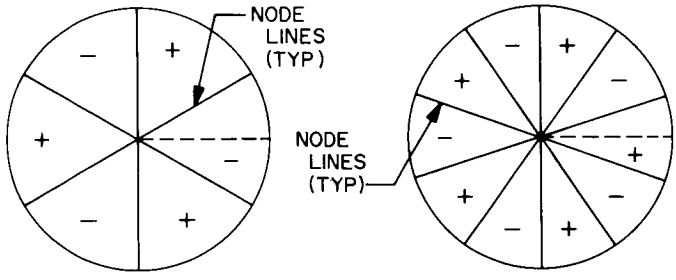

Fig. 3.2. Nodal patterns of the asymmetric flexural modes

The coordinate system and the forces and displacements corresponding to the variables required by the program are shown in Fig. 3.3. Assume that the shell boundary at X, 0, Z is a radial nodal line. For this case, a particle on this boundary will not translate radially or meridianally, and will not rotate about a circumferential axis. To represent these conditions, the required displacement constraints referenced to the overall coordinate system are:

$$\left.\begin{aligned} u_X &= 0 \\ u_Z &= 0 \\ \theta_Y &= 0 \end{aligned}\right\} \quad \text{(nodal line at X, 0, Z)} \tag{3.1}$$

This set of symmetry conditions is adequate to describe the characteristics of the nodal line even though further definition is possible. For example, an additional restraint can be formulated based upon the only allowable rotation at the boundary, which is about the meridianal axis (θ_ϕ in Fig. 2.3). One can write

$$\theta_X = \theta_\phi \cos\phi$$

$$\theta_Z = \theta_\phi \sin\phi$$

Eliminating θ_ϕ, find

$$\theta_X = \theta_Z \operatorname{ctn}\phi$$

which can be imposed as an additional constraint. However, if this constraint is not imposed, then certain modes computed using Eq. (1) should yield this constraint naturally and provide a check on the analysis. It is recommended that boundary conditions should be formulated on as simple a basis as possible consistent with the problem being solved.

Consider the meridianal line X, 0, Z as an antinode. For this case, a particle on the boundary will not translate circumferentially, and will not rotate about a meridianal axis; therefore

$$\begin{aligned} u_Y &= 0 \\ &\qquad \text{(antinodal line at X, 0, Z)} \\ \theta_X &= 0 \end{aligned} \tag{3.2}$$

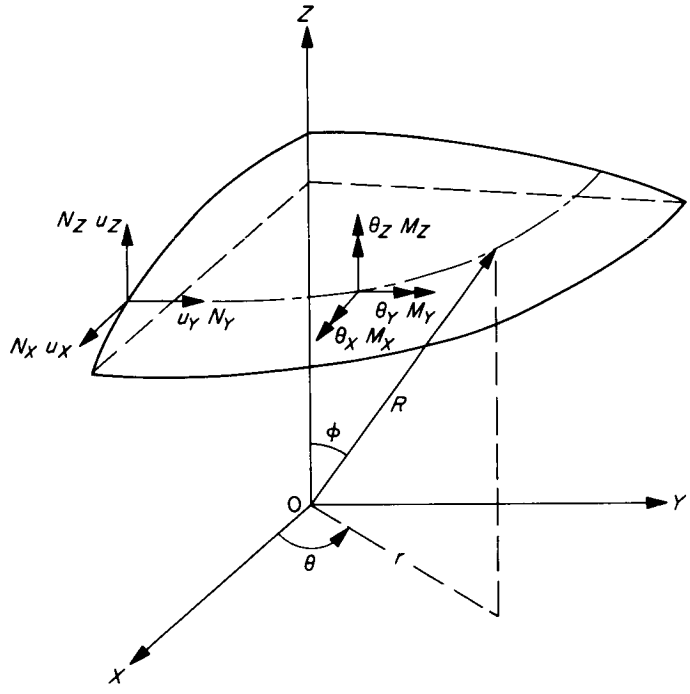

Fig. 3.3. Displacement variables and coordinates

At the gridpoint at the apex of the sector, the variables θ_θ and θ_ϕ lose their directional significance (Fig. 2.3). However, arguing that at this point several nodal lines meet, each requiring certain directional rotations to be zero, the only way of satisfying all of the conditions is to disallow any rotation at this point. Thus, the boundary conditions at the apex gridpoint of the sector will be taken as

$$U_X = 0$$

$$U_Y = 0$$

$$U_Z = 0$$

$$\theta_X = 0$$

$$\theta_Y = 0$$

$$\theta_Z = 0 \qquad (3.3)$$

This completes the definition of types of boundary conditions for the flexural modes. It should be noted that along the outer edge of the shell none of the displacements or rotations are zero, the forces and moments being zero. However, for the dynamics part of the analysis the force and moment conditions are not used because they are inertial; hence, they are proportional to displacements and rotations which have already been specified.

3.3 Element Geometry

The facet geometry should be selected consistent with the data that is to be determined. In the present case, only the lower flexural modes are to be determined. Assume that the fifth flexural mode is the highest mode of interest. The arc of a half wavelength of the fifth mode is 1/10 (360 deg) = 36 deg. Assuming that only a rough outline of the mode shape is required, two or three displacement values within this angular span should be sufficient, implying a separation of radial gridpoint lines of 12 to 15 deg.

The number of gridpoint circles is dependent upon the number of radial displacements required. For the low-frequency flexural modes, only two or three

radial displacements values are generally needed; however, if torsional modes are of interest, more gridpoint circles should be used. In the present case six gridpoint circles are used; hence, the shell sector is subdivided as indicated in Fig. 3.4.

Good practice in locating gridpoints is that the resultant triangles have sides that are approximately equal in length (equilateral). Hence, not all intersecting points in Fig. 3.4 will be used; however, one possible array, which reflects some internal symmetry, is shown in Fig. 3.5. Also shown in Fig. 3.5 is the gridpoint numbering. With respect to the overall coordinates X, Y, Z, each gridpoint location is listed in Table 3-1.

3.4 Gridpoint Referenced Boundary Conditions

The boundary conditions defined by Eqs. (3) and (4) are general expressions not referenced to any particular gridpoints. With reference to the gridpoint numbering arrangement of Fig. 3.5, the boundary conditions for the two types of vibration modes are listed in Tables 3-2 and 3-3.

Table 3-1. Gridpoint coordinates

Gridpoint	x	y	z
1	0.0	0.0	28.50
2	1.800	0.0	28.44
3	1.273	1.273	28.44
4	0.0	1.800	28.44
5	3.500	0.0	28.28
6	3.233	1.339	28.28
7	2.475	2.475	28.28
8	1.339	3.233	28.28
9	0.0	3.500	28.28
10	5.200	0.0	28.02
11	5.100	1.014	28.02
12	4.326	2.889	28.02
13	2.889	4.326	28.02
14	1.014	5.100	28.02

Table 3-1 (Cont'd)

Gridpoint	x	y	z
15	0.0	5.200	28.02
16	6.900	0.0	27.65
17	6.375	2.640	27.65
18	4.879	4.879	27.65
19	2.640	6.375	27.65
20	0.0	6.900	27.65
21	8.700	0.0	27.14
22	8.533	1.697	27.14
23	8.038	3.329	27.14
24	7.234	4.833	27.14
25	6.152	6.152	27.14
26	4.833	7.234	27.14
27	3.329	8.033	27.14
28	1.697	8.533	27.14
29	0.0	8.700	27.14
30	10.60	0.0	26.46
31	10.40	2.068	26.46
32	9.793	4.056	26.46
33	8.814	5.889	26.46
34	7.495	7.495	26.46
35	5.889	8.814	26.46
36	4.056	9.793	26.46
37	2.068	10.40	26.46
38	0.0	10.60	26.46

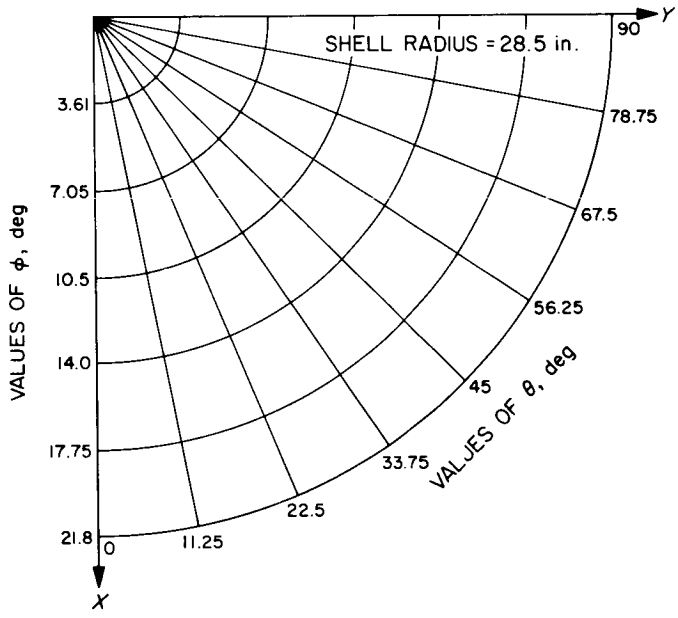

Fig. 3.4. Subdivision of shell sector

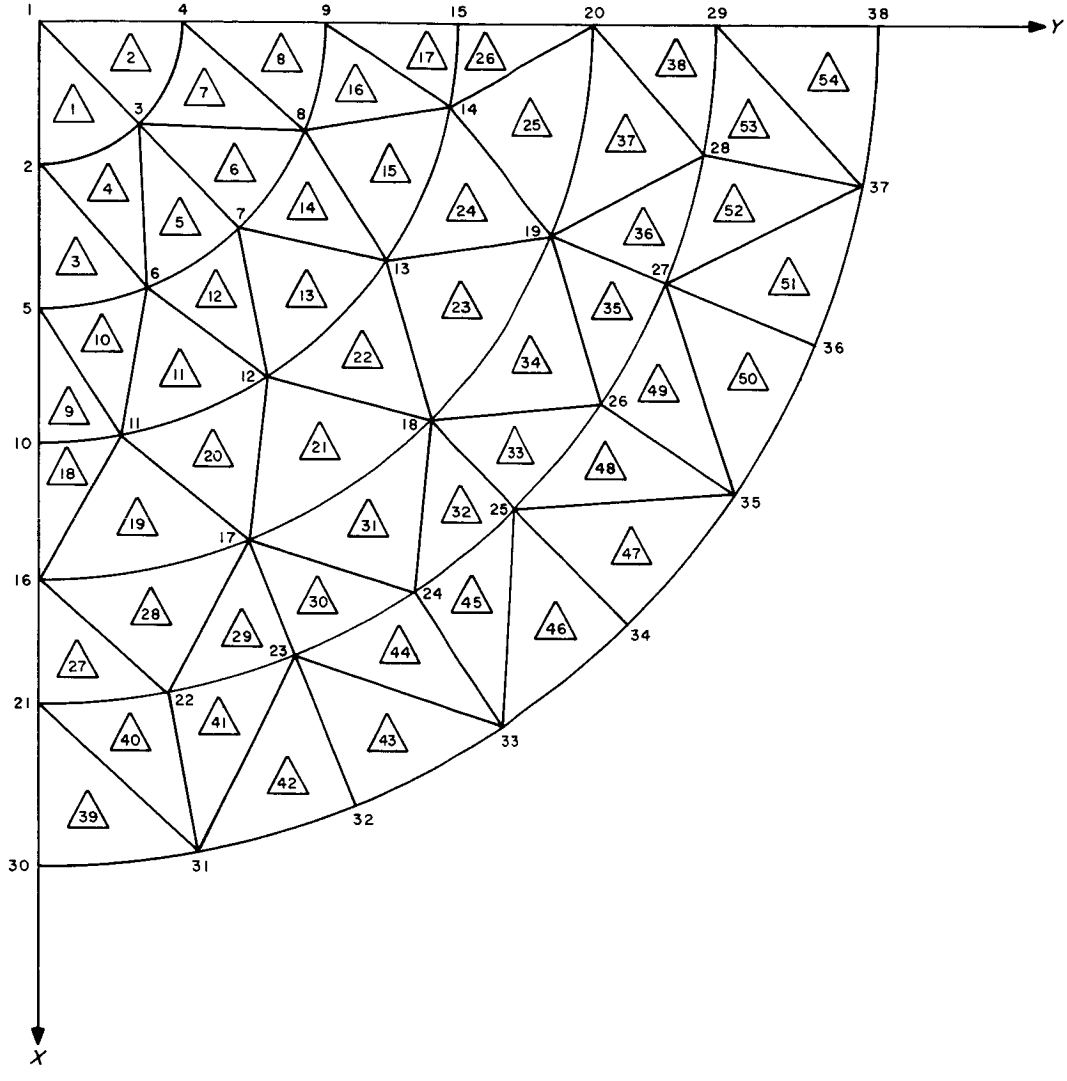

Fig. 3.5. Arrangement of facets

Table 3-2. Boundary conditions for symmetric modes

Gridpoint i	u_{X_i}	u_{Y_i}	u_{Z_i}	θ_{X_i}	θ_{Y_i}	θ_{Z_i}
2	0.0	1.0	0.0	1.0	0.0	1.0
5	0.0	1.0	0.0	1.0	0.0	1.0
10	0.0	1.0	0.0	1.0	0.0	1.0
16	0.0	1.0	0.0	1.0	0.0	1.0
21	0.0	1.0	0.0	1.0	0.0	1.0
30	0.0	1.0	0.0	1.0	0.0	1.0
1	0.0	0.0	0.0	0.0	0.0	0.0
4	1.0	0.0	0.0	0.0	1.0	1.0
9	1.0	0.0	0.0	0.0	1.0	1.0
15	1.0	0.0	0.0	0.0	1.0	1.0
20	1.0	0.0	0.0	0.0	1.0	1.0
29	1.0	0.0	0.0	0.0	1.0	1.0
38	1.0	0.0	0.0	0.0	1.0	1.0

Table 3-3. Boundary conditions for asymmetric modes

Gridpoint i	u_{X_i}	u_{Y_i}	u_{Z_i}	θ_{X_i}	θ_{Y_i}	θ_{Z_i}
2	0.0	1.0	0.0	1.0	0.0	1.0
5	0.0	1.0	0.0	1.0	0.0	1.0
10	0.0	1.0	0.0	1.0	0.0	1.0
16	0.0	1.0	0.0	1.0	0.0	1.0
21	0.0	1.0	0.0	1.0	0.0	1.0
30	0.0	1.0	0.0	1.0	0.0	1.0
1	0.0	0.0	0.0	0.0	0.0	0.0
4	0.0	1.0	1.0	1.0	0.0	1.0
9	0.0	1.0	1.0	1.0	0.0	1.0
15	0.0	1.0	1.0	1.0	0.0	1.0
20	0.0	1.0	1.0	1.0	0.0	1.0
29	0.0	1.0	1.0	1.0	0.0	1.0
38	0.0	1.0	1.0	1.0	0.0	1.0

3.5 Estimation of Matrix Size

In the SAMIS program, two subprograms, which have limited capacity, generally control the size of problems that can be solved without partitioning*. The ROOT subprogram (which calculates eigenvalues) is limited to 130 deg of freedom (either local or generalized). The CHOL subprogram (which solves simultaneous equations) is limited to core storage of 20,000 words. However, for CHOL only the diagonal and upper off-diagonal elements and two column vectors of the dimension of the matrix equation being solved must be stored. Thus the largest solid matrix of order b that can be handled in CHOL is defined by the equation:

$$\left(\frac{b^2}{2} + \frac{b}{2}\right) + 2b = 20,000$$

from which b = 197. Since stiffness matrices are generally very sparse, the limit on b is greatly relaxed in most structural problems.

A rapid estimate of the size of the stiffness matrix that will be generated can be made after the triangular array and gridpoint numbering have been defined. Consider, as an example, the triangular grid and gridpoint numbering of the idealized quarter shell (Fig. 3.5). A chart is prepared by designating a row and column for each gridpoint as shown in Fig. 3.6. Coupling between gridpoints is then indicated by filling in the appropriate squares. This is done only for the diagonal and upper off-diagonal, since this is the data used in CHOL. The CHOL subprogram in SAMIS is band-limited, which means that of all the matrix elements in the upper off-diagonal only the zero and nonzero elements below the heavy solid line in Fig. 3.6 are stored. Each square below this line represents a 6 x 6 matrix; thus, if the squares are counted and multiplied by 36, an estimate of the total number of elements that must be stored is obtained. In the present example, the number of squares is 270, which corresponds to 9720 storage locations. Note that in this problem elimination of rows and columns by imposition of the symmetry conditions will reduce slightly the storage needed for this matrix. In some problems this reduction will be significant and should be accounted for in the calculation. A tabular method of estimating the amount of storage space required is defined in Ref. 2.

*Current development of the program is aimed at elimination of these limitations.

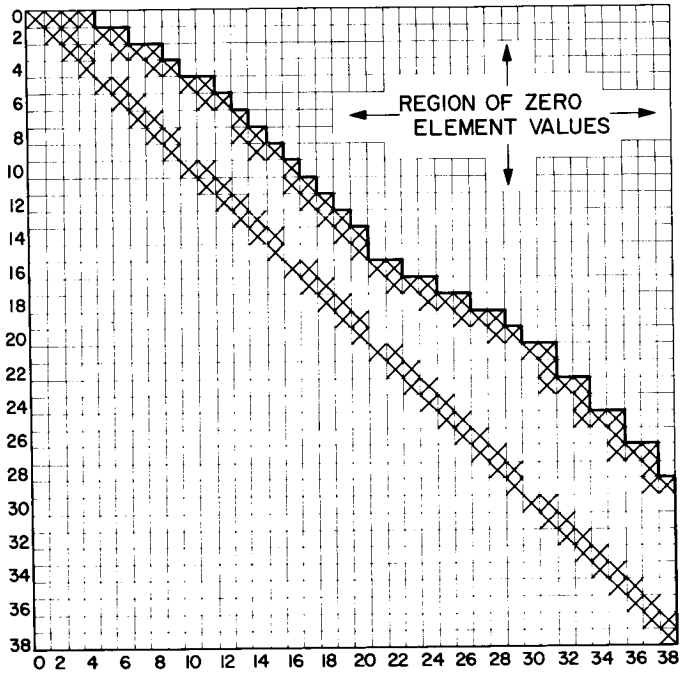

Fig. 3.6. Definition of matrix array

Should it be found that the matrix does not fit in core, then the problem must be solved by partitioning the matrix equation one or more times. This procedure is outlined in Section 5.0.

The procedure outlined above for estimating the storage size of the matrix shows that the bandwidth of storable data is controlled by the sequence of gridpoint numbering. Optimum gridpoint numbering results in a minimum-bandwidth matrix.

3.6 Influence of Rigid Body Modes

The constraints imposed on the 90-deg shell sector for the symmetric and asymmetric modes are not sufficient to eliminate all rigid body modes. For the symmetric mode case, a rigid rotation of the shell about the Z-axis can occur. For the asymmetric mode case, a rotation about the meridian defined as a nodal line can occur (shallow shell). The presence of these rigid body modes causes the stiffness matrix to be nonpositive-definite. This offers no problem if the mass matrix is inverted in solving the dynamics problem, because the ROOT subprogram will determine the eigenvalues and eigenvectors of zero-frequency modes. However, if the mass matrix is singular, which is often the case (e.g., rotary inertias neglected), inversion of the nonsingular partition of the mass matrix will lead to less accurate low-frequency eigenvalues than if the stiffness matrix is inverted. This occurs because round-off errors have a greater influence on the lower-valued roots, and in inverting the mass matrix the actual eigenvalues are determined; whereas if the stiffness matrix is inverted, the reciprocals of the eigenvalues are determined. Thus, in most problems the stiffness matrix should be inverted. To do this the influence of the rigid body modes must be eliminated. The process of eliminating these modes is outlined below for the two cases of interest in this problem.

3.7 Elimination of the Rigid Body Mode for the Symmetric Mode Case

For a rigid body rotation of magnitude Υ about the Z-axis, the displacements of a gridpoint j, as shown in Fig. 3.7, are defined by the equations

$$u_{jX} = -x_j (1 - \cos\Upsilon) - y_j \sin\Upsilon$$

$$u_{jY} = -y_j (1 - \cos\Upsilon) + x_j \sin\Upsilon \qquad (3.4)$$

where x_j and y_j are the original coordinates of gridpoint j.

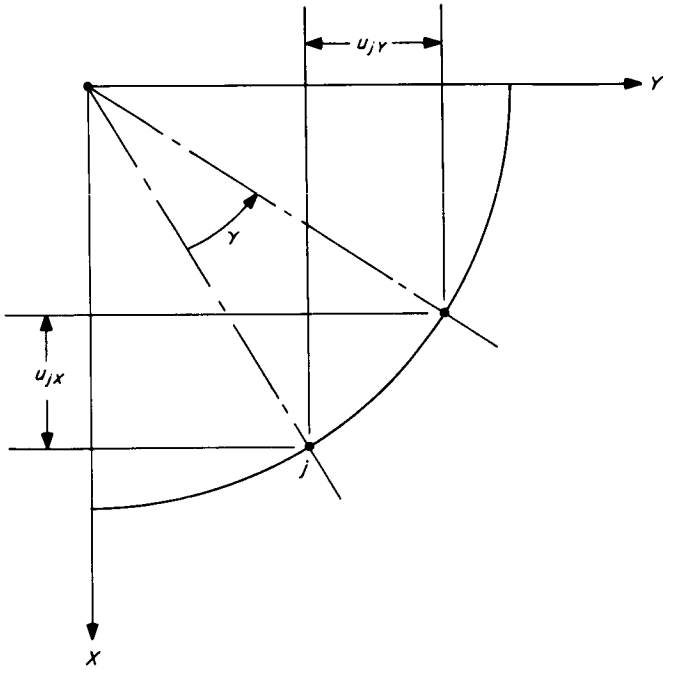

Fig. 3.7. Rigid body rotation, symmetric modes

The general orthogonality condition between two modes r and s is

$$\sum_{j=1}^{N} \left[u_{jX}^{(r)} \, m_j \, u_{jX}^{(s)} + u_{jY}^{(r)} \, m_j \, u_{jY}^{(s)} \right] = 0 \qquad (3.5)$$

which is valid whether the modes are rigid body or elastic. Substituting Eq. (4) into (5) and making the small angle approximation, yields

$$\sum_{j=1}^{N} \left[-y_j \, m_j \, u_{jX}^{(s)} + x_j \, m_j \, u_{jY}^{(s)} \right] = 0$$

We now want to expand this equation and solve for one of the gridpoint displacements in terms of the others. For convenience we will select the lowest nonzero term which is $u_{2Y}^{(s)}$, which gives:

$$u_{2Y}^{(s)} = \sum_{j=3}^{N} \frac{x_j \, m_j \, u_{jX}^{(s)} - y_j \, m_j \, u_{jX}^{(s)}}{x_2 \, m_2}$$

Further expansion of this equation yields

$$u_{2Y}^{(s)} = \frac{x_3 m_3}{x_2 m_2} u_{3Y}^{(s)} - \frac{y_3 m_3}{x_2 m_2} u_{3X}^{(s)} - \frac{y_4 m_4}{x_2 m_2} u_{4X}^{(s)} + \frac{x_5 m_5}{x_2 m_2} u_{5Y}^{(s)}$$

$$+ \frac{x_6 m_6}{x_2 m_2} u_{6Y}^{(s)} - \frac{y_6 m_6}{x_2 m_2} u_{6X}^{(s)} + \cdots \sum_{j=7}^{38} \frac{x_j m_j \, u_{jY}^{(s)} - y_j m_j \, u_{jX}^{(s)}}{x_2 m_2}$$

The displacement $u_{2Y}^{(s)}$ is dependent upon the remaining variables which are still independent. For these can write

$$u_{3X}^{(s)} = u_{3X}^{(s)}$$

$$u_{3Y}^{(s)} = u_{3Y}^{(s)}$$

$$\vdots$$

$$u_{38Y}^{(s)} = u_{38Y}^{(s)}$$

Imposing the notation that a displacement in the X direction have subscript 1 and a displacement in the Y direction have subscript 2, we can write the above results in matrix format as follows (notation consistent with SAMIS):

$$\begin{Bmatrix} u_{22} \\ u_{31} \\ u_{32} \\ u_{41} \\ u_{52} \\ \cdot \\ \cdot \\ \cdot \\ \cdot \\ u_{382} \end{Bmatrix}^{(s)}_{O} = \begin{bmatrix} -\frac{y_3 m_3}{x_2 m_2} & \frac{x_3 m_3}{x_2 m_2} & -\frac{y_4 m_4}{x_2 m_2} & +\frac{x_5 m_5}{x_2 m_2} & \frac{x_6 m_6}{x_2 m_2} & \cdots \\ 1.0 & 0 & 0 & 0 & 0 & \\ 0 & 1.0 & 0 & 0 & 0 & \\ 0 & 0 & 1.0 & 0 & 0 & \\ 0 & 0 & 0 & 1.0 & 0 & \\ & & & & & \ddots \\ & & & & & 1.0 \end{bmatrix} \begin{Bmatrix} u_{31} \\ u_{32} \\ u_{41} \\ u_{52} \\ \cdot \\ \cdot \\ \cdot \\ \cdot \\ \cdot \\ u_{382} \end{Bmatrix}^{(s)}_{N} \tag{3.6}$$

This equation may be interpreted as a variable transformation, which in compact notation may be written as

$$\{\delta\}_O = [T] \{\delta\}_N$$

where $\{\delta\}_O$ is the original displacement vector and $\{\delta\}_N$ is the transformed displacement vector.

3.8 Elimination of the Rigid Body Mode for the Asymmetric Mode Case

For the asymmetric modes a rigid body rotation can occur about a diametrical nodal line as shown in Fig. 3.8. Assuming a rotation of magnitude γ the displacements of gridpoint j are given by:

$$\begin{aligned} u_{jY} &= -y_j (1 - \cos\gamma) - \bar{z}_j \sin\gamma \\ u_{jz} &= -\bar{z}_j (1 - \cos\gamma) + y_j \sin\gamma \end{aligned} \tag{3.7}$$

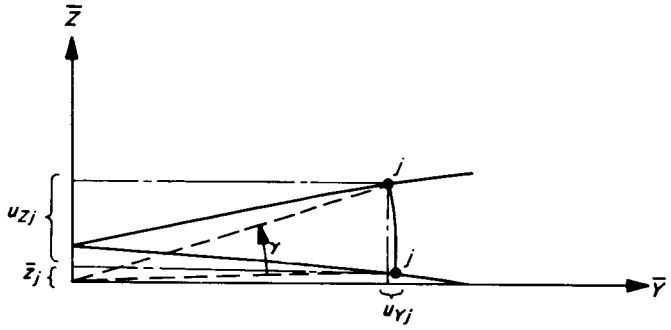

Fig. 3.8. Rigid body rotation, asymmetric modes

where y_j and $\bar{z}_j$ are the original coordinates of gridpoint j in terms of coordinates $\bar{Y}\bar{Z}$ and defined in Fig. 3.8. Making the small-angle approximation we obtain from Eq. (3.7)

$$u_{jY} = -\bar{z}_j \gamma$$

$$u_{jZ} = y_j \gamma$$

Now, using Eq. (3.5), substituting for the displacements and solving for $u_{3Z}^{(s)}$, we obtain

$$u_{3Z}^{(s)} = \frac{\bar{z}_2 m_2}{y_3 m_3} u_{2Y}^{(s)} + \frac{\bar{z}_3 m_3}{y_3 m_3} u_{3Y}^{(s)} + \frac{\bar{z}_4 m_4}{y_3 m_3} u_{4Y}^{(s)}$$

$$+ \frac{\bar{z}_5 m_5}{y_3 m_3} u_{5Y}^{(s)} + \cdots\cdots\cdots \frac{\bar{z}_N m_N}{y_3 m_3} u_{NY}^{(s)}$$

$$- \frac{y_4 m_4}{y_3 m_3} u_{4Z}^{(s)} - \frac{y_6 m_6}{y_3 m_3} u_{6Z}^{(s)} - \cdots\cdots \frac{y_N m_N}{y_3 m_3} u_{NZ}^{(s)}$$

Imposing the notation that a displacement in the Y direction have subscript 2 and a displacement in the Z direction have subscript 3, we can write the variable transformation equation as follows:

$$\begin{Bmatrix} u_{22} \\ u_{32} \\ u_{33} \\ u_{42} \\ u_{43} \\ \cdot \\ \cdot \\ \cdot \\ \cdot \\ u_{382} \end{Bmatrix}_O^{(s)} = \begin{bmatrix} 1.0 & 0 & 0 & 0 & 0 \cdots \\ 0 & 1.0 & 0 & 0 & 0 \cdots \\ \frac{\bar{z}_2 m_2}{y_3 m_3} & \frac{\bar{z}_3 m_3}{y_3 m_3} & \frac{\bar{z}_4 m_4}{y_3 m_3} & \frac{y_4 m_4}{y_3 m_3} & \cdots\cdots \\ 0 & 0 & 1.0 & 0 & \\ 0 & 0 & 0 & 1.0 & \cdots\cdots \\ & & & \ddots & \\ & & & & 1.0 \end{bmatrix} \begin{Bmatrix} u_{22} \\ u_{32} \\ u_{42} \\ u_{43} \\ \cdot \\ \cdot \\ \cdot \\ \cdot \\ u_{383} \end{Bmatrix}_N^{(s)} \quad (3.8)$$

It should be noted that if additional rigid body modes were present in the system, a more complicated transformation would have to be defined and applied. The worst case would occur if all six rigid body modes had to be swept from the system. This was unnecessary in the present problem because, through the application of the symmetry boundary conditions, the remaining two rotational modes and the three translational modes were eliminated.

3.9 Method of Dynamic Analysis

Just as in the stress problem, the manipulations required in the SAMIS to solve for the mode shapes and frequencies of the free shallow shell are controlled by a set of pseudo instructions. For the dynamic analysis, the pseudo program will be used twice, once to obtain the symmetric modes, and a second time for the asymmetric modes. The set of pseudo instructions used in this problem is listed in Table 3-4. These instructions demonstrate the use of comment cards, which appear in the listing for user purposes, but are not interpreted during problem solution. The comment cards are identified by the letter C in the first column. The mathematical manipulations the numbered instructions describe are explained in the individual synopses of the instructions that follow.

Instructions 1.0 through 3.0 direct the formation of the structure mass and stiffness matrices.

1.0 BILD:
1.5 CONT: Generate the element stiffness matrices (KER001 through KER054) and the element mass matrices (MER001 through MER054) for the 54 elements of the shell idealization. The stiffness matrices are stored in sequence on tape 9, locations 001 through 054. Similarly the mass matrices are stored on tape 10. The units digit of the number in the E field specifies the type of mass matrix that is to be generated (see BILD description in Ref. 1 for details of this option). The continue instruction (CONT) must be used when element mass matrices are generated.

2.0 ADDS
3.0 ADDS Add the element mass and stiffness matrices to form the complete structure matrices. These are:

a. MAR001: the structure mass matrix which is stored on tape 11, location 1.

Table 3-4. Listing of the pseudo instructions for the calculation of the mode shapes and frequencies of the unsupported shell

Pseudo instruction No.	Field A		Field B		Field D	Field C		Field E
	Tape No.	Matrix name	Tape No.	Matrix name	Pseudo instruction name	Tape No.	Matrix name	Control No.
C								
C Shallow shell problem, low frequency flexural modes of free shell.								
C								
C Formation of the structure mass and stiffness matrices.								
C								
1.0	09001	KER001			BILD			5402
1.5	10001	MER001			CONT			
2.0	10001	MER001			ADDS	11001	MAR001	5400
3.0	9001	KER001			ADDS	11002	KAR001	5400
C								
C Imposition of symmetry and boundary conditions.								
C								
4.0	9001	VTR001			READ			
5.0	9001	VTR001			COLS	9002	VTC001	
6.0	9002	VTC001			FLIP	9003	VFR001	
7.0	11002	KAR001	9002	VTC001	MULT	10001	KVC001	
8.0	09003	VFR001	10001	KVC001	MULT	10002	KTC001	
9.0	10002	KTC001			ROWS	11003	KTR001	
10.0	11001	MAR001	9002	VTC001	MULT	10001	MVC001	
11.0	9003	VFR001	10001	MVC001	MULT	10002	MTC001	
C								
C Decomposition of the mass matrix.								
C								
12.0	10002	MTC001			ROWS	11004	MTR001	
13.0	11004	MTR001	9002	MRR001	CHIN	11005	MIR001	
14.0	9002	MRR001			FLIP	10001	MFC001	
C								
C Formation of the dynamic matrix.								
C								
15.0	11003	KTR001	10001	MFC001	CHOL	10002	KBC001	
16.0	9002	MRR001	10002	KBC001	MULT	11006	DYC001	
17.0	11006	DYC001			DECO	10001	DYD001	
C								
C Determination of eigenvalues and eigenvectors.								
C								
18.0	10001	DYD001	10002	EVD001	ROOT	10003	EID001	-100
19.0	10002	EVD001			CODE	9002	EVC001	
C								
C Inverse Transformation of the eigenvectors.								
C								
20.0	11005	MIR001	9002	EVC001	MULT	11007	ETC001	
21.0	11007	ETC001			COLS	10004	ETC001	
22.0	9001	VTR001	10004	ETC001	MULT	11007	ETC001	

Table 3-4 (cont'd)

Pseudo instruction No.	Field A		Field B		Field D	Field C		Field E
	Tape No.	Matrix name	Tape No.	Matrix name	Pseudo instruction name	Tape No.	Matrix name	Control No.
C C Printout of results. C								
23.0	10003	EID001			INKS			1
24.0	11007	ETC001			INKS			1
25.0					HALT			
4.0	10001	WAR001			READ			
5.0	10001	WAR001	11002	KAR001	WASH	11003	KTR001	
11.0	10001	WAR001	11001	MAR001	WASH	10002	MTC001	

b. KAR001: the structure stiffness matrix which is stored on tape 11, location 2.

Instructions 4.0 through 11.0 direct imposition of symmetry and boundary conditions.

4.0 READ: Transfer the variable transformation matrix VTR001 from the data input tape to tape 9, location 001.

5.0 COLS: Column-list the variable transformation matrix and store the resultant matrix VTC001 on tape 9, location 002.

6.0 FLIP: Transpose VTC001; title the resultant matrix VFR001 and store it on tape 9, location 003.

7.0 MULT
8.0 MULT
9.0 ROWS
10.0 MULT
11.0 MULT

Transform the stiffness matrix KAR001 and the mass matrix MAR001 by a pre- and post-multiplication consistent with the following mathematical treatment of the problem:

After combining the stiffness and mass matrices the dynamic equation is of the form

$$\lambda^2 [M]\{\delta\} = [K]\{\delta\}$$

where, as yet, the system is unconstrained. The variable transformation matrix contains the transformation to eliminate the rigid body modes, Eq. (3.6) or (3.8), depending upon the problem being run, and the zero diagonal elements to impose zero displacement conditions, Table 3-2 or 3-3. The transformation is defined by:

$$\{\delta\} = [V]\{\delta^*\}$$

where $\{\delta^*\}$ is the vector of nonzero displacement variables. Imposing this transformation on the dynamic equation leads to

$$\lambda^2 [M][V]\{\delta^*\} = [K][V]\{\delta^*\}$$

Premultiplying by $[V]^T$:

$$\lambda^2 [V]^T [M] [V] \{\delta^*\} = [V]^T [K] [V] \{\delta^*\}$$

or

$$\lambda^2 [M^*] \{\delta^*\} = [K^*] \{\delta^*\}$$

where

$$[K^*] \equiv [KTR001]$$

$$[M^*] \equiv [MTR001]$$

Instructions 12.0 through 14.0 involve decomposition of the mass matrix, which is required to maintain matrix symmetry.

12.0 ROWS: Row-list the mass matrix and store the output matrix MTR001 on tape 11, location 004.

13.0 CHIN: Triangular decompose the mass matrix MTR001 using the Choleski Decomposition technique. The upper triangular decomposition matrix is MRR001 and is stored on tape 9, location 002. The inverse of MRR001 is designated MIR001 and is stored on tape 11, location 005.

14.0 FLIP: Transpose the matrix MRR001, and designate the resultant matrix MFC001 and store it on tape 10, location 001.

Instructions 15.0 through 17.0 direct formulation of the dynamic matrix. By instructions 18.0 and 19.0 the eigenvalues and eigenvectors are determined.

15.0 CHOL
16.0 MULT } Perform a matrix inversion and triple product consistent with the following mathematical requirements.

Starting with

$$\lambda^2 [U]^T [U] \{\delta^*\} = [K^*] \{\delta^*\}$$

where

$$[U]^T [U] = [M^*] \quad \text{(From CHIN)}$$

Define

$$\{\bar{\delta}\} = [U]\{\delta^*\}$$

then

$$\{\delta^*\} = [U]^{-1}\{\bar{\delta}\}$$

Substitute into the matrix equation to obtain

$$\lambda^2 [U]^T \{\bar{\delta}\} = [K^*] [U]^{-1} \bar{\delta}$$

Premultiply by $[U] [K^*]^{-1}$:

$$\lambda^2 [U] [K^*]^{-1} [U]^T \{\bar{\delta}\} = [I]\{\bar{\delta}\}$$

Instruction 15.0 determines $[K^*]^{-1} [U]^T$, and instruction 16.0 determines $[U] [K^*]^{-1} [U]^T$. The necessity for decomposing the mass matrix (or stiffness matrix) is to obtain a symmetric dynamic matrix. If the stiffness matrix were simply inverted to obtain $[K^*]^{-1} [M]$, the resultant matrix would not be symmetric as required by ROOT.

17.0 DECO: Decode the matrix DYC001. Title the decoded matrix DYD001 and store it on tape 10, location 001.

18.0 ROOT: Calculate the eigenvectors EVD001 (stored on tape 10, location 002) and the eigenvalues EID001 (stored on tape 10, location 003). The -100 in the E field instructs the printout of all eigenvalues directly from ROOT. This provides the

interpretation of the eigenvalues as frequency (see the ROOT description in Ref. 2 for details of this option).

19.0 CODE: Recode the eigenvectors as EVC001 and store them on tape 9, location 002.

Instructions 20.0 through 22.0 perform the inverse transformation of the eigenvectors. Instructions 23.0 and 24.0 direct printout of the results.

20.0 MULT: Transform the eigenvectors to obtain $\{\delta^*\}$ as per the relation already cited:

$$\{\delta^*\} = [U]^{-1}\{\bar{\delta}\}$$

where the $\{\bar{\delta}\}$ correspond to the set EVC001.

21.0 COLS: Transfer matrix ETC001 from tape 11, location 007 to tape 10, location 004. In this pseudo instruction program the data on tape 11 are saved for possible program recovery.

22.0 MULT: Perform the transformation from $\{\delta^*\}$ to $\{\delta\}$ as per the relation

$$\{\delta\} = [V]\{\delta^*\}$$

The $\{\delta\}$ are the eigenvectors of the shell referenced to the overall coordinate system X, Y, Z.

23.0 INKS
24.0 INKS } The eigenvalues EID001 (stored on tape 10, location 003) and the eigenvectors ETC001 (stored on tape 11, location 007) are transferred to the data printout tape with appropriate single-line titles.

25.0 HALT: HALT operation on this problem.

It should be noted that, in this set of pseudo instructions, if tape 11 is saved the program has built-in recovery at various instructions such as 4, 13, and 17.

In many problems it is not required to eliminate rigid body modes because the structure is adequately supported. For these problems only a WASH operation is needed. The

pseudo instruction modifications required by this option are listed at the bottom of Table 3-4. These instructions replace instructions 4 through 11 when only a WASH operation is used. If desired, a further reduction is to omit the WASH instructions and define boundary conditions by the continuity numbers in the element data. However, with this option the structural matrices must be regenerated if the boundary conditions are changed.

3.10 Description of Input Data

In the present example, the pseudo instruction program is headed by a generation phase (BILD); thus the order of listing of input data is the same as in the stress problem (Section 2.0).

Regarding each type of input, the following comments apply:

a. Pseudo instructions: The listing is given in Table 3-4.
b. Material table: Same as that used in the statics problem.
c. Zero card: Required after material table in all programs.
d. Element data: The format of the element data for the dynamics problem is defined in Ref. 1, Tables 7-4 and 7-6. In general, less data must be supplied for the dynamics problem than for the stress problem. The two cards of element input data for element 1 (Fig. 3.5) having gridpoints 1, 2, 3 are given in Fig. 3.9.

The matrix data and title cards have the same format as outlined in Section 2.0. A complete listing of the input data for the dynamics problem is given in Appendix E.

3.11 Interpretation of Output Data

In the present example, output from the program is obtained from three instructions of the pseudo instruction program. In instruction 18.0, the -100 flags printout of all eigenvalues. By instructions 23.0 and 24.0 the eigenvalues EID001 are again printed out as well as the eigenvectors ETC001 (with appropriate title cards).

In this problem the initial dimension of the program-generated mass matrix MAR001 is 114 (three times number of gridpoints). However, by the coordinate

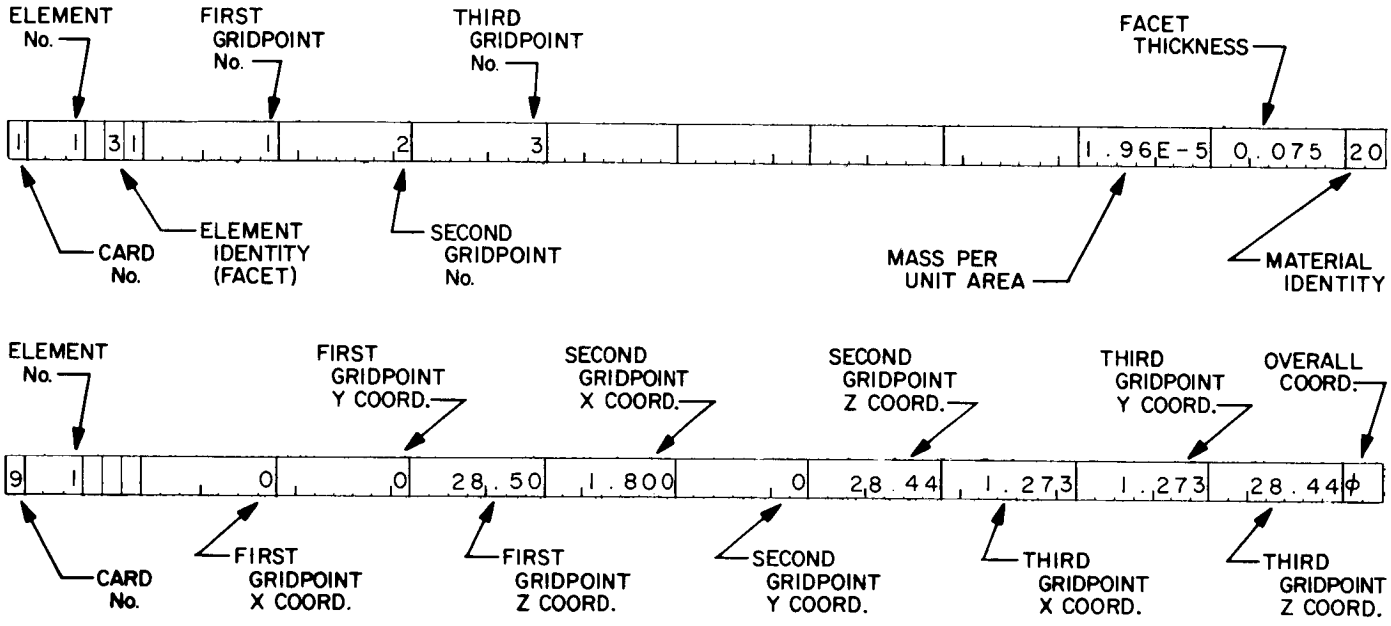

Fig. 3.9. Element data for Element 1 of shell dynamics problem

transformation of the mass matrix the order is reduced to 86 for the symmetric modes and to 92 for the asymmetric modes.

The output from instruction 18.0 is shown in Table 3-5 for the symmetric mode case. Only 50 of the 86 eigenvalues are shown, although the entire 86 were listed by the instruction. In most problems the natural frequencies will appear in one or the other of the two columns on the right. If the stiffness matrix is inverted, the frequencies appear in the last column, starting with the lowest value. If the mass matrix is inverted, the frequencies appear in the next to last column starting with the largest value. The remaining three columns are provided in the event a problem is solved in which the eigenvalues have a different interpretation from that given above.

The printout by instruction 23.0, which is shown in Table 3-6, is the complete set of eigenvalues, which are identical to those in the column of eigenvalues in Table 3-5. For ordinary structural problems this printout is not as useful as the direct printout from ROOT because the actual natural frequencies must still be computed. However, it should be noted from this printout that the eigenvalue matrix is a diagonal square matrix suitable for scaling purposes in specialized problems.

A sample listing of the eigenvectors is given in Table 3-7. In this listing, column 10 corresponds to eigenvalue 01, column 20 to eigenvalue 02, etc. The row numbers define the gridpoint number and direction at which the deflection occurs. For example, the row code 352 defines the displacement as that at gridpoint 35 in the overall Y direction (component 2). For the first flexural mode this displacement has a relative value of 9.219.

It should be noted that the eigenvectors generated by ROOT are normalized to unit length. However, in the process of transformation by the inverse of the decomposed mass matrix to express displacements in their original form, the vector length is changed. This change in length, however, assures that the generalized mass matrix is a unit diagonal matrix.

3.12 Summary and Discussion of Results

Several of the flexural natural modes and frequencies of the shallow spherical shell were obtained by three different methods. Theoretical values were computed

Table 3.5 Printout of eigenvalues for the symmetric modes by the printout option of ROOT

EIGENVALUES OF MATRIX DYD 1

ROOT NO.	EIGENVALUE	SQUARE ROOT	RECIPROCAL	SQ.RT./2PI	RECIP/2PI
1	0.2176E-04	0.4665E-02	0.2144E 03	0.7424E-03	0.3412E 02
2	0.8187E-06	0.9048E-03	0.1105E 04	0.1440E-03	0.1759E 03
3	0.1719E-06	0.4146E-03	0.2412E 04	0.6599E-04	0.3839E 03
4	0.7999E-07	0.2828E-03	0.3536E 04	0.4501E-04	0.5627E 03
5	0.1946E-07	0.1395E-03	0.7168E 04	0.2220E-04	0.1141E 04
6	0.1627E-07	0.1276E-03	0.7839E 04	0.2030E-04	0.1248E 04
7	0.1611E-07	0.1269E-03	0.7879E 04	0.2020E-04	0.1254E 04
8	0.1370E-07	0.1170E-03	0.8544E 04	0.1863E-04	0.1360E 04
9	0.1014E-07	0.1007E-03	0.9931E 04	0.1603E-04	0.1581E 04
10	0.6350E-08	0.7969E-04	0.1255E 05	0.1268E-04	0.1997E 04
11	0.5185E-08	0.7201E-04	0.1389E 05	0.1146E-04	0.2210E 04
12	0.4455E-08	0.6675E-04	0.1498E 05	0.1062E-04	0.2385E 04
13	0.2149E-08	0.4635E-04	0.2157E 05	0.7377E-05	0.3433E 04
14	0.1594E-08	0.3993E-04	0.2504E 05	0.6355E-05	0.3986E 04
15	0.1352E-08	0.3678E-04	0.2719E 05	0.5853E-05	0.4328E 04
16	0.1338E-08	0.3658E-04	0.2734E 05	0.5822E-05	0.4351E 04
17	0.1305E-08	0.3613E-04	0.2768E 05	0.5750E-05	0.4405E 04
18	0.1144E-08	0.3382E-04	0.2957E 05	0.5383E-05	0.4706E 04
19	0.6551E-09	0.2560E-04	0.3907E 05	0.4074E-05	0.6218E 04
20	0.5315E-09	0.2305E-04	0.4338E 05	0.3669E-05	0.6904E 04
21	0.4241E-09	0.2059E-04	0.4856E 05	0.3277E-05	0.7729E 04
22	0.3341E-09	0.1828E-04	0.5471E 05	0.2909E-05	0.8708E 04
23	0.3086E-09	0.1757E-04	0.5693E 05	0.2796E-05	0.9060E 04
24	0.2990E-09	0.1729E-04	0.5784E 05	0.2752E-05	0.9205E 04
25	0.2416E-09	0.1554E-04	0.6433E 05	0.2474E-05	0.1024E 05
26	0.1648E-09	0.1284E-04	0.7790E 05	0.2043E-05	0.1240E 05
27	0.1631E-09	0.1277E-04	0.7830E 05	0.2033E-05	0.1246E 05
28	0.1559E-09	0.1249E-04	0.8008E 05	0.1987E-05	0.1275E 05
29	0.1458E-09	0.1207E-04	0.8282E 05	0.1922E-05	0.1318E 05
30	0.1365E-09	0.1168E-04	0.8559E 05	0.1860E-05	0.1362E 05
31	0.1265E-09	0.1125E-04	0.8891E 05	0.1790E-05	0.1415E 05
32	0.1068E-09	0.1033E-04	0.9677E 05	0.1645E-05	0.1540E 05
33	0.1042E-09	0.1021E-04	0.9798E 05	0.1624E-05	0.1559E 05
34	0.9991E-10	0.9996E-05	0.1000E 06	0.1591E-05	0.1592E 05
35	0.8768E-10	0.9364E-05	0.1068E 06	0.1490E-05	0.1700E 05
36	0.8403E-10	0.9167E-05	0.1091E 06	0.1459E-05	0.1736E 05
37	0.7833E-10	0.8851E-05	0.1130E 06	0.1409E-05	0.1798E 05
38	0.7292E-10	0.8539E-05	0.1171E 06	0.1359E-05	0.1864E 05
39	0.7091E-10	0.8421E-05	0.1188E 06	0.1340E-05	0.1890E 05
40	0.6899E-10	0.8306E-05	0.1204E 06	0.1322E-05	0.1916E 05
41	0.6134E-10	0.7832E-05	0.1277E 06	0.1246E-05	0.2032E 05
42	0.5813E-10	0.7624E-05	0.1312E 06	0.1213E-05	0.2088E 05
43	0.5680E-10	0.7536E-05	0.1327E 06	0.1199E-05	0.2112E 05
44	0.5382E-10	0.7336E-05	0.1363E 06	0.1168E-05	0.2169E 05
45	0.5234E-10	0.7235E-05	0.1382E 06	0.1151E-05	0.2200E 05
46	0.5142E-10	0.7171E-05	0.1395E 06	0.1141E-05	0.2219E 05
47	0.4866E-10	0.6976E-05	0.1434E 06	0.1110E-05	0.2282E 05
48	0.4847E-10	0.6962E-05	0.1436E 06	0.1108E-05	0.2286E 05
49	0.4528E-10	0.6729E-05	0.1486E 06	0.1071E-05	0.2365E 05
50	0.4276E-10	0.6539E-05	0.1529E 06	0.1041E-05	0.2434E 05

Table 3-6. Printout of eigenvalues for the symmetric modes by the INKS option

EID 1 EIGENVALUES-SYMMETRIC MODES PAGE 1

ROW	COL	ELEMENT	ROW	COL	ELEMENT	ROW	COL	ELEMENT	ROW	COL	ELEMENT
01	01	0.2176E-04	02	02	0.8187E-06	03	03	0.1719E-06	04	04	0.7999E-07
05	05	0.1946E-07	06	06	0.1627E-07	07	07	0.1611E-07	08	08	0.1370E-07
09	09	0.1014E-07	10	10	0.6350E-08	11	11	0.5185E-08	12	12	0.4455E-08
13	13	0.2149E-08	14	14	0.1594E-08	15	15	0.1352E-08	16	16	0.1338E-08
17	17	0.1305E-08	18	18	0.1144E-08	19	19	0.6551E-09	20	20	0.5315E-09
21	21	0.4241E-09	22	22	0.3341E-09	23	23	0.3086E-09	24	24	0.2990E-09
25	25	0.2416E-09	26	26	0.1648E-09	27	27	0.1631E-09	28	28	0.1559E-09
29	29	0.1458E-09	30	30	0.1365E-09	31	31	0.1265E-09	32	32	0.1068E-09
33	33	0.1042E-09	34	34	0.9991E-10	35	35	0.8768E-10	36	36	0.8403E-10
37	37	0.7833E-10	38	38	0.7292E-10	39	39	0.7091E-10	40	40	0.6899E-10
41	41	0.6134E-10	42	42	0.5813E-10	43	43	0.5680E-10	44	44	0.5382E-10
45	45	0.5234E-10	46	46	0.5142E-10	47	47	0.4866E-10	48	48	0.4847E-10
49	49	0.4528E-10	50	50	0.4276E-10	51	51	0.4004E-10	52	52	0.3921E-10
53	53	0.3879E-10	54	54	0.3592E-10	55	55	0.3489E-10	56	56	0.3061E-10
57	57	0.2953E-10	58	58	0.2856E-10	59	59	0.2580E-10	60	60	0.2514E-10
61	61	0.2509E-10	62	62	0.2389E-10	63	63	0.2270E-10	64	64	0.2192E-10
65	65	0.2160E-10	66	66	0.2158E-10	67	67	0.1997E-10	68	68	0.1979E-10
69	69	0.1912E-10	70	70	0.1864E-10	71	71	0.1836E-10	72	72	0.1763E-10
73	73	0.1712E-10	74	74	0.1650E-10	75	75	0.1593E-10	76	76	0.1531E-10
77	77	0.1426E-10	78	78	0.1411E-10	79	79	0.1394E-10	80	80	0.1387E-10
81	81	0.1357E-10	82	82	0.1050E-10	83	83	0.1047E-10	84	84	0.9511E-11
85	85	0.5620E-11	86	86	0.5620E-11						

THIS COMPLETES PRINTOUT OF MATRIX 10003 EID 1.

Table 3-7. Printout of the eigenvectors for the symmetric modes

ETC 1 EIGENVECTORS-SYMMETRIC MODES PAGE 1

ROW	COL	ELEMENT	ROW	COL	ELEMENT	ROW	COL	ELEMENT	ROW	COL	ELEMENT
22	01	0.2355E-01	31	01	0.3661E-01	32	01	0.3664E-01	33	01	0.1542E 01
41	01	0.2351E-01	52	01	0.2200E-00	61	01	0.2414E-00	62	01	0.2683E-00
63	01	0.4160E 01	71	01	0.3255E-00	72	01	0.3256E-00	73	01	0.5881E 01
81	01	0.2682E-00	82	01	0.2415E-00	83	01	0.4160E 01	91	01	0.2199E-00
102	01	0.7469E 00	111	01	0.4523E-00	112	01	0.7919E 00	113	01	0.5011E 01
121	01	0.1041E 01	122	01	0.1038E 01	123	01	0.1210E 02	131	01	0.1038E 01
132	01	0.1042E 01	133	01	0.1210E 02	141	01	0.7918E 00	142	01	0.4523E-00
143	01	0.5011E 01	151	01	0.7467E 00	162	01	0.1812E 01	171	01	0.1948E 01
172	01	0.2194E 01	173	01	0.1634E 02	181	01	0.2641E 01	182	01	0.2641E 01
183	01	0.2312E 02	191	01	0.2193E 01	192	01	0.1948E 01	193	01	0.1634E 02
201	01	0.1811E 01	212	01	0.3735E 01	221	01	0.2174E 01	222	01	0.3951E 01
223	01	0.1406E 02	231	01	0.3948E 01	232	01	0.4495E 01	233	01	0.2599E 02
241	01	0.5040E 01	242	01	0.5088E 01	243	01	0.3397E 02	251	01	0.5374E 01
252	01	0.5374E 01	253	01	0.3679E 02	261	01	0.5088E 01	262	01	0.5041E 01
263	01	0.3397E 02	271	01	0.4494E 01	272	01	0.3948E 01	273	01	0.2599E 02
281	01	0.3950E 01	282	01	0.2174E 01	283	01	0.1406E 02	291	01	0.3735E 01
302	01	0.6929E 01	311	01	0.3968E 01	312	01	0.7311E 01	313	01	0.2082E 02
321	01	0.7220E 01	322	01	0.8296E 01	323	01	0.3849E 02	331	01	0.9222E 01
332	01	0.9353E 01	333	01	0.5032E 02	341	01	0.9858E 01	342	01	0.9858E 01
343	01	0.5448E 02	351	01	0.9353E 01	352	01	0.9223E 01	353	01	0.5032E 02
361	01	0.8296E 01	362	01	0.7221E 01	363	01	0.3849E 02	371	01	0.7310E 01
372	01	0.3969E 01	373	01	0.2082E 02	381	01	0.6929E 01	22	02	0.7016E-02
31	02	0.4470E-02	32	02	-0.4491E-02	33	02	-0.1195E-03	41	02	-0.7038E-02
52	02	-0.5122E-02	61	02	0.8425E-01	62	02	0.3687E-01	63	02	0.6014E 00
71	02	-0.2136E-02	72	02	0.2066E-02	73	02	-0.2438E-03	81	02	-0.3690E-01
82	02	-0.8427E-01	83	02	-0.6016E 00	91	02	0.5083E-02	102	02	-0.1456E-00
111	02	-0.4687E-00	112	02	-0.1924E-00	113	02	-0.3141E 01	121	02	-0.3986E-00
122	02	-0.1503E-00	123	02	-0.2724E 01	131	02	0.1502E-00	132	02	0.3986E-00
133	02	0.2724E 01	141	02	0.1924E-00	142	02	0.4687E-00	143	02	0.3141E 01

from equations derived by Johnson and Reissner as set forth in Ref. 6. Experimental values were determined from impulse response acceleration-recordings of the shallow spherical shell suspended from a single wire. Finally, values predicted by application of the finite element method were obtained by use of SAMIS as described. The natural frequencies obtained by the three methods are presented in Table 3-8.

Table 3-8. Natural frequencies of the shallow spherical shell

Mode description	Theoretical frequency, cps	Experimental frequency, cps	SAMIS computed frequency, conf. No. 1, cps	SAMIS computed frequency, conf. No. 2*, cps
First symmetric Two nodal diameters	36.0	37.2	34.1	34.8
First asymmetric Three nodal diameters	86.6	90.0	91.5	--
Second symmetric Four nodal diameters	154	150	178	167
Second asymmetric Five nodal diameters	236	240	278	--
Third symmetric Six nodal diameters	332	--	387	370
Third asymmetric Seven nodal diameters	--	--	491	--

*These results are discussed subsequently in this paragraph.

The in-plane and out-of-plane mode displacements for the first symmetric and asymmetric modes are shown in Figs. 3.10 and 3.12. The out-of-plane displacements for the second and third modes are shown in Figs. 3.11 and 3.13. Corresponding theoretical and experimental mode shapes were not determined due to the complexity of the measurements and calculations required to obtain these data.

The computed results for the shallow shell show general agreement with theory. The first symmetric and asymmetric mode frequencies agree with theoretical and experimental results well within normal engineering accuracy. However, the computed frequencies for the higher modes show greater divergence from experimental values than was expected. For these modes, the shapes possess the required symmetry, except near the apex of the shell (Fig. 3.11). For the second mode, the displacements at gridpoints 6 and 8 are opposite in polarity to displacements of the remainder of the structure. Similar behavior is observed in the third mode at gridpoint 7 (Fig. 3.11). These displacement anomalies significantly distort the mode shapes, and were suspected to be the conditions causing the large error in frequency. Study of the triangular array (Fig. 3.5) revealed that, for the second mode, element number 11 (typical) was required to represent a large change in slope (including polarity) between gridpoints 11 and 12. For the third mode, similar conditions existed for elements 13 and 22. To alleviate this condition, the structure was further subdivided, increasing the number of elements from 54 to 68 (Fig. 3.14). Solution for the symmetric modes and frequencies only was repeated. The results obtained show significant improvement in the frequency prediction (comparison of the fifth and sixth columns in Table 3-8) and correction of the modal displacements to more physically rational shapes (Fig. 3.15). For the symmetric modes, comparison of theoretical and SAMIS computed frequencies indicates -3 percent error in the first mode, +8.4 percent error in the second mode, and +11.4 percent error in the third mode. It is suspected that part of this error may be due to the particular mass lumping technique that was used. This technique was to place one-third the mass of each element at each of its nodes. This method of mass lumping as well as several others is currently under study.

The mode shapes obtained from use of both the original and the refined triangular arrays exhibit, in general, smooth variations that phase correctly over the shell surface (with the exception already noted). Nodal lines are distinctly susceptible of interpolation for all modes and have approximately the correct angular spacing.

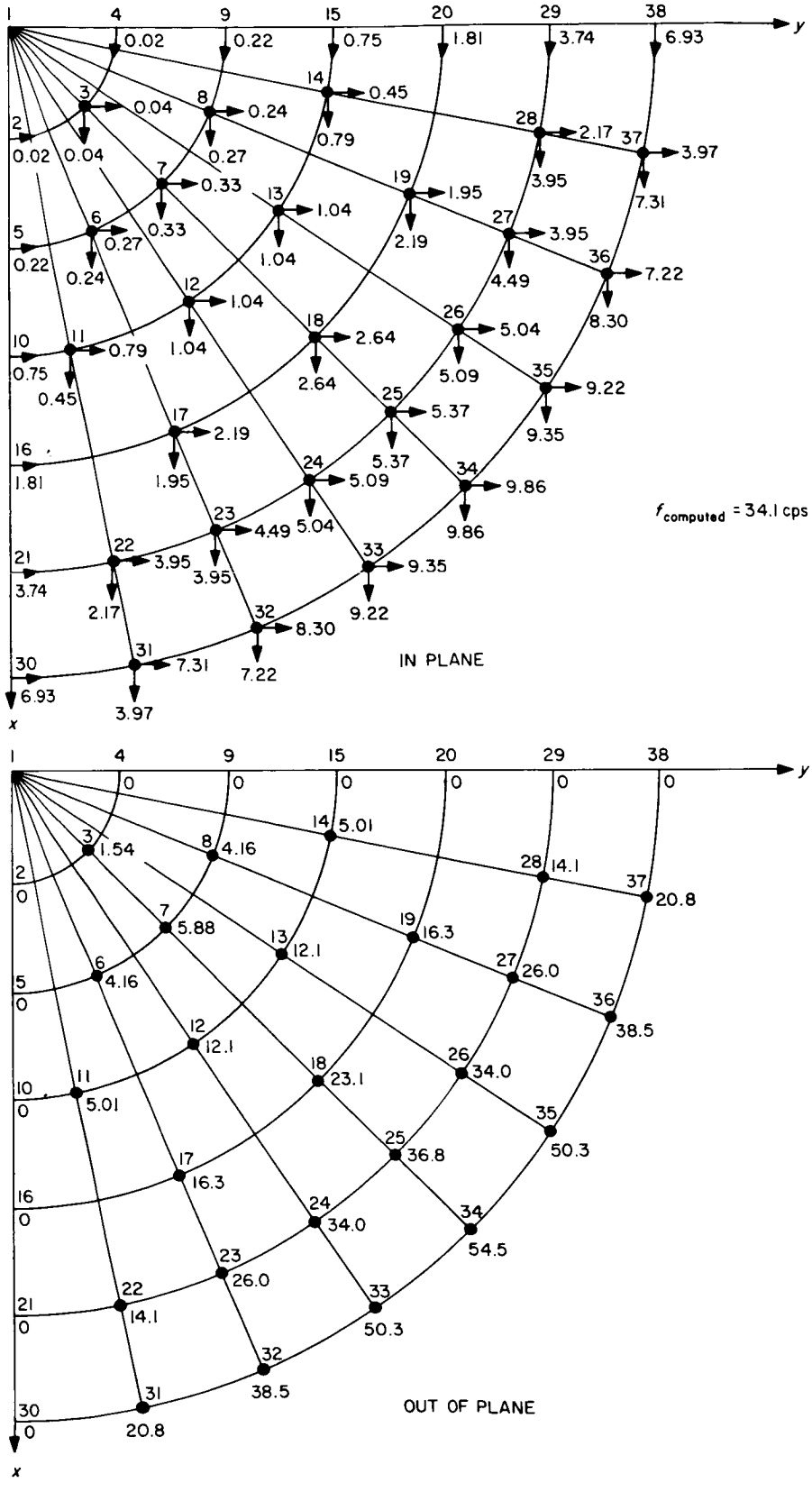

Fig. 3.10. Computed shape of the first symmetric mode

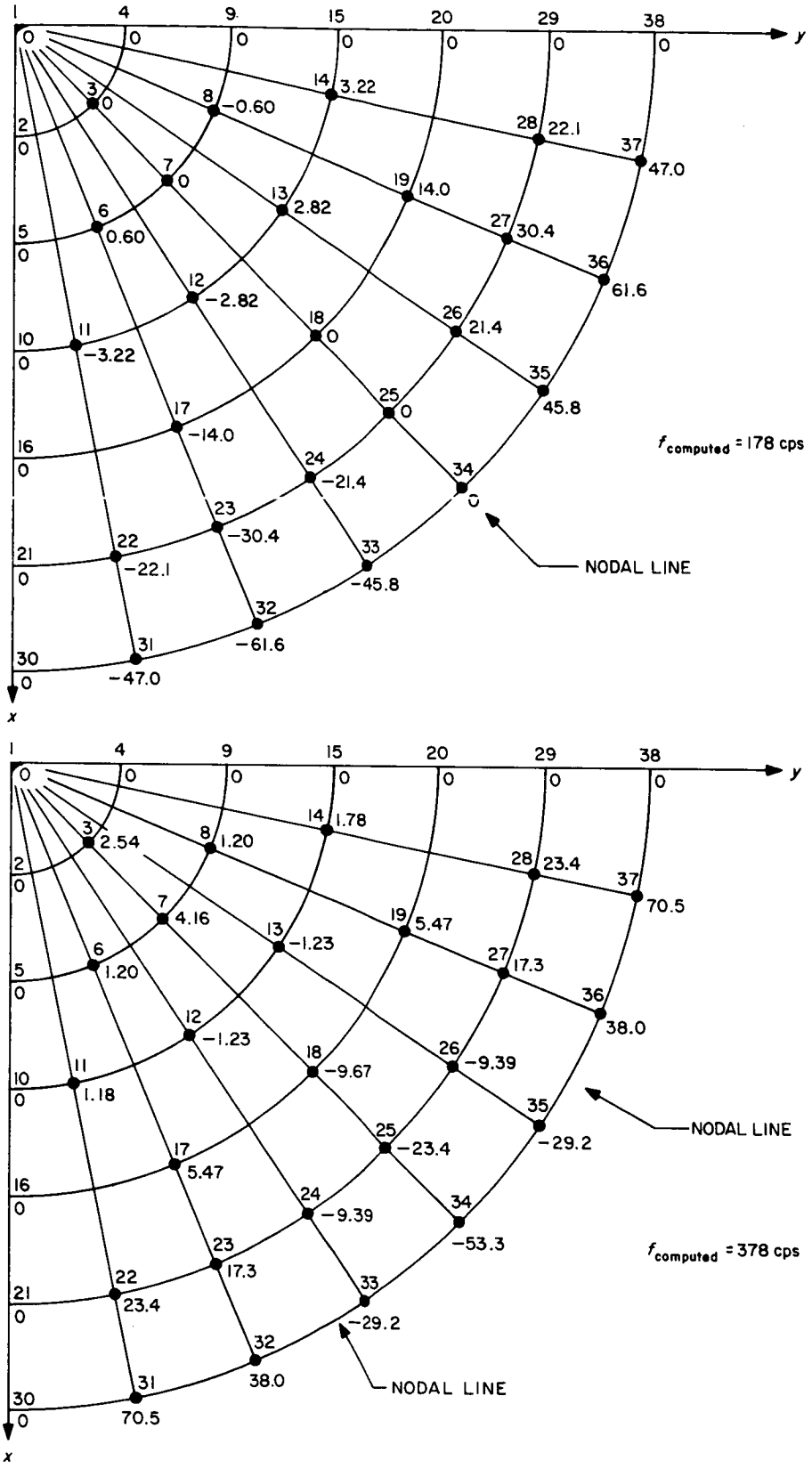

Fig. 3.11. Out-of-plane displacements of the second and third symmetric modes

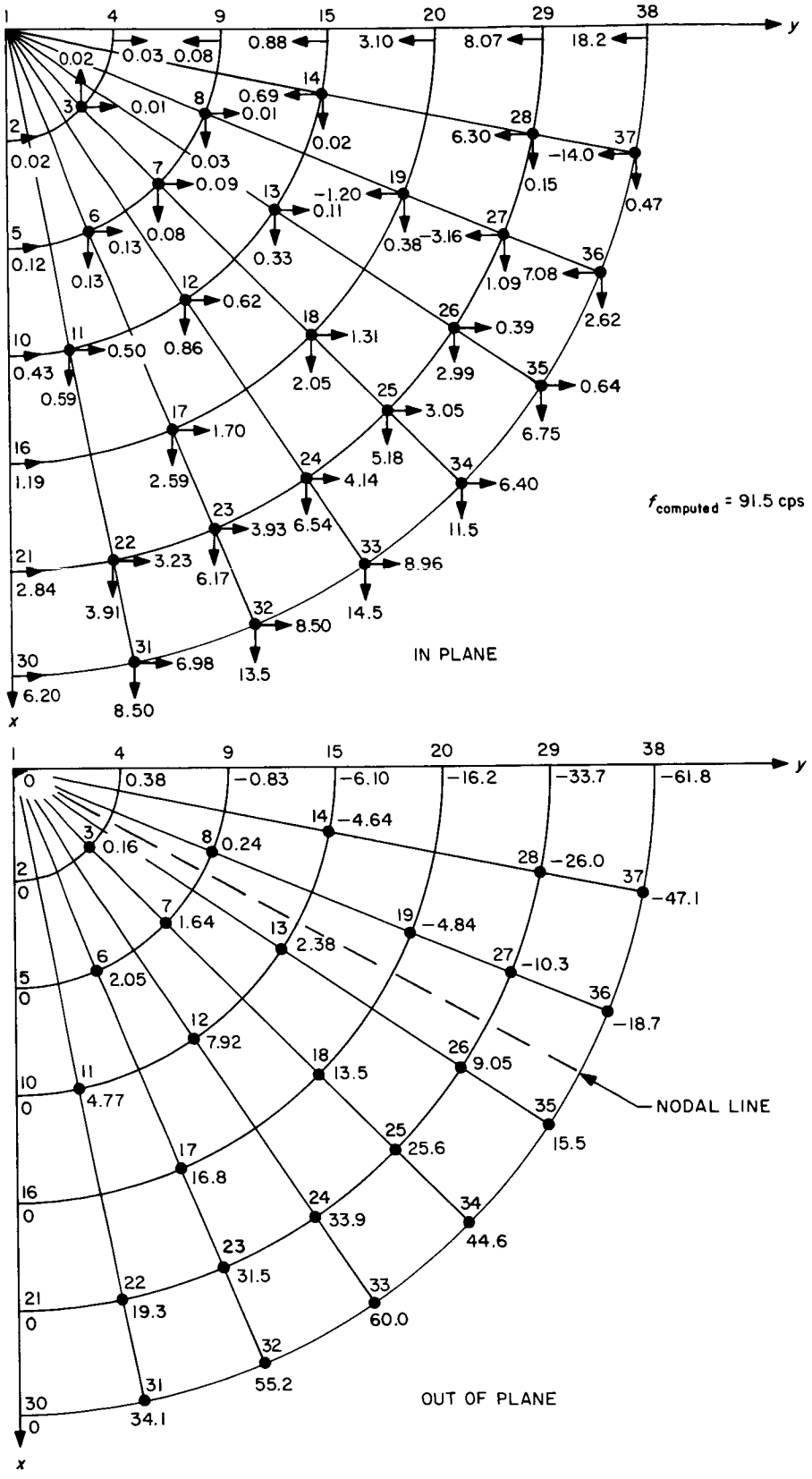

Fig. 3.12. Computed shape of first asymmetric mode

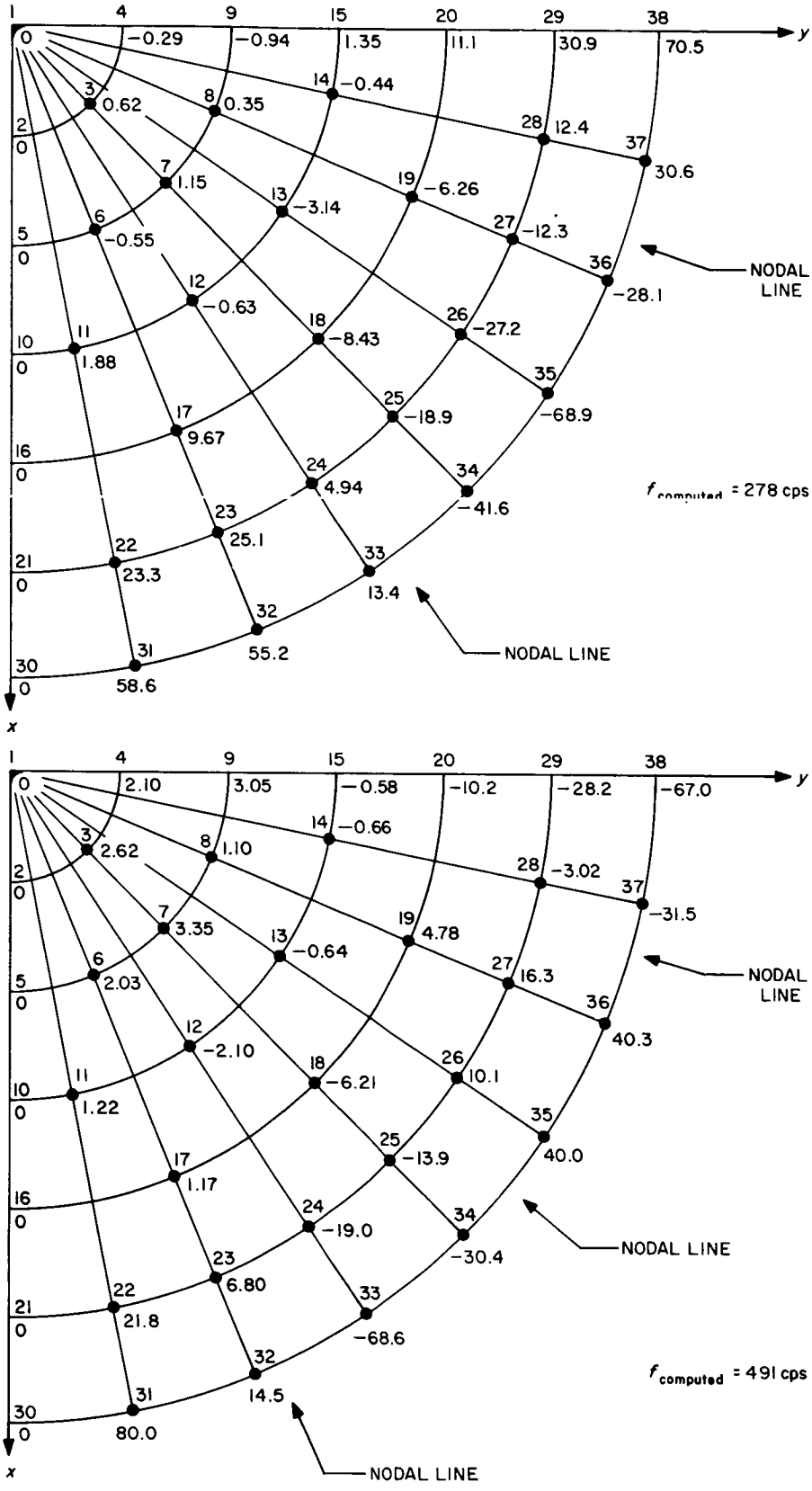

Fig. 3.13. Out-of-plane displacements of the second and third asymmetric modes

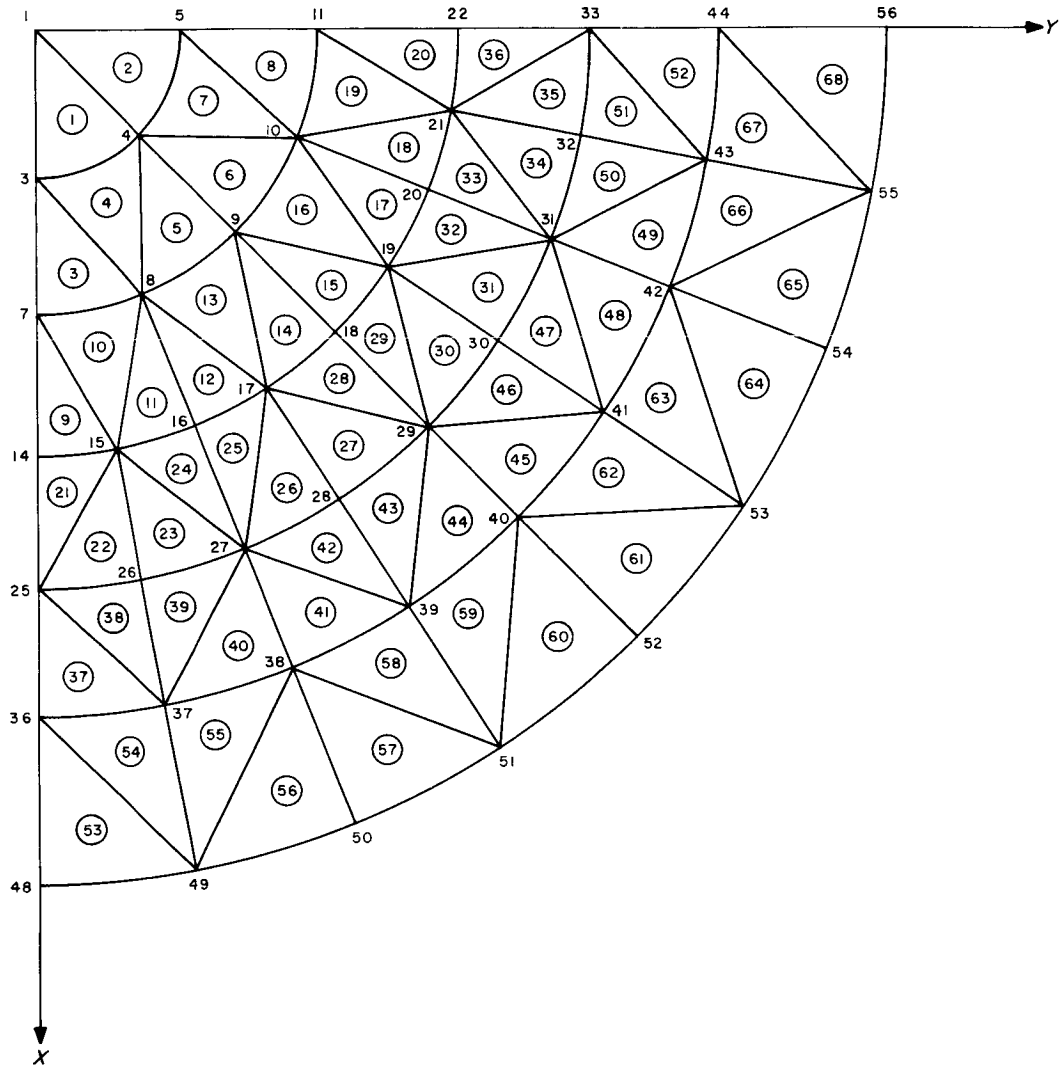

Fig. 3.14. Refined triangular element idealization of shell sector

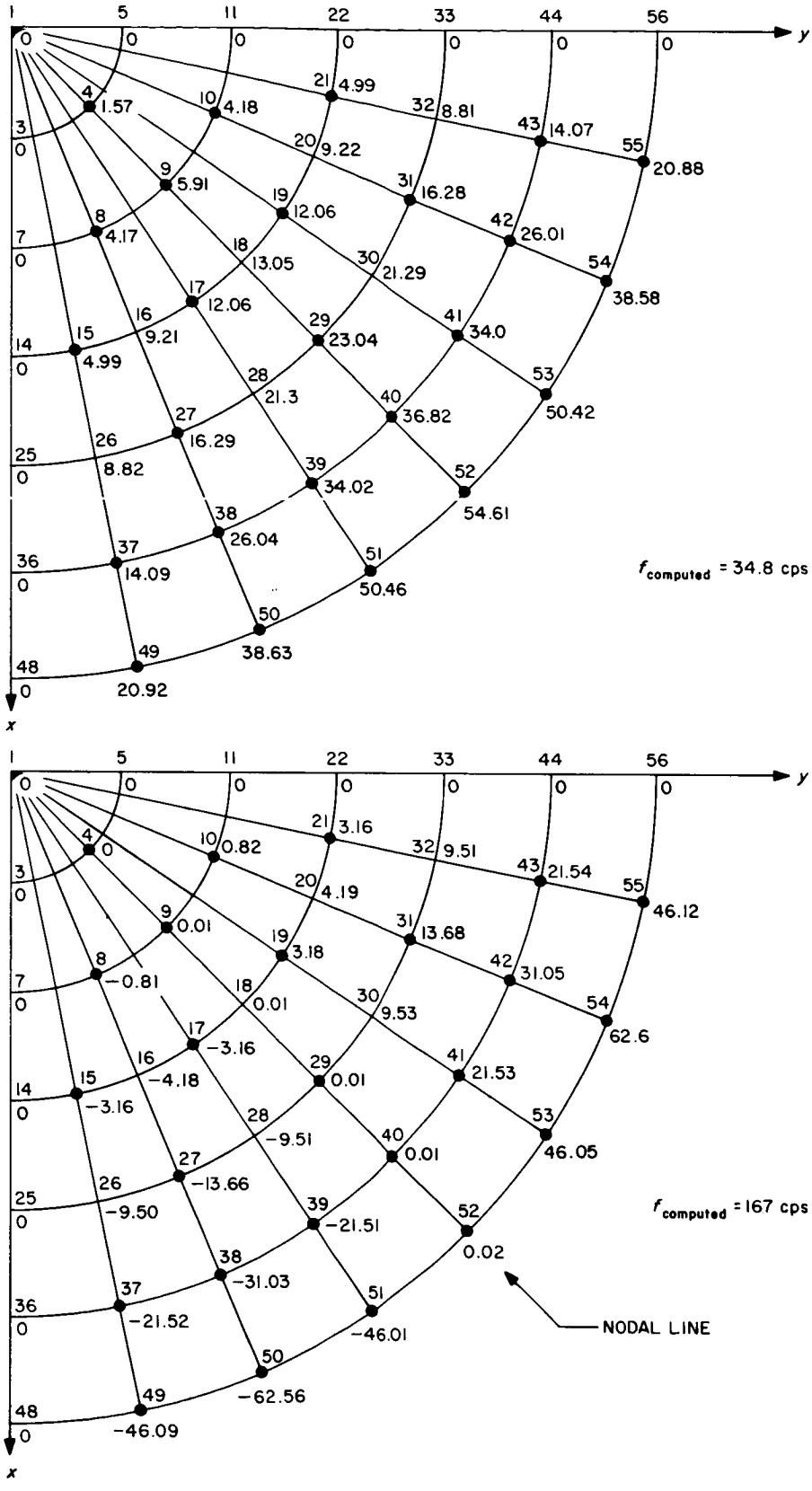

Fig. 3.15. Refined out-of-plane symmetric modes

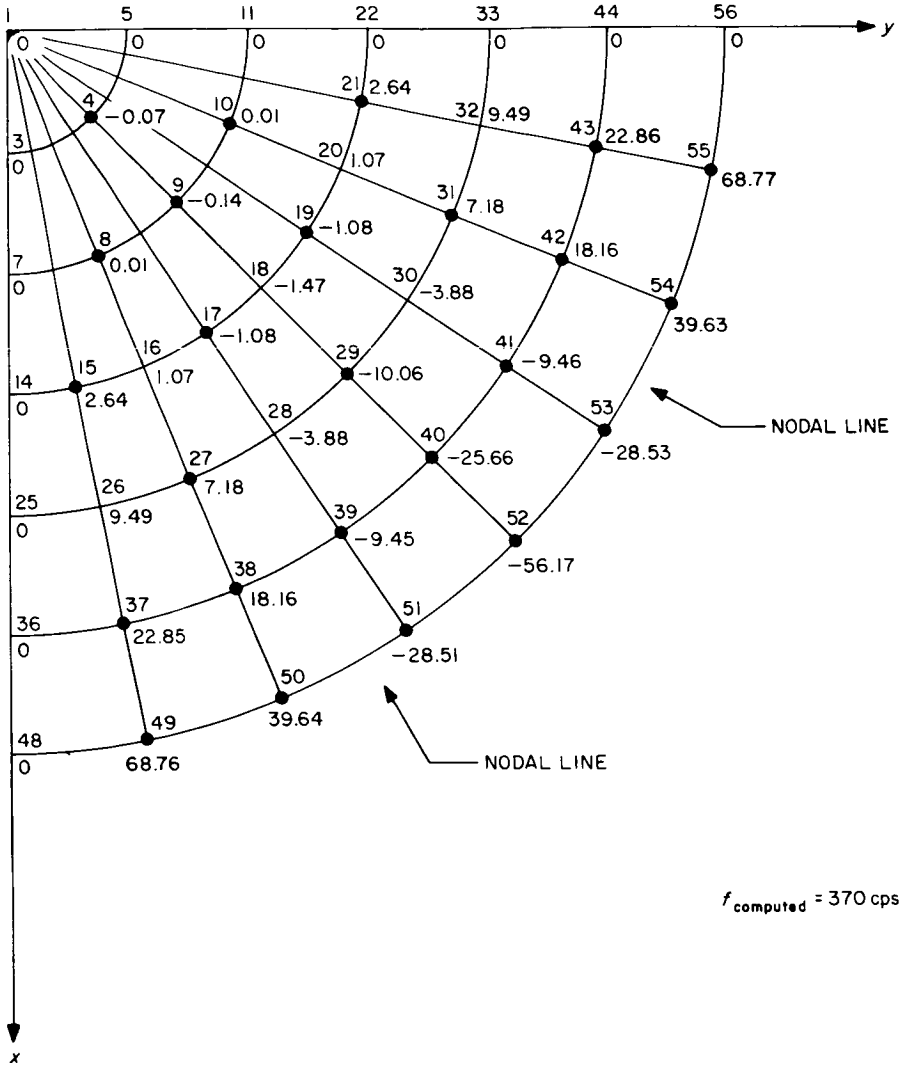

Fig. 3.15 (Cont'd)

The single-step refinement procedure of the shell dynamics problem described above typifies one approach the user may adopt in gaining confidence in problem solutions. Generally, if errors have been made in element data, or if a poor structural idealization has been made, these conditions will be reflected in peculiarities in the solutions. It has been the experience of the JPL users that input errors of this type cause variations in a solution that tend to be localized in the same region as the original error, and recognition of this has speeded correction of several problems.

In conclusion, it should be noted that in the idealization of Fig. 3.14 the gridpoint numbering is not consecutive. In general, this procedure should be followed in representation of complex structures to allow for idealization changes or for utilization of the node discontinuity capability.

3.13 Alternate Concepts of Dynamic Analysis

Mathematically, the form of the dynamic equation usually encountered in analyses with the SAMIS program is:

$$\lambda^2 \begin{bmatrix} m & 0 \\ 0 & 0 \end{bmatrix} \begin{Bmatrix} \delta_1 \\ \delta_2 \end{Bmatrix} = \begin{bmatrix} k_{11} & k_{12} \\ k_{21} & k_{22} \end{bmatrix} \begin{Bmatrix} \delta_1 \\ \delta_2 \end{Bmatrix}$$

That is, the stiffness representation of the structure is more refined than the inertial representation. One condition that leads to this inconsistency of rank is neglect of rotary inertia effects in generation of the structure mass matrix. For structures with 6 degrees of freedom per gridpoint, this condition results in a mass matrix one-half the order of the stiffness matrix.

A second condition that causes inconsistency is the capacity limitation of the eigenvector and eigenvalue computation subprogram ROOT. Since in most problems the lowest frequencies are of interest, the stiffness matrix is inverted and the final form of the dynamic matrix is (see paragraph 3.9):

$$[D] = [U][K]^{-1}[U]^T$$

where

$$[U]^T [U] = [m]$$

Thus, the size of $[D]$ is defined by the order of $[m]$, which must be less than 131 to satisfy the requirements of ROOT. Therefore, in discretizing a structure, a maximum of 130 mass coefficients may be specified on the diagonal. For planar truss and frame structures this limitation is not normally severe because of the directional motion characteristics of this type of structure. However, for three-dimensional frame and shell structures, a gridpoint may move significant amounts in several directions, each direction requiring a diagonal mass coefficient. Thus, if symmetry conditions cannot be applied and user intuition regarding the shapes of the modes is not firm, an assumed inertial representation within the 130 coefficient limitation may not be satisfactory.

Two methods are outlined below that aid in alleviating the limitation on matrix order for dynamic problems. Both methods involve transfer from local to a set of generalized coordinates.

Assume for a given problem that the stiffness matrix has been generated and constraints have been imposed consistent with specified boundary conditions. Then, assuming that more than 130 discrete mass coefficients would be required to discretize the structure adequately, an alternate approach of defining 130 or less vector locations of major inertial significance is selected. Next, a unit force is applied sequentially at each preselected vector location. For this loading the static problem is solved by inverting the stiffness matrix. That is, starting with

$$[K] \{\delta\} = \{F\}$$

where

$$\{F\} = \overset{1 \longleftrightarrow n}{\begin{Bmatrix} 1 & 0 & 0 \\ 0 & 0 & 1 \\ 0 & 0 & 0 \\ \cdot & 1 & \cdot \\ \cdot & \cdot & \cdot \end{Bmatrix}} \quad (n \leq 130)$$

the solution is:

$$\{\delta\} = [K]^{-1} \{F\}$$

where $\{\delta\}$ is a set of static deflection shapes of the constrained structure for unit applied forces. This set of shapes is interpreted as a generalized set and applied to the dynamics equation as follows:

$$\{\delta\} = [D]\{q\}$$

and

$$\lambda^2 [m] \{\delta\} = [K]\{\delta\}$$

Hence

$$\lambda^2 [D]^T [m][D]\{q\} = [D]^T [K][D]\{q\} \tag{3.9}$$

This equation may be written

$$\lambda^2 [\overline{m}]\{q\} = [\overline{K}]\{\overline{q}\}$$

The solution for the λ_i^2 and $\{q_i\}$ is effected by methods outlined in Section 3.9. The mass matrix $[m]$ in Eq. (9) is the set of coefficients assigned to the originally selected 130 or less stations on the structure. The coefficients of the matrix aligned with each orthogonal coordinate should represent the total mass of the structure. Use of the static deflection shapes as pseudo modal functions essentially distributes each point mass proportionately to each shape, which in turn relates directly to the stiffness properties of the structure. This technique often provides a more accurate representation of the structure per number of variables than if a set of discrete displacement variables is used.

The second method of solving problems with more than 130 mass points is by component mode synthesis techniques, as reported in Refs. 9 and 10. With this approach, subsystems of the total structure are isolated, analyzed, and finally combined with other subsystems, after each has been transformed to separate generalized coordinates. To demonstrate the procedure, consider a structure made up of two parts, subsystems A and B. For each subsystem, referenced to its own natural

coordinates, the mass and stiffness equations are generated. In the present example we have:

$$[m_A]\{\ddot{U}_A\} + [K_A]\{U_A\} = \{0\}$$

$$[m_B]\{\ddot{U}_B\} + [K_B]\{U_B\} = \{0\}$$

For each subsystem, appropriate eigenvectors $[\phi_{ij}]$ are computed, which provide the transformation to generalized coordinates, namely

$$\{U_{ij_A}\} = [\phi^n_{ij_A}]\{q^n_A\}$$

$$\{U_{ij_B}\} = [\phi^n_{ij_B}]\{q^n_B\}$$

The eigenvectors $[\phi_{ij}]$ may be a superposition of several types, namely the normal modes of the subsystem, rigid body modes, constraint modes* and/or attachment modes**. The process of forming the modal functions is repeated for all subsystems.

To combine the subsystems, a constraint condition must be imposed so that displacements of subsystem A match displacements of subsystem B at common points. However, in general, each subsystem is referenced to its own local coordinate system, so in order to match displacements a coordinate transformation is required. The transformation is simply the three-dimensional vector transformation involving direction cosines, which will be designated $\bar{\gamma}_A$ and $\bar{\gamma}_B$ for the two subsystems. At present, each transformation matrix must be generated by hand.

*See Ref. 7.
**See Ref. 8.

For subsystem A assume gridpoints i and j are to be matched with gridpoints of subsystem B. The matrix of direction cosines for subsystem A is, therefore,

$$[\gamma_A] = \begin{array}{c} \\ i1 \\ i2 \\ i3 \\ i4 \\ i5 \\ i6 \\ j1 \\ j2 \\ j3 \\ j4 \\ j5 \\ j6 \end{array} \begin{array}{c} \begin{array}{cccccc} i1 & i2 & i3 & i4 & i5 & i6 \end{array} \\ \left[\begin{array}{cccccc} \bar{\gamma}_A & & & 0 & & 0 \\ & & & & & \\ & & & & & \\ 0 & & & \bar{\gamma}_A & & 0 \\ & & & & & \\ & & & & & \\ 0 & & & 0 & & \bar{\gamma}_A \\ & & & & & \\ & & & & & \end{array}\right. \end{array} \begin{array}{c} \begin{array}{cccccc} j1 & j2 & j3 & j4 & j5 & j6 \end{array} \\ \left.\begin{array}{cccccc} 0 & & & 0 & & 0 \\ & & & & & \\ & & & & & \\ 0 & & & 0 & & 0 \\ & & & & & \\ & & & & & \\ 0 & & & 0 & & 0 \\ & & & & & \\ & & & & & \end{array}\right] \end{array}$$

A similar matrix can be written for subsystem B, assuming gridpoints k and ℓ are involved.

$$[\gamma_B] = \begin{array}{c} \\ k1 \\ k2 \\ k3 \\ k4 \\ k5 \\ k6 \\ \ell 1 \\ \ell 2 \\ \ell 3 \\ \ell 4 \\ \ell 5 \\ \ell 6 \end{array} \begin{array}{c} \begin{array}{cccccc} k1 & k2 & k3 & k4 & k5 & k6 \end{array} \\ \left[\begin{array}{cccccc} \bar{\gamma}_B & & & 0 & & 0 \\ & & & & & \\ & & & & & \\ 0 & & & \bar{\gamma}_B & & 0 \\ & & & & & \\ & & & & & \\ 0 & & & 0 & & \bar{\gamma}_B \\ & & & & & \\ & & & & & \end{array}\right. \end{array} \begin{array}{c} \begin{array}{cccccc} \ell 1 & \ell 2 & \ell 3 & \ell 4 & \ell 5 & \ell 6 \end{array} \\ \left.\begin{array}{cccccc} 0 & & & 0 & & 0 \\ & & & & & \\ & & & & & \\ 0 & & & 0 & & 0 \\ & & & & & \\ & & & & & \\ 0 & & & 0 & & 0 \\ & & & & & \\ & & & & & \end{array}\right] \end{array}$$

Next by operations within SAMIS, the total γ matrix is defined, of the form:

$$[\gamma] = \left[\gamma_A \mid -\gamma_B\right]$$

which is to be premultiplied by the matrix of modal functions, namely

$$[\phi] = \left[\begin{array}{c|c} \phi_A & 0 \\ \hline 0 & \phi_B \end{array}\right]$$

to obtain

$$[B] = [\gamma]\ [\phi] = \left[\gamma_A\ \phi_A \mid -\gamma_B\ \phi_B\right]$$

This equation is actually an expression of the condition

$$\left\{U_{ij_A}\right\} - \left\{U_{k\ell_B}\right\} = \left\{0\right\}$$

or in terms of the generalized variables is:

$$\left[\gamma_A\ \phi_A \mid -\gamma_B\ \phi_B\right] \{q\} = \{0\} \tag{3.10}$$

However, in equating the displacements of the two subsystems, the number of independent variables is reduced in Eq. (3.10). Hence, the equation can be written in the form:

$$\left[\begin{array}{c|c} \Phi^{DD} & \Phi^{DI} \\ \hline \Phi^{ID} & \Phi^{II} \end{array}\right] \left\{\begin{array}{c} q^D \\ \hline q^I \end{array}\right\} = \left\{\begin{array}{c} 0 \\ \hline 0 \end{array}\right\} \tag{3.11}$$

where $\{q^D\}$ are the dependent variables, the number of which is equal to the number of displacements that have been equilibrated. At present, selection of the dependent set is arbitrary, and is subject to the same consideration as selection of redundant

members in the force method of analysis with respect to maximizing accuracy (Ref. 9). Solving Eq. (3.11) for the dependent set yields:

$$\left\{q^D\right\} = \left[\Phi^{DD}\right]^{-1} \left[\Phi^{DI}\right] \left\{q^I\right\}$$

and the final transformation matrix is formed, namely:

$$\begin{Bmatrix} q^I \\ -- \\ q^D \end{Bmatrix} = \left[\begin{array}{c} I \\ \hline \left[\Phi^{DD}\right]^{-1} \left[\Phi^{DI}\right] \end{array}\right] \left\{q^I\right\}$$

or

$$\{q\} = [T] \left\{q^I\right\} \tag{3.12}$$

This transformation will be used in subsequent calculations. The calculations leading up to definition of $[T]$ involve only real arithmetic and can be performed with the current version of SAMIS once the Υ matrix has been generated.

With the modal functions defined, the matrix equations for each subsystem can be expressed in terms of generalized coordinates. For subsystem A:

$$\left[\overline{m}_A\right] \left\{\ddot{q}_A\right\} + \left[\overline{K}_A\right] \left\{q_A\right\} = \{0\}$$

where

$$\left[\overline{m}_A\right] = \left\{\phi_A\right\}^T \left[m_A\right] \left\{\phi_A\right\}$$

$$\left[\overline{K}_A\right] = \left\{\phi_A\right\}^T \left[K_A\right] \left\{\phi_A\right\}$$

After generalizing the subsystem equations, the subsystem matrices are superimposed to form the dynamic equation of the composite system, each

subsystem still being referenced to local coordinates. The form of the matrix equation is

$$\left[\begin{array}{c|c} \overline{m}_A & 0 \\ \hline 0 & \overline{m}_B \end{array}\right] \left\{\begin{array}{c} \ddot{q}_A \\ \hline \ddot{q}_B \end{array}\right\} + \left[\begin{array}{c|c} \overline{K}_A & 0 \\ \hline 0 & \overline{K}_B \end{array}\right] \left\{\begin{array}{c} q_A \\ \hline q_B \end{array}\right\} = \left\{\begin{array}{c} 0 \\ \hline 0 \end{array}\right\}$$

Next, the transformation defined by Eq. (3.12) is applied to obtain

$$[T]^T [m] [T] \left\{\ddot{q}^I\right\} + [T]^T [K] [T] \left\{q^I\right\} = \{0\}$$

which may be written as

$$\lambda^2 [\mathcal{M}] \left\{q^I\right\} - [\mathcal{K}] \left\{q^I\right\} = \{0\} \tag{3.13}$$

Solution for the eigenvalues and eigenvectors is effected by methods defined in Section 3.9. After the eigenvectors have been determined, the mode shapes for the two subsystems in local coordinates are determined by transforming as follows:

$$\left\{\begin{array}{c} u_{ij_A} \\ \hline u_{ij_B} \end{array}\right\} = \left[\begin{array}{c|c} \phi_A & 0 \\ \hline 0 & \phi_B \end{array}\right] [T] \left\{q^I\right\}$$

where $\left\{q^I\right\}$ are the eigenvectors from Eq. (13).

It should be noted that the procedure outlined above for determining dynamic characteristics is also the preparatory process for solving the forced motion problem, as discussed in Refs. 7 and 8.

3.14 Use of Multiple Coordinate Systems

Most problems, particularly those with single component structures, are set up referenced to a single overall X, Y, Z coordinate system. With this arrangement, the gridpoint coordinates, loading vectors and gridpoint displacements are referenced to the overall system, and the member stress resultants are referenced to either the analyst's specified or computer-generated local coordinates. However, for some problems it is convenient to use more than one set of overall coordinates. In these

cases, use of several sets either reduces the amount of input data to be prepared or simplifies the interpretation of computed results.

An interesting example which demonstrates the applicability of multiple coordinate systems is the analysis of a pivotable antenna and mount (Fig. 3.16). Assume that it is necessary to determine the static response or dynamic characteristics of this configuration for several positions of the dish relative to the pedestal. If a single coordinate system X, Y, Z is used to define the geometry of the dish and pedestal, then the data must be regenerated for each position of the dish.

The alternate procedure is to first define the geometry of the pedestal with respect to the X, Y, Z coordinate system and to define the geometry of the dish with respect to the x, y, z coordinate system. Individual element and the system stiffness, stress, and loading matrices are next generated by use of the SAMIS for each structural component--in this case the pedestal and dish. Mathematically, the dynamic equations for the two component systems are:

$$\lambda^2 \left[M_P\right] \left\{\delta_P\right\} = \left[K_P\right] \left\{\delta_P\right\} \tag{3.14}$$

$$\lambda^2 \left[M_D\right] \left\{\delta_D\right\} = \left[K_D\right] \left\{\delta_D\right\} \tag{3.15}$$

At this point the two systems are referenced to different coordinate systems; hence, the next step is to join them by matching displacements at common gridpoints--gridpoints 1 and 2 in Fig. 3.16. Assume displacement components of the pedestal at gridpoints 1 and 2 are aligned with the dish displacements as follows:

$$\left\{\delta P_{1\text{-}2}\right\} = \left[\gamma\right] \left\{\delta D_{1\text{-}2}\right\}$$

or, accounting for all displacements, we can write:

$$\begin{Bmatrix} \delta P_{1\text{-}2} \\ \hline \delta P_{3\text{-}n} \end{Bmatrix} = \left[\begin{array}{c|c} \gamma & 0 \\ \hline 0 & I \end{array}\right] \begin{Bmatrix} \delta D_{1\text{-}2} \\ \hline \delta P_{3\text{-}N} \end{Bmatrix}$$

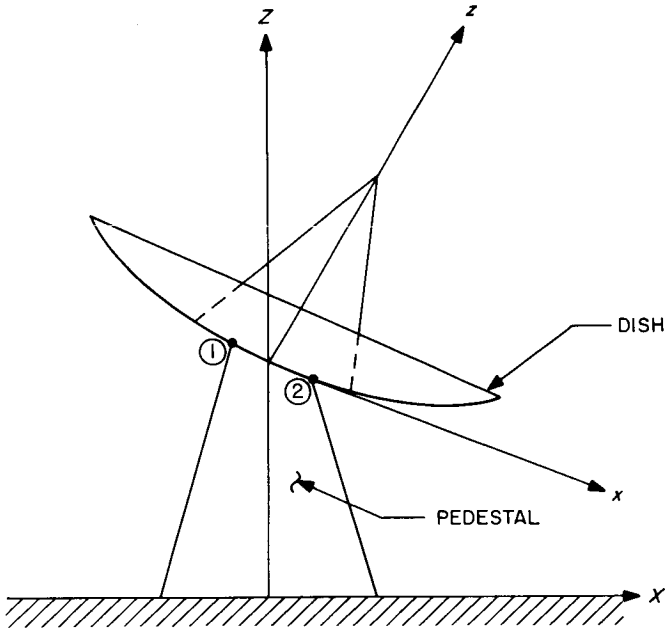

Fig. 3.16. Antenna and mount

or

$$\left\{\delta_P\right\} = [T]\left\{\begin{matrix}\delta_{D_{1-2}} \\ \hline \delta_{P_{3-N}}\end{matrix}\right\} \tag{3.16}$$

The transformation matrix $[T]$ is made up of a direction cosine matrix $[\gamma]$, which may be repeated several times depending upon the number of common gridpoints between the two systems, and a diagonal unit matrix needed to retain all remaining displacement components of the pedestal. Imposing this transformation on Eq. (3.14) leads to

$$\lambda^2[T]^T[M_P][T]\left\{\begin{matrix}\delta_{D_{1-2}} \\ \hline \delta_{P_{3-N}}\end{matrix}\right\} = [T]^T[K_P][T]\left\{\begin{matrix}\delta_{D_{1-2}} \\ \hline \delta_{P_{3-N}}\end{matrix}\right\}$$

By this transformation the codes of the displacement vector, mass matrix, and stiffness matrix have been made compatible with those of the dish at the attachment points. Hence, the mass and stiffness matrices of the two systems can be superimposed to define composite matrices for the entire structure.

It is apparent that all matrix operations required in the above manipulations can be commanded by pseudo instructions if the matrix of direction cosines $[\gamma]$ is first computed and utilized to define the transformation matrix $[T]$.

The advantage of this scheme is that location of the dish relative to the pedestal is controlled by the matrix of direction cosines. Hence, to change the orientation of the dish requires only that $[\gamma]$ be changed. This is a rather simple procedure compared to the alternative of regenerating element input data for each geometric configuration. Furthermore, the mode shapes of the dish will be defined with respect to the dish-oriented coordinates x, y, z, and the pedestal dynamic characteristics will be defined with respect to its natural coordinate system X, Y, Z (except for gridpoints common with dish), which eases interpretation of the results.

4.0 THE LINE ELEMENT, STATIC AND DYNAMIC PROBLEMS

4.1 Three-Dimensional Frame Structure

A three-dimensional frame structure, for which independent load and deflection data are available from Ref. 8, was set up and analyzed with the SAMIS program to check the program formulation of the line element. The structure is composed of circular cross-section beam members. A set of hypothetical values for the cross-sectional area (0.001 in.^{2}), shear areas (0.003 in.^{2}), and moments of inertia (0.001 in.^{4}) is assumed for each member. The structure is composed of 35 members, which are arranged to form a nonsymmetric array. For the static problem, a loading of 1000 lb at gridpoint 13 in the -Z direction is applied as shown in Fig. 4.1. For this problem, gridpoint displacements, reaction forces, and member forces were determined.

To check the calculation of modal properties of the structure, the first option of the mass generation routine was used, which concentrates half the mass of each element at the element gridpoints.

The static and dynamic results obtained from the SAMIS program were found to be in complete agreement with results reported in Ref. 10.

Of interest here is the format of the element input data for a typical element of the structure. Consider element 8, which extends from gridpoint 3 to gridpoint 5. The three cards of element input data are shown in Fig. 4.2. It is assumed that this data is for a dynamics problem, since card No. 2 is included, which provides only the value of the mass per unit length of the element.

The output format for the beam problem is similar to the facet output. For this problem the displacements of the gridpoints are referenced to the overall coordinate system X, Y, Z. The stresses are referenced to each element's local coordinates. The stress component identification is defined in Ref. 1, Table 5-4.

4.2 Planar Frame Structure, Prismatic Members

A three-member frame structure, in which each member has a rectangular cross-section, was set up to check the program for correct generation of the structural stiffness matrix. The structure is shown in Fig. 4.3 with the overall coordinates X, Y, Z and member local coordinates $x_i y_i z_i$ defined consistent with the ordering of gridpoints in the element data. The total structure stiffness matrix was

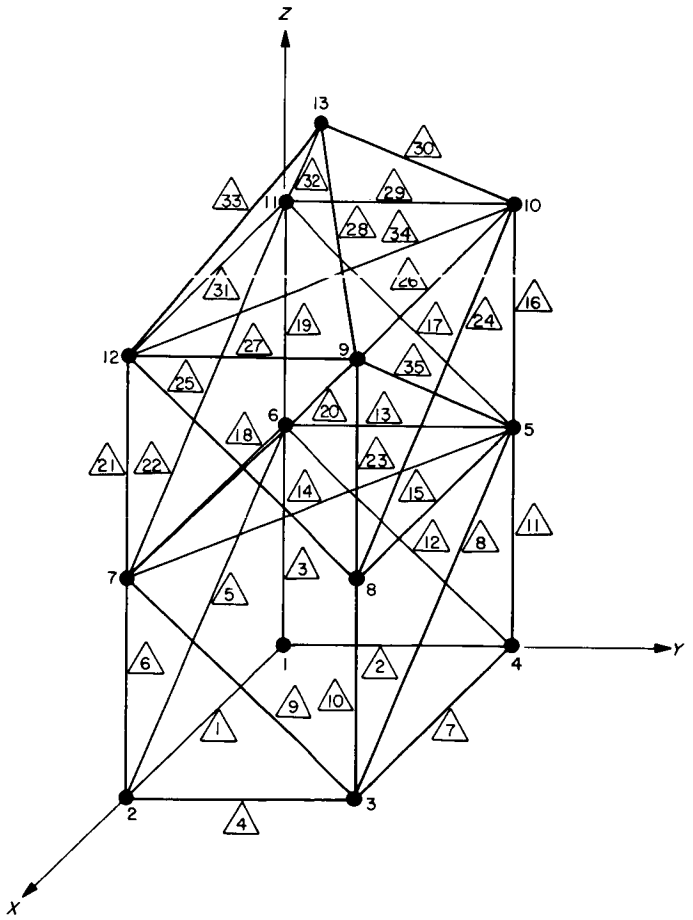

Fig. 4.1. Three-dimensional frame structure

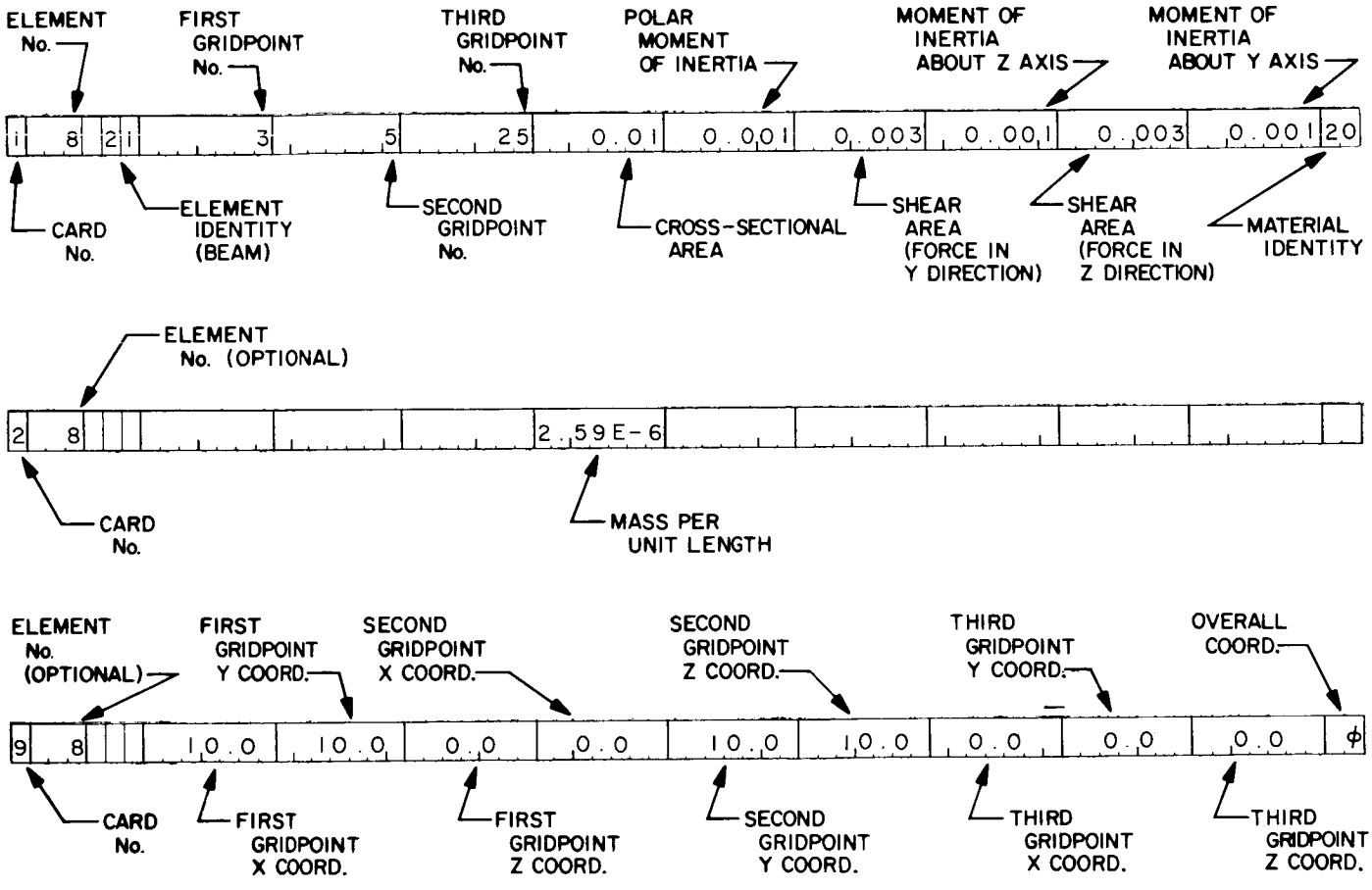

Fig. 4.2. Sample element data for beam problem

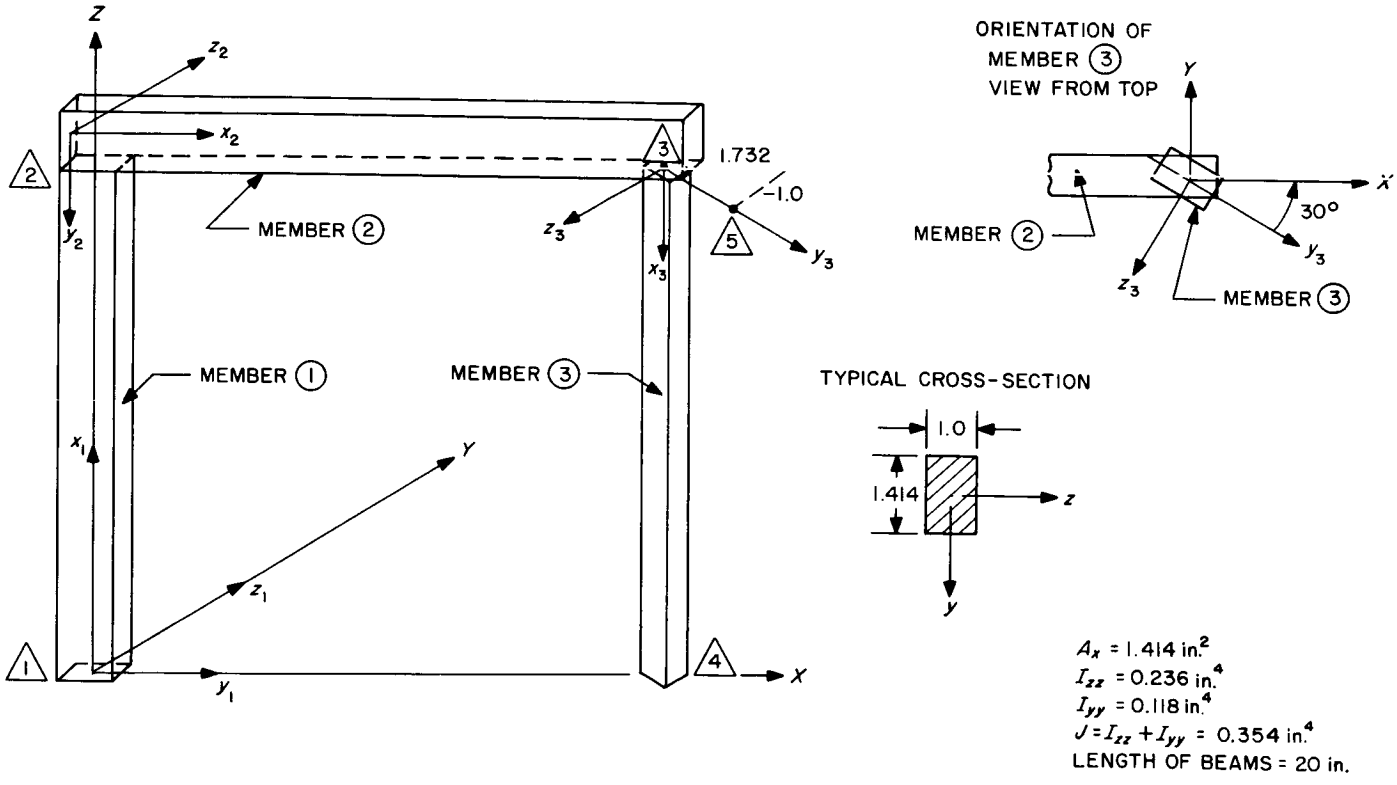

Fig. 4.3. Coordinates and geometry of planar three-member frame structure

generated by the program and compared with a hand-derived stiffness matrix. The comparison between the two was exact.

Of interest is the format of the element input data for this problem. In the previous example of the three-dimensional frame structure, because the element cross-sections are circular, the location of the gridpoint that defines the local x-y plane of each element is arbitrary and may even be ignored. However, in the present case, the location of the third gridpoint must be considered carefully; otherwise the interpretation of the member stresses will be incorrect. For the three elements, the element input data is that shown in Fig. 4.4. For member (1), the elastic gridpoint numbers are (1) and (2), which define the direction of the local x axis. The third gridpoint, which is (3), is used to define the local x-y plane for this member, which is the $x_1 y_1$ plane. The clamped end condition at gridpoint (1) is specified by the sequence 999999 on card 2. For member (2) the third gridpoint is (1) which leads to definition of the $x_2 y_2$ plane as the local plane. For member (3), a local coordinate system, skewed with respect to the XYZ system, is selected to align with the principal axes of the member cross-section. For this member, the third gridpoint is (5) as shown in Fig. 4.2. The clamped condition at gridpoint (4) is indicated by the sequence 999999 on card 2. Based upon these definitions of the local axes, the moment of inertia I_{zz} is larger than I_{yy} for each element, and is so referenced in the element data.

FORTRAN CODING FORM

Program		Punching Instructions	Graphic		Card Form #	Page of
Programmer	Date		Punch			Identification 73–80

C FOR COMMENT

Statement Number (1)	(2–5)	Cont. (6)	7	8–15	16–21	22–28	29–35	36–42	43–49	50–56	57–63	64–70	71–72
1	1	2	1	1	2	3	1.414	0.354	0.0	0.236	0.0	0.118	20
2	1	2	1	999999									
9	1	2	1	0.0	0.0	0.0	0.0	0.0	20.0	20.0	0.0	20.0	ϕ
1	2	2	1	2	3	1	1.414	0.354	0.0	0.236	0.0	0.118	20
9	2	2	1	0.0	0.0	20.0	20.0	0.0	20.0	0.0	0.0	0.0	ϕ
1	3	2	1	3	4	5	1.414	0.354	0.0	0.236	0.0	0.118	20
2	3	2	1		999999								
9	3	2	1	20.0	0.0	20.0	20.0	0.0	0.0	21.732	-1.0	0.0	ϕ

JPL 2051-1 SEP 65

Fig. 4.4. Element input data for three-member frame structure

5.0 MISCELLANEOUS TOPICS

5.1 Automatic Matrix Partitioning and Applications

In most statics problems involving solution of the equation:

$$[K]\{\delta\} = \{P\}$$

the applied loads are zero at many gridpoints. Partitioning on this basis, the above equation can be put into the form:

$$\left[\begin{array}{c|c} K_{11} & K_{12} \\ \hline K_{21} & K_{22} \end{array}\right] \left\{\begin{array}{c} \delta_1 \\ \hline \delta_2 \end{array}\right\} = \left\{\begin{array}{c} P \\ \hline 0 \end{array}\right\} \tag{5.1}$$

Normal procedure in solving this equation is to determine the relationship between $\{\delta_1\}$ and $\{\delta_2\}$ from the lower set of equations, then substitute this result into the upper set to obtain:

$$\left[K_{11} - K_{12} K_{22}^{-1} K_{21}\right]\{\delta_1\} = \{P\}$$

or

$$[\bar{K}]\{\delta_1\} = \{P\}$$

At this point $[\bar{K}]$ is inverted to solve for the displacements $\{\delta_1\}$ due to a specific loading $\{P\}$, that is:

$$\{\delta_1\} = [\bar{K}]^{-1}\{P\} \equiv \left[K_{11} - K_{12} K_{22}^{-1} K_{21}\right]^{-1}\{P\} \tag{5.2}$$

It is noteworthy that if the stiffness matrix of Eq. (1) is inverted, the resultant flexibility matrix has the matrix coefficient of Eq. (5.2) in the partition location corresponding to K_{11}. To demonstrate this, designate the flexibility matrix by $[f]$; then by definition

$$\left[\begin{array}{c|c} f_{11} & f_{12} \\ \hline f_{21} & f_{22} \end{array}\right] \left[\begin{array}{c|c} K_{11} & K_{12} \\ \hline K_{21} & K_{22} \end{array}\right] = \left[\begin{array}{c|c} I & 0 \\ \hline 0 & I \end{array}\right] \tag{5.3}$$

or

$$[f_{11}]\ [K_{11}] + [f_{21}]\ [K_{21}] = [I] \tag{5.4}$$

$$[f_{11}]\ [K_{12}] + [f_{21}]\ [K_{22}] = [0] \tag{5.5}$$

$$[f_{12}]\ [K_{11}] + [f_{22}]\ [K_{21}] = [0] \tag{5.6}$$

$$[f_{12}]\ [K_{12}] + [f_{22}]\ [K_{22}] = [I] \tag{5.7}$$

Solving Eq. (5.5) for $[f_{12}]$ and substituting into Eq. (5.4) leads to

$$[f_{11}] = \left[K_{11} - K_{12}\, K_{22}^{-1}\, K_{21}\right]^{-1}$$

Similarly, it is found that:

$$[f_{21}] = -\,[f_{11}]\ \left[K_{12}\, K_{22}^{-1}\right]$$

$$[f_{22}] = \left[K_{22} - K_{21}\, K_{11}^{-1} K_{12}\right]^{-1}$$

$$[f_{12}] = -\,[f_{22}]\ \left[K_{21}\, K_{11}^{-1}\right]$$

Thus, the f_{11} partition of the flexibility matrix is exactly the coefficient matrix that is required to be multiplied by the loading matrix.

Symbolically, if the stiffness matrix of Eq. (5.1) is input as the $[A]$ matrix, and the loading matrix as the $[B]$ matrix, then the following result is automatically determined by use of the CHOL subprogram:

$$\left[\begin{array}{c|c} f_{11} & f_{12} \\ \hline f_{21} & f_{22} \end{array}\right] \left\{\begin{array}{c} P \\ \hline o \end{array}\right\} = [f_{11}]\ \{P\}$$

which is the desired result as defined by Eq. (5.2). Thus, by input of

$$\left[\begin{array}{c|c} K_{11} & K_{12} \\ \hline K_{21} & K_{22} \end{array}\right]$$

and $\left\{\begin{array}{c} P \\ \hline o \end{array}\right\}$ into CHOL, the desired output defined by Eq. (2) is obtained. It is to be noted that if a unit diagonal matrix is input as the $[B]$ matrix into CHOL along with any matrix $[A]$ of larger order than $[B]$, the output is automatically $\left[A_{11}-A_{12}A_{22}^{-1}A_{21}\right]^{-1}$, in which A_{11} has the same dimension as $[B]$.

This capability can be used in numerous problems. Consider the dynamic matrix equation in which the mass matrix is of lower order than the stiffness matrix:

$$\lambda^2 \left[\begin{array}{c|c} m & o \\ \hline o & o \end{array}\right] \left\{\begin{array}{c} \delta_1 \\ \hline \delta_2 \end{array}\right\} = \left[\begin{array}{c|c} K_{11} & K_{12} \\ \hline K_{21} & K_{22} \end{array}\right] \left\{\begin{array}{c} \delta_1 \\ \hline \delta_2 \end{array}\right\}$$

The mass matrix is decomposed into:

$$[U]^T [U] = [m]$$

or

$$\lambda^2 \left[\begin{array}{c|c} U^T & o \\ \hline o & o \end{array}\right] \left[\begin{array}{c|c} U & o \\ \hline o & o \end{array}\right] \left\{\begin{array}{c} \delta_1 \\ \hline \delta_2 \end{array}\right\} = \left[\begin{array}{c|c} K_{11} & K_{12} \\ \hline K_{21} & K_{22} \end{array}\right] \left\{\begin{array}{c} \delta_1 \\ \hline \delta_2 \end{array}\right\}$$

We define

$$\{\delta^*\} = [U] \{\delta\}$$

Then

$$\lambda^2 \left[\begin{array}{c|c} U^T & o \\ \hline o & o \end{array}\right] \left\{\begin{array}{c} \delta^* \\ \hline o \end{array}\right\} = \left[\begin{array}{c|c} K_{11} & K_{12} \\ \hline K_{21} & K_{22} \end{array}\right] [U]^{-1} \{\delta^*\}$$

The stiffness matrix is input to CHOL as the [A] matrix, and the

$$\left[\begin{array}{c|c} U^T & o \\ \hline o & o \end{array}\right]$$

as the [B] matrix. The output of CHOL is:

$$\left[\begin{array}{c|c} K_{11} & K_{12} \\ \hline K_{21} & K_{22} \end{array}\right]^{-1} \left[\begin{array}{c|c} U^T & o \\ \hline o & c \end{array}\right]$$

which is equivalent to:

$$\left[K_{11} - K_{12}K_{21}^{-1}K_{21}\right]^{-1}[U]^T$$

Thus, the dynamic equation automatically reduces to:

$$\lambda^2[U]\left[K_{11} - K_{12}K_{22}^{-1}K_{21}\right]^{-1}[U]^T\{\delta^*\} = [I]\{\delta^*\}$$

which is the desired form of the equation from which the eigenvalues and eigenvectors are determined using ROOT.

In the event the stiffness matrix of Eq. (5.1) has a diagonal and upper off-diagonal that exceed core, the matrix must be partitioned "manually" through the use of additional pseudo instructions. A set of pseudo instructions that performs this partitioning is given in Table 5-1. These 13 instructions operate on stiffness matrix KTR001, which presumably has already been generated and constrained. Description of each pseudo instruction follows:

14.00 READ: Transfer from the data input tape to tape 12, locations 001 and 002, the two matrices WAR001 and WAR002, respectively.

Table 5-1. Pseudo instructions for matrix partitioning

```
14.00   12001  WAR001  12002  WAR002  READ
14.05   12001  WAR001  11001  KTR001  WASH  10001  KWR001  2
14.10   12001  WAR001                 FLIP  11002  WFC001
14.15   11002  WFC001                 ROWS  13001  WFR001
14.20   13001  WFR001  10001  KWR001  WASH  13002  KAR001  2
14.25   10001  KWR001  13002  KAR001  SUBS  11002  KLR001
14.30   11002  KLR001                 COLS  11003  KLC001
14.35   11003  KLC001                 FLIP  11004  KUR001
14.40   12002  WAR002  11001  KTR001  WASH  13001  KBR001  2
14.45   13001  KBR001  11003  KLC001  CHOL  12001  KDC001
14.50   11004  KUR001  12001  KDC001  MULT  10001  KIC001
14.55   10001  KIC001                 ROWS  10002  KIR001
14.60   13002  KAR001  10002  KIR001  SUBS  11002  KPC001
```

14.05 WASH: Extract certain rows and columns from the stiffness matrix KTR001 by special pre- and postmultiplication. Store the partition of KTR001 on tape 10, location 001. The explicit operation is:

Starting with the complete stiffness matrix

$$[K] = \left[\begin{array}{c|c} K_{11} & K_{12} \\ \hline K_{21} & K_{22} \end{array}\right]$$

the left column partition $\begin{bmatrix} K_{11} \\ K_{21} \end{bmatrix}$ is isolated by use of WASH, option 2 (as indicated in E field). The matrix WAR001 has column codes that match those of K_{11} and row codes that are different from any codes used in K. Elements equal unity in WAR001. Note that since rows and columns of $[K]$ are prescribed by element codes, the selection of the row or column codes of $[K_{11}]$ and $[K_{22}]$ is dependent only upon the element codes used in the WASH matrix. To minimize computer time, general practice should be to select strongly coupled elements for $[K_{11}]$ and lightly coupled elements for $[K_{22}]$. With this arrangement $[K_{22}]$ is efficiently inverted in forming $\left[K_{11}-K_{12}K_{22}^{-1}K_{21}\right]$ Since $[K_{12}]\ [K_{22}]^{-1}\ [K_{21}]$ will be a full matrix, the fact that $[K_{11}]$ is also full, is of little consequence.

14.10 FLIP
14.15 ROWS } Row-list the transpose of the WASH matrix.

14.20 WASH: Extract the $[K_{11}]$ matrix from the $\begin{bmatrix} K_{11} \\ K_{12} \end{bmatrix}$ partition by special pre- and postmultiplication with the matrix WFR001. Title the $[K_{11}]$ matrix KAR001 and store it on tape 13, location 002.

14.25 SUBS: Subtract $[K_{11}]$ from $\begin{bmatrix} K_{11} \\ K_{21} \end{bmatrix}$ to obtain $[K_{21}]$. This matrix is titled KLR001 and is stored on tape 11, location 002.

14.30 COLS / 14.35 FLIP: Convert $[K_{21}]$ to $[K_{12}]$. Designate $[K_{12}]$ KUR001 and store on tape 11, location 004.

14.40 WASH: Extract the $[K_{22}]$ partition from the total $[K]$ matrix by special pre- and postmultiplication. Matrix WAR002 has row and column codes that match those of $[K_{22}]$ and element values of unity. Option 2 of WASH is used. Matrix $[K_{22}]$ is designated KBR001 and is stored on tape 13, location 001.

14.45 CHOL: Form the matrix produce $[K_{22}]^{-1}[K_{21}]$ from input of $[K_{22}]$ (KBR001) and $[K_{21}]$ (KLC001). Designate the resultant matrix KDC001 and store on tape 12, location 001.

14.50 MULT: Multiply together $[K_{12}]$ (KUR001) and $[K_{22}]^{-1}[K_{21}]$ (KDC001) to form $[K_{12}][K_{22}]^{-1}[K_{21}]$ (KIC001).

14.55 ROWS: Row-list the matrix KIC001 and title the new matrix KIR001. It is stored on tape 10, location 002.

14.60 SUBS: By subtraction form $\left[K_{11} - K_{12} K_{22}^{-1} K_{21}\right]$. This matrix is titled KPC001 and is stored on tape 11, location 002. Except for degenerate cases this matrix is a full matrix.

These pseudo instructions are an example set suitable for insertion into a pseudo instruction program. They would necessarily have to be modified, particularily in tape assignments, upon insertion into a program set.

Another use of the partitioning capability can be demonstrated by considering the problem of a stiffened cylinder subjected to a transverse normal load as shown in Fig. 5.1. Because of symmetry, only one-half of the cylinder cross-section needs to be idealized and analyzed. However, even with this reduction, if one-half of the cylinder is idealized by a network of triangular elements as shown in Section C, it is apparent that the total structural stiffness matrix would greatly exceed the computational capacity of the SAMIS. However, partitioning this structure and solving a lower-order matrix equation, can be used to retain the effect of a fine grid array.

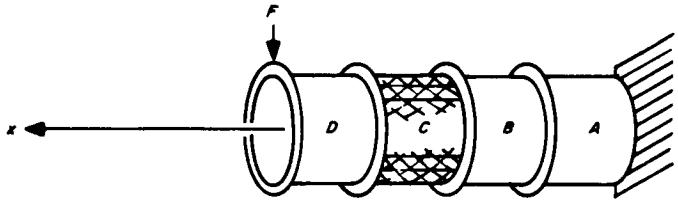

Fig. 5.1. Stiffened cylinder

The procedure centers on first analyzing each section of the total cylinder. Consider Section A as having been idealized by an array of triangular plate elements and a number of beam elements that represent the ring stiffener. The stiffness matrix for Section A is generated using SAMIS, which takes the form:

$$[K_A]\ \{\delta_A\} = \{P_A\}$$

At this stage, gridpoints in Section A which border on Section B or the clamped edge, and gridpoints at which deflections are to be computed or forces are to be applied, are separated and designated as $\delta_A^{(1)}$. All remaining displacement components are designated $\delta_A^{(2)}$. Thus the matrix equation partitions into

$$\left[\begin{array}{c|c} K_A^{11} & K_A^{12} \\ \hline K_A^{21} & K_A^{22} \end{array}\right] \left\{\begin{array}{c} \delta_A^{(1)} \\ \hline \delta_A^{(2)} \end{array}\right\} = \left\{\begin{array}{c} P_A \\ \hline o \end{array}\right\} \qquad (5\text{-}8)$$

In actual manipulations, the matrix K_A and a unit diagonal matrix of the same dimension and coding as the rows of $\left\{\delta_A^{(1)}\right\}$ are input to CHOL as the [A] and [B] matrices, respectively. The output of CHOL is:

$$[f_A] = \left[K_A^{11} - K_A^{22}\ K_A^{22^{-1}}\ K_A^{21}\right]^{-1}$$

This matrix is next inverted and designated $[\bar{K}_A]$. Thus, we have

$$[\bar{K}_A] \left\{\delta_A^{(1)}\right\} = \{P_A\}$$

where $[\bar{K}_A]$ is, in general, a solid matrix of the same order as $\delta_A^{(1)}$. This process is repeated for all remaining sections of the cylinder, until finally four stiffness matrices have been determined that have the following interpretation:

$$[\bar{K}_A] \left\{\delta_A^{(1)}\right\} = \{P_A\}$$

$$[\bar{K}_B] \left\{\delta_B^{(1)}\right\} = \{P_B\}$$

$$[\bar{K}_C] \left\{\delta_C^{(1)}\right\} = \{P_C\}$$

$$[\bar{K}_D] \left\{\delta_D^{(1)}\right\} = \{P_D\}$$

These matrix equations are superimposed to obtain a representation of the entire structure, i.e.:

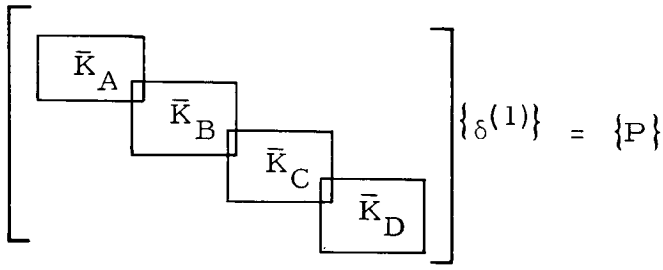

or

$$[\bar{K}_S] \{\delta^{(1)}\} = \{P\} \tag{5.9}$$

If precautions have been taken to control the dimension of $\{\delta^{(1)}\}$, then the final stiffness matirx $[\bar{K}_S]$ will still fit in core or the matrix size will have been reduced such that a single partitioning of the equation is all that is required to solve for the $\{\delta^{(1)}\}$ in terms of specified applied loads $\{P\}$. The only restriction on this procedure is that in the initial solution of the problem only the displacements $\{\delta^{(1)}\}$ are determined. If the remaining structural displacements are needed, then supplemental manipulations with the individual section equations, e.g., Equation (8), are necessary.

5.2 The Node Discontinuity Concept

Computational ability to account for displacement discontinuity at the joints of adjoining finite elements is very easily effected in the SAMIS. Consider the beam element, which has a stiffness matrix of order 12 when the beam is arbitrarily

oriented in three-dimensional space. Six of the variables are referenced to each of its gridpoints. For gridpoints designated i and j the stiffness matrix for element k is of the form

$$
\begin{array}{c}
\\
i1 \\
\downarrow \\
i6 \\
j1 \\
\downarrow \\
j6
\end{array}
\begin{array}{c}
\begin{array}{cc} i1 \longrightarrow i6 & j1 \longrightarrow j6 \end{array} \\
\left[\begin{array}{c|c} K_{ii}^{(h)} & K_{ij}^{(h)} \\ \hline K_{ji}^{(h)} & K_{jj}^{(h)} \end{array}\right]
\end{array}
$$

Combining the stiffness matrices for the structure shown in Fig. 5.2, which is made up of two elements, leads to the following matrix equation:

$$
\left[\begin{array}{c|c|c}
K_{11}^{(1)} & K_{12}^{(1)} & \\ \hline
K_{21}^{(1)} & K_{22}^{(1)} + K_{22}^{(2)} & K_{24}^{(2)} \\ \hline
 & K_{42}^{(2)} & K_{44}^{(2)}
\end{array}\right]
\left\{\begin{array}{c}
u_{11} \\ u_{12} \\ u_{13} \\ \theta_{14} \\ \theta_{15} \\ \theta_{16} \\ \hline
u_{21} \\ u_{22} \\ u_{23} \\ \theta_{24} \\ \theta_{25} \\ \theta_{26} \\ \hline
u_{41} \\ u_{42} \\ u_{43} \\ \theta_{44} \\ \theta_{45} \\ \theta_{46}
\end{array}\right\}
=
\left\{\begin{array}{c}
P_{11} \\ P_{12} \\ P_{13} \\ m_{14} \\ m_{15} \\ m_{16} \\ \hline
P_{21} \\ P_{22} \\ P_{23} \\ m_{24} \\ m_{25} \\ m_{26} \\ \hline
P_{41} \\ P_{42} \\ P_{43} \\ m_{44} \\ m_{45} \\ m_{46}
\end{array}\right\}
$$

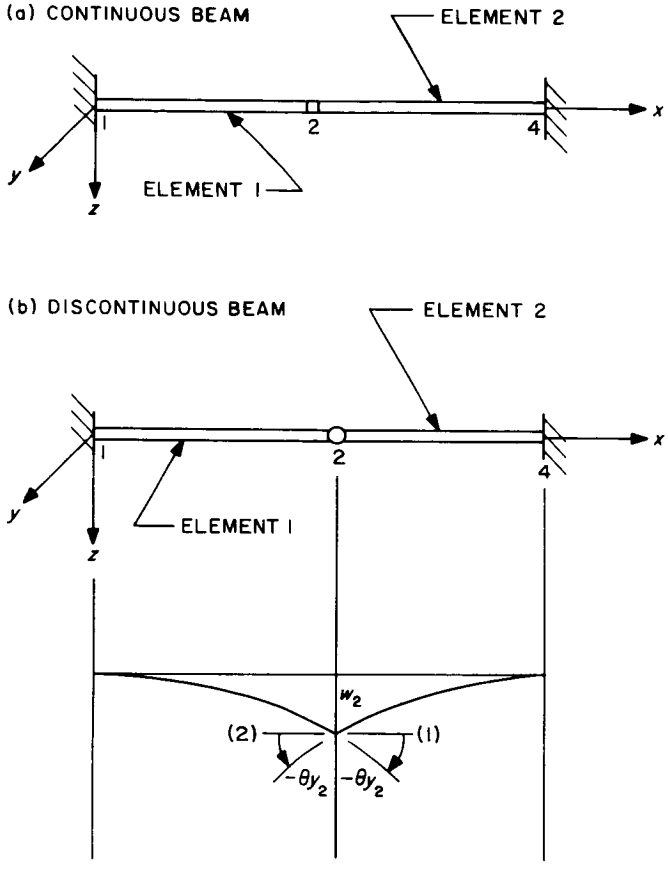

Fig. 5.2. Two-member beam

Note that at gridpoint 2 the two-element stiffness matrices combine, resulting in only six independent variables at this gridpoint. Hence, in going from element 1 to element 2, across joint 1, continuity of displacements is maintained.

Consider now the case when joint 2 is a hinge connection with a single axis of rotation along the y axis. The twelve displacement variables at gridpoints 1 and 4 and five of the displacement variables at gridpoint 2 are unaffected by this structural modification. However, the slope at gridpoint 2 is now discontinuous, having a value $\theta_{y_2}^{(1)}$ on the element 1 side of the joint and a value $\theta_{y_2}^{(2)}$ on the element 2 side of the joint. Hence, instead of eighteen displacement variables, we now have nineteen, and superpositioning of the stiffness matrices must yield a matrix equation of the form

$$
\begin{bmatrix}
K_{11}^{(1)} & K_{12}^{(1)} & K_{12}^{(1)} & 0 & 0 \\
K_{21}^{(1)} & K_{22}^{(1)} + K_{22}^{(2)} & K_{22}^{(1)} & K_{22}^{(2)} & K_{24}^{(2)} \\
\leftarrow K_{21}^{(1)} \rightarrow & \leftarrow K_{22}^{(1)} \rightarrow & & & \leftarrow 0 \rightarrow \\
\leftarrow 0 \rightarrow & \leftarrow K_{22}^{(2)} \rightarrow & & & \leftarrow K_{24}^{(2)} \rightarrow \\
0 & K_{42}^{(2)} & 0 & K_{42}^{(2)} & K_{44}^{(2)}
\end{bmatrix}
\begin{Bmatrix}
u_{11} \\ u_{12} \\ u_{13} \\ \theta_{14} \\ \theta_{15} \\ \theta_{16} \\
u_{21} \\ u_{22} \\ u_{23} \\ \theta_{24} \\ \theta_{26} \\
\theta_{25}^{(1)} \\ \theta_{25}^{(2)} \\
u_{41} \\ u_{42} \\ u_{43} \\ \theta_{44} \\ \theta_{45} \\ \theta_{46}
\end{Bmatrix}
=
\begin{Bmatrix}
P_{11} \\ P_{12} \\ P_{13} \\ m_{14} \\ m_{15} \\ m_{16} \\
P_{21} \\ P_{22} \\ P_{23} \\ m_{24} \\ m_{26} \\
m_{25}^{(1)} \\ m_{25}^{(2)} \\
P_{41} \\ P_{42} \\ P_{43} \\ m_{44} \\ m_{45} \\ m_{46}
\end{Bmatrix}
$$

It should be noted that not only has a new displacement variable been generated, but also the corresponding force variable has been split into two independent variables at the joint. Thus, if a moment M_y is applied at joint 2, the user must determine the fraction of this moment that is applied to each member.

In the SAMIS, the mechanism for identifying additional variables when discontinuities are present is by incrementing the gridpoint number of one of the elements during the generation of the stiffness matrices. Thus, in the present example, if the discontinuity condition is flagged in the element data of element 1, the coding of the variable $\theta_{y_2}^{(1)}$ would change, but the coding of $\theta_{y_2}^{(2)}$ would not. Since the gridpoint number 3 has not been assigned, the coding could be: $\theta_{y_2}^{(1)} \longrightarrow 35$ and $\theta_{y_2}^{(2)} \longrightarrow 25$; thus, the element stiffness matrices become:

$$
\begin{array}{c|c|c}
 & 11\ 12\ 13\ 14\ 15\ 16 & 21\ 22\ 23\ 24\ 26\ 35 \\
\hline
\begin{matrix}11\\12\\13\\14\\15\\16\end{matrix} & K_{11}^{(1)} & K_{12}^{(1)} \\
\hline
\begin{matrix}21\\22\\23\\24\\26\\35\end{matrix} & K_{21}^{(1)} & K_{22}^{(1)}
\end{array}
\quad \text{and} \quad
\begin{array}{c|c|c}
 & 21\ 22\ 23\ 24\ 25\ 26 & 41\ 42\ 43\ 44\ 45\ 46 \\
\hline
\begin{matrix}21\\22\\23\\24\\25\\26\end{matrix} & K_{22}^{(2)} & K_{24}^{(2)} \\
\hline
\begin{matrix}41\\42\\43\\44\\45\\46\end{matrix} & K_{42}^{(2)} & K_{44}^{(2)}
\end{array}
$$

Superposition of these matrices then yields the necessary nineteen degrees of freedom.

The node discontinuity capability in SAMIS has been used in the analysis of a solar panel structure. The actual panel was constructed of corrugated sheet, with a second facing sheet to which solar cells were mounted. Two large beams support the panel and attach to adjacent structure (see Fig. 5.3). This design was idealized by three planes of beam elements. In the idealization, the corrugations were lumped into equivalent beams lying transverse to the support beams. The facing sheet was idealized by criss-cross beams that modeled the in-plane stiffness of the sheet. The discontinuity conditions arose because of the extreme shear flexibility of the corrugation resulting in displacement discontinuity between gridpoints in the support beams and gridpoints in the facing sheet. This discontinuity was accounted for in the following manner. Gridpoints

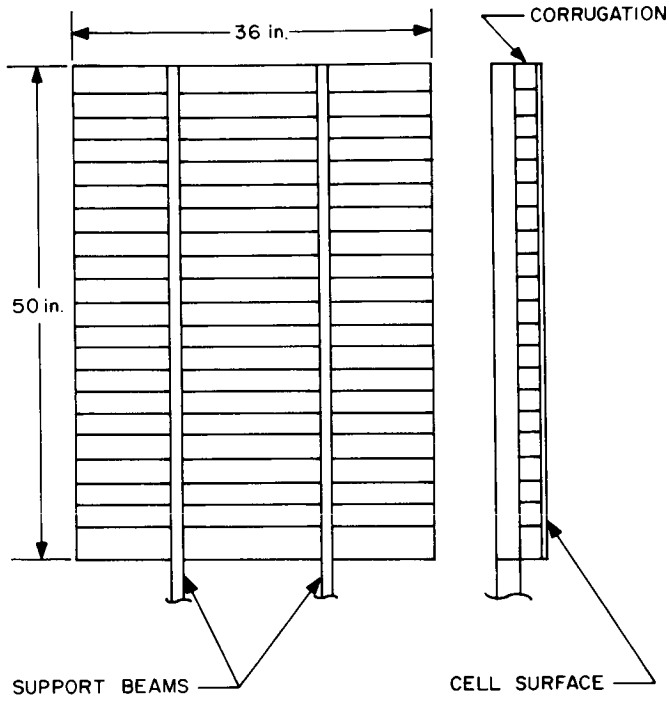

Fig. 5.3. Sketch of solar panel

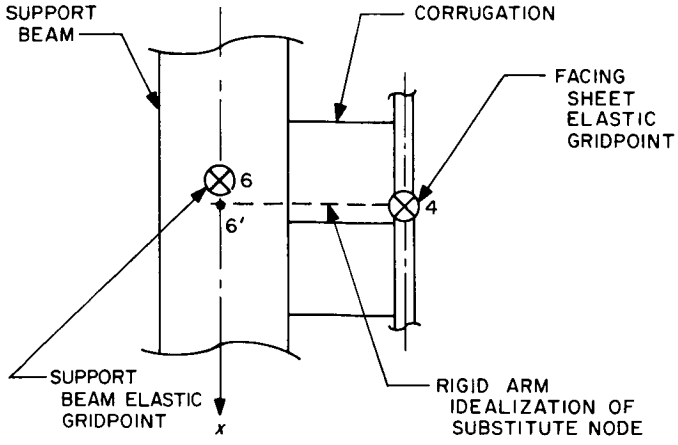

Fig. 5.4. Definition of substitute node

on the facing sheet were transferred to corresponding elastic gridpoint locations on the support beam. Physically this is equivalent to assuming a rigid massless arm attached to the facing sheet and gridpoint forces acting at the substitute gridpoint. The elastic gridpoints (4 and 6) and a substitute gridpoint (6') are shown in Fig. 5.4. All displacement components at gridpoints 6 and 6' are coded identically, except the axial displacement (along x axis). For this component the discontinuity condition was used in which the support beam retained the 61 designation; however, the substitute node 6' was designated 51. To complete the idealization, a stiffness matrix representing a linear spring was input which had the form:

$$\begin{array}{c} \\ 51 \\ 61 \end{array} \begin{array}{c} \begin{array}{cc} 51 & 61 \end{array} \\ \left[\begin{array}{c|c} k & -k \\ \hline -k & k \end{array}\right] \end{array}$$

The stiffness coefficient k was sized to represent the stiffness of the tributary corrugations in shear.

ACKNOWLEDGMENT

The theoretical and numerical work performed by Prof. H. E. Williams to provide closed form solutions for the shallow shell loading problems is gratefully acknowledged.

REFERENCES

1. Melosh, R. J., Diether, P. A., and Brennan, M., Structural Analysis and Matrix Interpretative System (SAMIS) Program Report, Technical Memorandum 307, Jet Propulsion Laboratory, Pasadena, California, September 1, 1966.

2. Melosh, R. J., and Christiansen, H. N., Structural Analysis and Matrix Interpretative System (SAMIS) Technical Report, Technical Memorandum 311, Jet Propulsion Laboratory, Pasadena, California, November 1, 1966.

3. Timoshenko, S., Theory of Plates and Shells, 2nd ed., ch. 16, McGraw-Hill Book Co., New York, 1959.

4. Sepetoski, W. K., et al, "A Digital Computer Program for the General Axially Symmetric Thin-Shell Problem," ASME paper No. 62-WA-31, November 25, 1962.

5. Utku, Senol, Computation of Stresses in Triangular Finite Elements, Technical Report 32-948, Jet Propulsion Laboratory, Pasadena, California, July 1, 1966.

6. Johnson, M. W., and Reissner, E., "On Transverse Vibrations of Shallow Spherical Shells," Quarterly of Applied Mathematics, Vol. 15, 1958, pp. 367-380.

7. Hurty, W. C., Dynamic Analysis of Structural Systems by Component Mode Synthesis, Technical Report 32-530, Jet Propulsion Laboratory, Pasadena, California, January 15, 1964.

8. Bamford, R. M., Modal Combination Program, Technical Memorandum 33-290, Jet Propulsion Laboratory, Pasadena, California, August 15, 1966.

9. Denke, P. H., A Computerized Static and Dynamic Aircraft Structural Analysis System—Engineering Aspects and Mathematical Formulation of the Problem, Paper 3213, Douglas Aircraft Co., Long Beach, California.

10. Wada, B. K., Stiffness Matrix Structural Analysis, Technical Report 32-774, Jet Propulsion Laboratory, Pasadena, California, October 31, 1965.

11. Williams, H. E., Influence Coefficients of Shallow Spherical Shells, Technical Report 32-51, Jet Propulsion Laboratory, Pasadena, California, February 12, 1961.

12. Williams, H. E., JPL internal document.

APPENDIX A. Transformation of Orthogonal Vectors

Equations are derived for transforming a set of vectors in spherical coordinates to a set in rectangular coordinates. The notation and sign convention are shown in Fig. A-1.

In Fig. A-1, the vectors $\vec{e}_\zeta$, $\vec{e}_\theta$, $\vec{e}_\phi$, are unit vectors tangent to the respective coordinate lines. The unit vectors $\vec{e}_x$, $\vec{e}_y$, $\vec{e}_z$, are, as shown, in the rectangular system.

The unit vector $\vec{e}_\zeta$ can be found in terms of the rectangular system as follows:

$$\vec{e}_\zeta = \frac{x\vec{e}_x + y\vec{e}_y + z\vec{e}_z}{\sqrt{x^2 + y^2 + z^2}}$$

where, from Fig. A-1,

$$x = a \sin \phi \cos \theta$$

$$y = a \sin \phi \sin \theta$$

$$z = a \cos \phi$$

substituting these quantities into the expression for $\vec{e}_\zeta$ yields

$$\vec{e}_\zeta = \sin \phi \cos \theta \, \vec{e}_x + \sin \phi \sin \theta \, \vec{e}_y + \cos \phi \, \vec{e}_z \qquad \text{(A-1)}$$

The unit vector $\vec{e}_\phi$ can be found by differentiation

$$\vec{e}_\phi = \frac{\dfrac{\partial \vec{e}_\zeta}{\partial \phi}}{\left| \dfrac{\partial \vec{e}_\zeta}{\partial \phi} \right|}$$

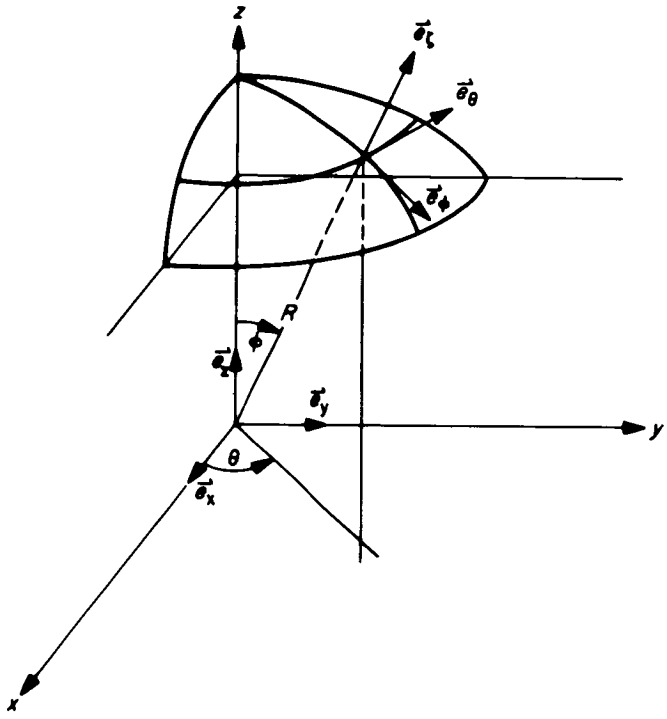

Fig. A-1. Sign convention and nomenclature

or,

$$\vec{e}_\phi = \cos\phi \cos\theta\ \vec{e}_x + \cos\phi \sin\theta\ \vec{e}_y - \sin\phi\ \vec{e}_z \tag{A-2}$$

Similarly, $\vec{e}_\theta$ is given by

$$\vec{e}_\theta = \frac{\dfrac{\partial \vec{e}_\zeta}{\partial\theta}}{\left|\dfrac{\partial \vec{e}_\zeta}{\partial\theta}\right|} = \frac{-\sin\phi \sin\theta\ \vec{e}_x + \sin\phi \cos\theta\ \vec{e}_y}{\sqrt{\sin^2\phi}}$$

or,

$$\vec{e}_\theta = -\sin\theta\,\vec{e}_x + \cos\theta\,\vec{e}_y \tag{A-3}$$

Now, the set of vectors

$$\vec{\psi}_\zeta = \psi_\zeta\ \vec{e}_\zeta \qquad \vec{\psi}_\phi = \psi_\phi\ \vec{e}_\phi \qquad \vec{\psi}_\theta = \psi_\theta\ \vec{e}_\theta$$

can be transformed into the xyz system by use of the unit vector relations, namely

$$\vec{\psi}_\zeta = \psi_\zeta\,(\sin\phi\cos\theta\ \vec{e}_x + \sin\phi\sin\theta\ \vec{e}_y + \cos\phi\ \vec{e}_z) \tag{A-4}$$

$$\vec{\psi}_\phi = \psi_\phi\,(\cos\phi\cos\theta\ \vec{e}_x + \cos\phi\sin\theta\ \vec{e}_y - \sin\phi\ \vec{e}_z) \tag{A-5}$$

$$\vec{\psi}_\theta = \psi_\theta\,(-\sin\theta\ \vec{e}_x + \cos\theta\ \vec{e}_y) \tag{A-6}$$

Let the vectors in the xyz system be denoted by

$$\vec{\xi}_x = \xi_x\ \vec{e}_x \qquad \vec{\xi}_y = \xi_y\ \vec{e}_y \qquad \vec{\xi}_z = \xi_z\ \vec{e}_z$$

These vectors can now be written in terms of the vectors $\vec{\psi}_i$ by summing the appropriate components in Eq. (A-4) - (A-6). Thus,

$$\vec{\xi}_x = (\psi_\zeta \sin\phi \cos\theta + \psi_\phi \cos\phi \cos\theta - \psi_\theta \sin\theta)\, \vec{e}_x \tag{A-7}$$

$$\vec{\xi}_y = (\psi_\zeta \sin\phi \sin\theta + \psi_\phi \cos\phi \sin\theta + \psi_\theta \cos\theta)\, \vec{e}_y \tag{A-8}$$

$$\vec{\xi}_z = (\psi_\zeta \cos\phi - \psi_\phi \sin\phi)\, \vec{e}_z \tag{A-9}$$

from which the inverse relations are obtained

$$\vec{\psi}_\zeta = (\xi_x \sin\phi \cos\theta + \xi_y \sin\phi \sin\theta + \xi_z \cos\phi)\, \vec{e}_\zeta \tag{A-10}$$

$$\vec{\psi}_\phi = (\xi_x \cos\phi \cos\theta + \xi_y \cos\phi \sin\theta - \xi_z \sin\phi)\, \vec{e}_\phi \tag{A-11}$$

$$\vec{\psi}_\theta = (-\xi_x \sin\theta + \xi_y \cos\theta)\, \vec{e}_\theta \tag{A-12}$$

APPENDIX B. Solution of Thermal Loading Problems

Calculation of temperature-induced displacements and stresses involves superposition of two linear loading states. One state consists of fixing all otherwise moveable gridpoints of the structure, then imposing the temperature conditions that induce loading. Formulation of this state yields gridpoint reaction forces that maintain the zero displacement constraint. These gridpoint forces are commonly referred to as "fixed-node forces."

The second loading state is the application of the fixed-node forces with reversed sense at the structural gridpoints. For this loading only the actual displacement constraints are imposed (boundary conditions), and deformation of all other gridpoints is computed.

Superposition of the displacements, stresses, and gridpoint forces from the two states is the solution of the thermal loading problem. Obviously, superposition of the two states results in zero net external forces acting at all unconstrained gridpoints, as should be the case. Actual deformation of the structure is defined by the displacements computed from the loading in the second state. For stresses, numerical results from both loading states must be considered. Actual member stresses are the difference between the values computed based upon the displacements of the second loading state. and the values corresponding to the fixed-node loading.

In using the SAMIS program to solve thermal loading problems, most of the essential data is determined internal to the program. For example, the vector of fixed-node forces is simply the vector resulting from overlay (ADDS) of the individual loading vectors generated by BILD. By subjecting the analytic structural model to this loading (solution by CHOL) the temperature-induced displacements are obtained.

The element stresses that result from the fixed-node loading state are also computed internal to SAMIS. These values are stored as column 05 in each element stress matrix whenever these matrices are generated in a thermal loads problem. Thus, for a thermal problem, the element stress matrix has the following format:

	Codes corresponding to element stiffness matrix codes	05	
Stress component codes	S	Fixed-node stresses	= $[\bar{S}]$

For other than a thermal loading problem, column 05 does not appear in the matrix ($[S] \equiv [\bar{S}]$).

The usual procedure with SAMIS in computing element stresses is to form the product

$$\{\sigma\} = [\bar{S}] \{\delta\}$$

where $\{\delta\}$ is the vector of displacements for the entire structure, but because multiplication in SAMIS is by code matching, only those elements of $\{\delta\}$ are selected that correspond with those of each $[\bar{S}]$. In a thermal stress problem the product $[\bar{S}] \{\delta\}$ yields the stresses corresponding to the second loading state--from which the fixed-node stresses must still be subtracted to obtain the actual stresses.

Because of the code matching technique employed in SAMIS, computation of the actual thermal stresses is very easily effected. The displacement vector $\{\delta\}$ resulting from a thermal loading problem has the column code 05 and row codes corresponding to the gridpoint displacement components. The format is:

	05
Codes corresponding to gridpoint displacement components	δ

To this vector an element is added that has the row code 05, column code 05 and element value -1.0. This changes the format of $\{\delta\}$ to:

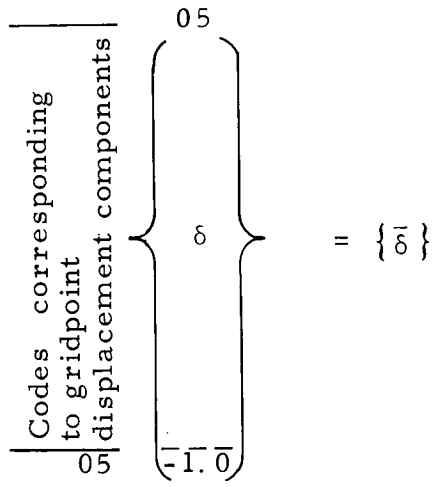

If this vector is used to form the product $[\bar{S}]\{\bar{\delta}\}$, the fixed-node stresses will automatically be subtracted from the stresses of state 2 to obtain the actual stresses in each member.

Addition of the element with codes 05, 05 and value -1.0 to the displacement vector due to thermal loading is a standard procedure with SAMIS and must be executed by use of pseudo instructions in all thermal stress problems if accurate stresses are to be computed.

APPENDIX C. Closed Form Solutions for the Static Loaded Shallow Spherical Shell

Constant Pressure Loading of a Restrained Shallow Spherical Shell

Following the notation and results of Ref. 11 the solution to the problem of the uniformly loaded, restrained spherical shell (Fig. C. 1) follows directly once the constants of integration C_1, C_2 have been determined. Requiring that the meridianal rotation (V) and the horizontal edge displacement (δ) vanish at the edge leads to

$$\tilde{C}_1 = 2\rho\, C_1/pa^2 = \frac{1-\nu}{a(\mu)} \cdot \left(\frac{ber'\mu}{\mu} + \frac{\nu}{\rho^2} \cdot \frac{bei'\mu}{\mu} \right)$$

$$\tilde{C}_2 = 2\rho\, C_2/pa^2 = \frac{1-\nu}{a(\mu)} \cdot \left(\frac{bei'\mu}{\mu} - \frac{\nu}{\rho^2} \cdot \frac{ber'\mu}{\mu} \right)$$

where

$$a(\mu) = bei\,\mu \cdot \frac{ber'\mu}{\mu} - ber\,\mu \cdot \frac{bei'\mu}{\mu} + (1+\nu) \cdot \left[\left(\frac{ber'\mu}{\mu} \right)^2 + \left(\frac{bei'\mu}{\mu} \right)^2 \right]$$

$$+ \frac{\nu}{\rho^2} \cdot \left(bei\,\mu \cdot \frac{bei'\mu}{\mu} + ber\,\mu \cdot \frac{ber'\mu}{\mu} \right)$$

and

$$EahV/\rho^2 = C_1 \cdot \left(-bei'x + \frac{\nu}{\rho^2} \cdot ber'x \right) + C_2 \cdot \left(ber'x + \frac{\nu}{\rho^2} \cdot bei'x \right)$$

$$Eh\delta/\sin\phi = -(1-\nu)pa^2/2 + \rho C_1 \cdot \left(\frac{1+\nu}{x} \cdot ber'x + bei\,x \right)$$

$$+ \rho C_2 \cdot \left(\frac{1+\nu}{x} \cdot bei'x - ber\,x \right)$$

and

$$\rho^4 = 12(1-\nu^2)\left(\frac{a}{h} \right)^2$$

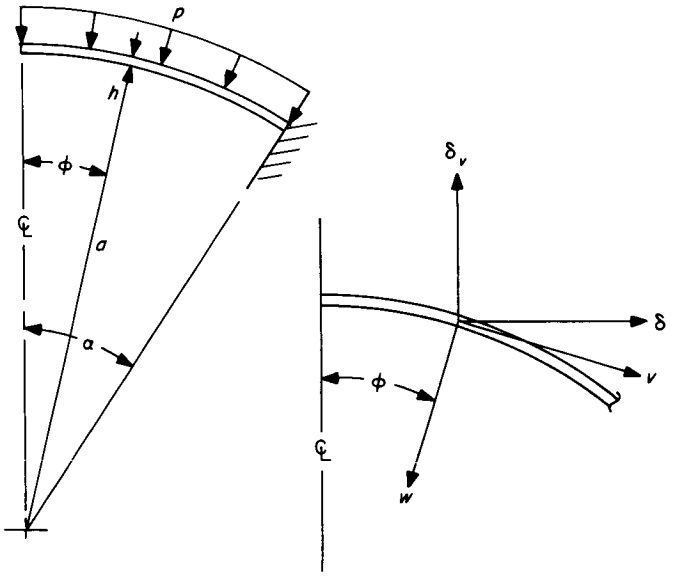

Fig. C. 1. Shell geometry and displacements

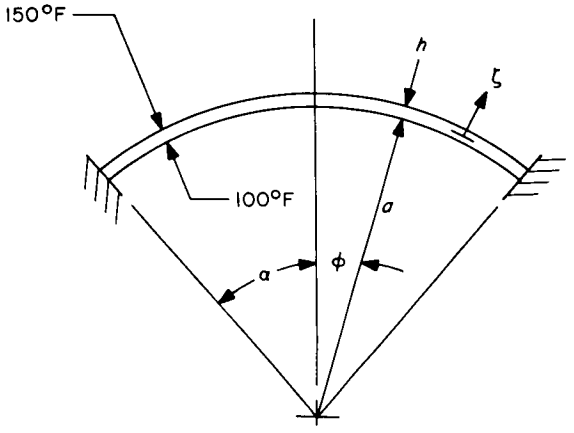

Fig. C. 2. Shell temperature state

The remaining quantities of interest follow as

$$-2N_\phi/pa = 1 + \tilde{C}_1 \cdot \frac{ber'x}{x} + \tilde{C}_2 \cdot \frac{bei'x}{x}$$

$$-2N_\theta/pa = 1 - \tilde{C}_1 \cdot \left(bei\, x + \frac{ber'x}{x}\right) + \tilde{C}_2 \cdot \left(ber\, x - \frac{bei'x}{x}\right)$$

$$2\rho Q_\phi/pa = \tilde{C}_1\, ber'x + \tilde{C}_2 \cdot bei'x$$

$$2\rho^2 M_\phi/pa^2 = \tilde{C}_1 \cdot \left[ber\, x + \frac{\nu}{\rho^2} \cdot bei\, x - (1-\nu) \cdot \left(\frac{bei'x}{x} - \frac{\nu}{\rho^2} \cdot \frac{ber'x}{x}\right)\right]$$

$$+ \tilde{C}_2 \cdot \left[bei\, x - \frac{\nu}{\rho^2} \cdot ber\, x + (1-\nu) \cdot \left(\frac{ber'x}{x} + \frac{\nu}{\rho^2} \cdot \frac{bei'x}{x}\right)\right]$$

$$2\rho^2 M_\theta/pa^2 = \tilde{C}_1 \cdot \left[\nu \cdot \left(ber\, x + \frac{\nu}{\rho^2} \cdot bei\, x\right) + (1-\nu) \cdot \left(\frac{bei'x}{x} - \frac{\nu}{\rho^2} \cdot \frac{ber'x}{x}\right)\right]$$

$$+ \tilde{C}_2 \cdot \left[\nu \cdot \left(bei\, x - \frac{\nu}{\rho^2} \cdot ber\, x\right) - (1-\nu) \cdot \left(\frac{ber'x}{x} + \frac{\nu}{\rho^2} \cdot \frac{bei'x}{x}\right)\right]$$

$$\frac{Eh}{a} \cdot \left(\delta_v + v_o\right) = (N_\theta - \nu N_\phi) \cdot \cos\phi - \frac{1+\nu}{\sin\phi} \cdot Q_\phi$$

The constant v_o can be chosen so that the vertical displacement δ_v vanishes at the edge $x = \mu$. The sign convention for the displacements is shown on Fig. C.1.

Thermal Stresses/Displacements in a Fully Restrained Shallow Spherical Shell

The stresses/displacements in a shallow spherical shell that is heated are taken to be those given by a particular solution of the heated shell on which is superposed a solution for a cold shell. The total solution is required to satisfy the fully restrained boundary condition. The loading is indicated in Fig. C.2.

The particular solution for the heated shell follows from Ref. 12 for a linearly varying temperature distribution through the thickness that is constant otherwise (Fig. C.2), assume

$$\Theta = T_o + \zeta T_1 ; \; T_o, \; T_1 \text{ - const.}$$

$$= \text{Temperature above ambient (strain free)}$$

It follows that

$$\epsilon_\theta = \alpha_t T_o - \frac{\alpha_t T_1 h^2}{24a} \cdot \frac{F\nu - 1}{1 - \nu} = \epsilon_T$$

$$\epsilon_\phi = \alpha_t T_o - \frac{\alpha_t T_1 h^2}{24a} \cdot \frac{F\nu - 1}{1 - \nu}$$

$$V_\theta = 0$$

$$M_\phi, \; M_\theta = (1+\nu) \cdot \alpha_t \, DT_1, \; D = Eh^3/12\left(1-\nu^2\right)$$

$$N_\phi, \; N_\theta, \; Q_\phi = 0$$

The solution for the cold shell is obtained from Ref. 11 once the constants C_1, C_2 are determined to satisfy the boundary conditions that

$$\epsilon_\theta \; (x = \mu) \Big|_{\text{cold}} = - \epsilon_T$$

$$V \; (x = \mu) = 0$$

with

$$\frac{Eah}{\rho} \cdot \epsilon_\theta \Big|_{cold} = C_1 \cdot \left(bei\, x + \frac{1+\nu}{x} \cdot ber'x\right)$$

$$+ C_2 \cdot \left(-ber\, x + \frac{1+\nu}{x} \cdot bei'x\right)$$

$$\frac{Eah}{\rho^2} \cdot V = C_1 \cdot \left(-bei'x + \frac{\nu}{\rho^2} \cdot ber'x\right)$$

$$+ C_2 \cdot \left(ber'x + \frac{\nu}{\rho^2} \cdot bei'x\right)$$

For the cold shell, it follows that

$$C_1 = -\frac{Eah\epsilon_T}{\rho a(\mu)} \cdot \left(\frac{ber'\mu}{\mu} + \frac{\nu}{\rho^2} \cdot \frac{bei'\mu}{\mu}\right)$$

$$C_2 = -\frac{Eah\epsilon_T}{\rho a(\mu)} \cdot \left(\frac{bei'\mu}{\mu} - \frac{\nu}{\rho^2} \cdot \frac{ber'\mu}{\mu}\right)$$

The total solution is then given by

$$N_\phi = -\frac{\rho}{a} \cdot \left(C_1 \cdot \frac{ber'x}{x} + C_2 \cdot \frac{bei'x}{x}\right)$$

$$N_\theta = \frac{\rho}{a} \cdot \left[C_1 \cdot \left(bei\, x + \frac{ber'x}{x}\right) - C_2 \cdot \left(ber\, x - \frac{bei'x}{x}\right)\right]$$

$$Q_\phi = \frac{1}{a} \cdot \left(C_1\, ber'x + C_2\, bei'x\right)$$

$$\frac{hM_\phi}{D} = (1+\nu) \cdot \alpha_t hT_1 + \frac{\rho^3}{Ea^2} \cdot \left\{ C_1 \cdot \left[\text{ber } x + \frac{\nu}{\rho^2} \cdot \text{bei } x - (1-\nu) \cdot \left(\frac{\text{bei}'x}{x} - \frac{\nu}{\rho^2} \cdot \frac{\text{ber}'x}{x} \right) \right] + C_2 \cdot \left[\text{bei } x - \frac{\nu}{\rho^2} \cdot \text{ber } x + (1-\nu) \cdot \left(\frac{\text{ber}'x}{x} + \frac{\nu}{\rho^2} \cdot \frac{\text{bei}'x}{x} \right) \right] \right\}$$

$$hM_\theta/D = (1+\nu)\, \alpha_t hT_1 + \frac{\rho^3}{Ea^2} \cdot \left\{ C_1 \left[\nu \cdot \left(\text{ber } x + \frac{\nu}{\rho^2} \text{ bei } x \right) + (1-\nu) \left(\frac{\text{bei}'x}{x} - \frac{\nu}{\rho^2} \cdot \frac{\text{ber}'x}{x} \right) \right] + C_2 \cdot \left[\nu \cdot \left(\text{bei } x - \frac{\nu}{\rho^2} \cdot \text{ber } x \right) - (1-\nu) \left(\frac{\text{ber}'x}{x} + \frac{\nu}{\rho^2} \cdot \frac{\text{bei}'x}{x} \right) \right] \right\}$$

$$\delta = a \sin\phi \cdot \left\{ \epsilon_T + \frac{\rho}{Eah} \cdot \left[C_1 \cdot \left(\text{bei } x + \frac{1+\nu}{x} \cdot \text{ber}'x \right) + C_2 \cdot \left(-\text{ber } x + \frac{1+\nu}{x} \cdot \text{bei}'x \right) \right] \right\}$$

$$\delta_v + v_o = a\epsilon_T \cdot \cos\phi + \frac{a}{Eh} \cdot \left(N_\theta - \nu N_\phi \right) \cdot \cos\phi - \frac{1+\nu}{Eh} \cdot \frac{aQ_\phi}{\text{Sin}\phi}$$

The constant (v_o) can be chosen so that $\delta_v (x = \mu) = 0$.

Appendix D. Input Data for Shallow Spherical Shell, Static Load Problem

A. Pseudo Instructions

```
1.0   09001  KAR001  10001  SSR001  BILD  11001  TLC001  -10800
2.0   09001  KAR001                 ADDS  13001  KKR001   10800
3.0   11001  TLC001                 ADDS  13002  TSC001   10800
4.0   09001  VTC001                 READ
5.0   09001  VTC001                 FLIP  11001  VFR001
6.0   11001  VFR001  13002  TSC001  MULT  09002  LTC001
7.0   13001  KKR001  09001  VTC001  MULT  12001  KPR001
8.0   12001  KPR001                 COLS  09003  KPC001
9.0   11001  VFR001   9003  KPC001  MULT  12001  KKC001
10.0  12001  KKC001                 ROWS  13001  KKR001
11.0   9002  LTC001                 COLS  13002  TSC001
12.0         WAR001                 READ
13.0         WAR001  13001  KKR001  WASH  11001  KWR001
14.0  11001  KWR001  13002  TSC001  CHOL  12001  DIC001
15.0  09001  VTC001                 ROWS         VTR001
16.0         VTR001  12001  DIC001  MULT  09004  DAC001
17.0  09004  DAC001                 COLS  12001  DIC001
18.0  12001  DIC001                 INKS                      1
19.0  13001  KKR001  12001  DIC001  MULT  11001  RFC001
20.0  11001  RFC001                 INKS                      1
21.0         ATC001                 READ
22.0         ATC001  12001  DIC001  ADDS         DTC001
23.0  10001  SSR001         DTC001  MULT  11001  SAC001   10800
24.0  11001  SAC001                 INKS                   10800
25.0                                HALT
```

B. Material Table

```
2014T6   530.   12.5E-6 16.0E+6  8.0E+6 16.0E+6    0       0       4.0E+6
         8.0E+6  8.0E+6           16.0E+6  4.0E+6            4.0E+6
```

C. Element Data

```
1   1 31      2       3       1                                                 .075 20
2                                                 50     530     150     100
9   1     1.3592          28.468 1.27720.46487 28.468                          28.5   0
1   2 31      3       2       4                                                 .075 20
2                                                 50     530     150     100
9   2     1.27720.46487 28.468 1.3592          28.468 1.92540.33950 28.433 0
1   3 31      2       5       4                                                 .075 20
2                                                 50     530     150     100
9   3     1.3592          28.468 2.8554          28.357 1.92540.33950 28.433 0
1   4 31      3       4       6                                                 .075 20
2                                                 50     530     150     100
9   4     1.27720.46487 28.468 1.92500.33950 28.430 2.683 0.97660 28.357 0
1   5 31      5       6       4                                                 .075 20
2                                                 50     530     150     100
9   5     2.8554          28.357 2.68320.97660 28.357 1.92540.33950 28.433 0
1   6 31      7       8       5                                                 .075 20
2                                                 50     530     150     100
9   6     4.3437          28.167 4.27770.75428 28.167 2.8554          28.357 0
1   7 31      6       5       8                                                 .075 20
2                                                 50     530     150     100
9   7     2.68320.97660 28.357 2.8554          28.357 4.27770.75428 28.167 0
1   8 31      8       9       6                                                 .075 20
2                                                 50     530     150     100
9   8     4.27770.75428 28.167 4.08171.4856  28.170 2.68320.97660 28.357 0
1   9 31     10      11       7                                                 .075 20
2                                                 50     530     150     100
9   9     5.8200          27.900 5.79780.50727 27.900 4.3437          28.167 0
1  10 31      8       7      11                                                 .075 20
2                                                 50     530     150     100
9  10     4.27770.75428 28.167 4.3437          28.167 5.79780.50727 27.900 0
1  11 31     11      12       8                                                 .075 20
2                                                 50     530     150     100
9  11     5.79780.50727 27.900 5.73161.0106  27.900 4.27770.75428 28.167 0
1  12 31     12      13       8                                                 .075 20
2                                                 50     530     150     100
9  12     5.73161.0106  27.900 5.62171.5063  27.900 4.27770.75428 28.167 0
1  13 31      9       8      13                                                 .075 20
2                                                 50     530     150     100
9  13     4.08171.4856  28.167 4.27770.75428 28.167 5.62171.5063  27.900 0
1  14 31     13      14       9                                                 .075 20
2                                                 50     530     150     100
9  14     5.62171.5063  27.900 5.46901.9906  27.900 4.08171.4856  28.167 0
1  15 31     11      10      15                                                 .075 20
2                                                 50     530     150     100
9  15     5.79780.50727 27.900 5.8200          27.900 6.7981          27.677 0
1  16 31     15      16      11                                                 .075 20
2                                                 50     530     150     100
9  16     6.7981          27.677 6.75210.78919 27.677 5.79780.50727 27.900 0
1  17 31     12      11      16                                                 .075 20
2                                                 50     530     150     100
9  17     5.73161.0106  27.900 5.79780.50727 27.900 6.75210.78919 27.677 0
1  18 31     16      17      12                                                 .075 20
2                                                 50     530     150     100
9  18     6.75210.78919 27.677 6.61481.5678  27.677 5.73161.0106  27.900 0
1  19 31     13      12      17                                                 .075 20
2                                                 50     530     150     100
9  19     5.62171.5063  27.900 5.73161.0106  27.900 6.61481.5678  27.677 0
1  20 31     17      18      13                                                 .075 20
2                                                 50     530     150     100
```

```
9 20     6.61481.5678  27.677 6.38812.3251  27.677 5.62171.5063  27.900 0
1 21 31      14      13      18                                    .075 20
2                                        50     530     150     100
9 21     5.46901.9906  27.900 5.62171.5063  27.900 6.38812.3251  27.677 0
1 22 31      19      20      15                                    .075 20
2                                        50     530     150     100
9 22     7.7600        27.423 7.74690.45117 27.423 6.7981        27.677 0
1 23 31      16      15      20                                    .075 20
2                                        50     530     150     100
9 23     6.75210.78919 27.677 6.7981        27.677 7.74690.45117 27.423 0
1 24 31      20      21      16                                    .075 20
2                                        50     530     150     100
9 24     7.74690.45117 27.423 7.70750.90086 27.423 6.75210.78919 27.677 0
1 25 31      21      22      16                                    .075 20
2                                        50     530     150     100
9 25     7.70750.90086 27.423 7.64211.3475  27.423 6.75210.78919 27.677 0
1 26 31      17      16      22                                    .075 20
2                                        50     530     150     100
9 26     6.61481.5678  27.677 6.75210.78919 27.677 7.64211.3475  27.423 0
1 27 31      22      23      17                                    .075 20
2                                        50     530     150     100
9 27     7.64211.3475  27.423 7.55081.7896  27.423 6.61481.5678  27.677 0
1 28 31      23      24      17                                    .075 20
2                                        50     530     150     100
9 28     7.55081.7896  27.423 7.43402.2256  27.423 6.61481.5678  27.677 0
1 29 31      18      17      24                                    .075 20
2                                        50     530     150     100
9 29     6.38812.3251  27.677 6.61481.5678  27.677 7.43402.2256  27.423 0
1 30 31      24      25      18                                    .075 20
2                                        50     530     150     100
9 30     7.43402.2256  27.423 7.29202.6541  27.423 6.38812.3251  27.677 0
1 31 31      26      27      19                                    .075 20
2                                        50     530     150     100
9 31     8.2453        27.281 8.24180.23977 27.281 7.7600        27.423 0
1 32 31      20      19      27                                    .075 20
2                                        50     530     150     100
9 32     7.74690.45117 27.423 7.7600        27.423 8.24180.23977 27.281 0
1 33 31      27      28      20                                    .075 20
2                                        50     530     150     100
9 33     8.24180.23977 27.281 8.21390.71866 27.281 7.74690.45117 27.423 0
1 34 31      21      20      28                                    .075 20
2                                        50     530     150     100
9 34     7.70750.90086 27.423 7.74690.45117 27.423 8.21390.71866 27.281 0
1 35 31      28      29      21                                    .075 20
2                                        50     530     150     100
9 35     8.21390.71866 27.281 8.15821.1950  27.281 7.70750.90086 27.423 0
1 36 31      22      21      29                                    .075 20
2                                        50     530     150     100
9 36     7.64211.3475  27.423 7.70750.90086 27.423 8.15821.1950  27.281 0
1 37 31      29      30      22                                    .075 20
2                                        50     530     150     100
9 37     8.15821.1950  27.281 8.07501.6674  27.281 7.64211.3475  27.423 0
1 38 31      23      22      30                                    .075 20
2                                        50     530     150     100
9 38     7.55081.7896  27.423 7.64211.3475  27.423 8.07501.6674  27.281 0
1 39 31      30      31      23                                    .075 20
2                                        50     530     150     100
9 39     8.07501.6674  27.281 7.96442.1340  27.281 7.55081.7896  27.423 0
1 40 31      24      23      31                                    .075 20
```

```
2                                                          50     530     150     100
9 40     7.43402.2256  27.423 7.55081.7896  27.423 7.96442.1340  27.281 0
1 41 31      31      32      24                                                .075 20
2                                                          50     530     150     100
9 41     7.96442.1340  27.281 7.82682.5935  27.281 7.43402.2256  27.423 0
1 42 31      25      24      32                                                .075 20
2                                                          50     530     150     100
9 42     7.29202.6541  27.423 7.43402.2256  27.423 7.82682.5935  27.281 0
1 43 31      32      33      25                                                .075 20
2                                                          50     530     150     100
9 43     7.82682.5935  27.281 7.74802.8201  27.281 7.29202.6541  27.423 0
1 44 31      27      26      34                                                .075 20
2                                                          50     530     150     100
9 44     8.24180.23977 27.281 8.2453        27.281 8.7201        27.133 0
1 45 31      34      35      27                                                .075 20
2                                                          50     530     150     100
9 45     8.7201        27.133 8.70540.50699 27.133 8.24180.23977 27.281 0
1 46 31      28      27      35                                                .075 20
2                                                          50     530     150     100
9 46     8.21390.71866 27.281 8.24180.23977 27.281 8.70540.50699 27.133 0
1 47 31      35      36      28                                                .075 20
2                                                          50     530     150     100
9 47     8.70540.50699 27.133 8.66121.0123  27.133 8.21390.71866 27.281 0
1 48 31      29      28      36                                                .075 20
2                                                          50     530     150     100
9 48     8.15821.1950  27.281 8.21390.71866 27.281 8.66121.0123  27.133 0
1 49 31      36      37      29                                                .075 20
2                                                          50     530     150     100
9 49     8.66121.0123  27.133 8.58761.5142  27.133 8.15821.1950  27.281 0
1 50 31      30      29      37                                                .075 20
2                                                          50     530     150     100
9 50     8.07501.6674  27.281 8.15821.1950  27.281 8.58761.5142  27.133 0
1 51 31      37      38      30                                                .075 20
2                                                          50     530     150     100
9 51     8.58761.5142  27.133 8.48502.0110  27.133 8.07501.6674  27.281 0
1 52 31      31      30      38                                                .075 20
2                                                          50     530     150     100
9 52     7.96442.1340  27.281 8.07501.6674  27.281 8.48502.0110  27.133 0
1 53 31      38      39      31                                                .075 20
2                                                          50     530     150     100
9 53     8.48502.0110  27.133 8.35382.5009  27.133 7.96442.1340  27.281 0
1 54 31      32      31      39                                                .075 20
2                                                          50     530     150     100
9 54     7.82682.5935  27.281 7.96442.1340  27.281 8.35382.5009  27.133 0
1 55 31      39      40      32                                                .075 20
2                                                          50     530     150     100
9 55     8.35382.5009  27.133 8.19422.9824  27.133 7.82682.5935  27.281 0
1 56 31      33      32      40                                                .075 20
2                                                          50     530     150     100
9 56     7.74802.8201  27.281 7.82682.5935  27.281 8.19422.9824  27.133 0
1 57 31      41      42      34                                                .075 20
2                                                          50     530     150     100
9 57     9.1924        26.977 9.19010.26736 26.977 8.7201        27.133 0
1 58 31      35      34      42                                                .075 20
2                                                          50     530     150     100
9 58     8.70540.50699 27.133 8.7201        27.133 9.19010.26736 26.977 0
1 59 31      42      43      35                                                .075 20
2                                                          50     530     150     100
9 59     9.19010.26736 26.977 9.15900.80135 26.977 8.70540.50699 27.133 0
```

```
1 60 31      36      35      43                                          .075 20
2                                          50     530     150     100
9 60     8.66121.0123  27.133 8.70540.50699 27.133 9.15900.80135 26.977 0
1 61 31      43      44      36                                          .075 20
2                                          50     530     150     100
9 31     9.15900.80135 26.977 9.09691.3325  26.977 8.66121.0123  27.133 0
1 62 31      37      36      44                                          .075 20
2                                          50     530     150     100
9 62     8.58761.5142  27.133 8.66121.0123  27.133 9.09691.3325  26.977 0
1 63 31      44      45      37                                          .075 20
2                                          50     530     150     100
9 63     9.09691.3325  26.977 9.00411.8592  26.977 8.58801.51400 27.130 0
1 64 31      38      37      45                                          .075 20
2                                          50     530     150     100
9 64     8.48502.0110  27.133 8.58761.5142  27.133 9.00411.8592  26.977 0
1 65 31      45      46      38                                          .075 20
2                                          50     530     150     100
9 65     9.00411.8592  26.977 8.88082.3796  26.977 8.48502.0110  27.133 0
1 66 31      39      38      46                                          .075 20
2                                          50     530     150     100
9 66     8.35382.5009  27.133 8.48502.0110  27.133 8.88082.3796  26.977 0
1 67 31      46      47      39                                          .075 20
2                                          50     530     150     100
9 67     8.88082.3796  26.977 8.72732.8919  26.977 8.35382.5009  27.133 0
1 68 31      40      39      47                                          .075 20
2                                          50     530     150     100
9 68     8.19422.9824  27.133 8.35382.5009  27.133 8.72732.8919  26.977 0
1 69 31      47      48      40                                          .075 20
2                                          50     530     150     100
9 69     8.72732.8919  26.977 8.63803.1440  26.977 8.19422.9824  27.133 0
1 70 31      42      41      49                                          .075 20
2                                          50     530     150     100
9 70     9.19010.26736 26.977 9.1924        26.977 9.6618        26.812 0
1 71 31      49      50      42                                          .075 20
2                                          50     530     150     100
9 71     9.6618        26.812 9.64550.56174 26.812 9.19010.26736 26.977 0
1 72 31      43      42      50                                          .075 20
2                                          50     530     150     100
9 72     9.15900.80135 26.977 9.19010.26736 26.977 9.64550.56174 26.812 0
1 73 31      50      51      43                                          .075 20
2                                          50     530     150     100
9 73     9.64550.56174 26.812 9.59651.1216  26.812 9.15900.80135 26.977 0
1 74 31      44      43      51                                          .075 20
2                                          50     530     150     100
9 74     9.09691.3325  26.977 9.15900.80135 26.977 9.59651.1216  26.812 0
1 75 31      51      52      44                                          .075 20
2                                          50     530     150     100
9 75     9.59651.1216  26.812 9.51501.6778  26.812 9.09691.3325  26.977 0
1 76 31      45      44      52                                          .075 20
2                                          50     530     150     100
9 76     9.00411.8592  26.977 9.09691.3325  26.977 9.51501.6778  26.812 0
1 77 31      52      53      45                                          .075 20
2                                          50     530     150     100
9 77     9.51501.6778  26.812 9.40132.2282  26.812 9.00411.8592  26.977 0
1 78 31      46      45      53                                          .075 20
2                                          50     530     150     100
9 78     8.88082.3796  26.977 9.00411.8592  26.977 9.40132.2282  26.812 0
1 79 31      53      54      46                                          .075 20
2                                          50     530     150     100
```

```
9 79     9.40132.2282  26.812 9.25592.7710  26.812 8.88082.3796  26.977 0
1 80 31      47      46      54                                    .075 20
2                                          50     530     150     100
9 80     8.72732.8919  26.977 8.88082.3796  26.977 9.25592.7710  26.812 0
1 81 31      54      55      47                                    .075 20
2                                          50     530     150     100
9 81     9.25592.7710  26.812 9.07913.3045  26.812 8.72732.8919  26.977 0
1 82 31      48      47      55                                    .075 20
2                                          50     530     150     100
9 82     8.63803.1440  26.977 8.72732.8919  26.977 9.07913.3045  26.812 0
1 83 31      56      57      49                                    .075 20
2                                          50     530     150     100
9 83    10.136         26.63710.132 0.29475 26.637 9.6618        26.812 0
1 84 31      50      49      57                                    .075 20
2                                          50     530     150     100
9 84     9.64550.56174 26.812 9.6618          26.81210.132 0.29475 26.637 0
1 85 31      57      58      50                                    .075 20
2                                          50     530     150     100
9 85    10.132 0.29475 26.63710.097 0.88345 26.637 9.64550.56174 26.812 0
1 86 31      51      50      58                                    .075 20
2                                          50     530     150     100
9 86     9.59651.1216  26.812 9.64550.56174 26.81210.097 0.88345 26.637 0
1 87 31      58      59      51                                    .075 20
2                                          50     530     150     100
9 87    10.097 0.88345 26.63710.029 1.4690  26.637 9.59651.1216  26.812 0
1 88 31      52      51      59                                    .075 20
2                                          50     530     150     100
9 88     9.51501.6778  26.812 9.59651.1216  26.81210.029 1.4690  26.637 0
1 89 31      59      60      52                                    .075 20
2                                          50     530     150     100
9 89    10.029 1.4690  26.637 9.92662.0497  26.637 9.51501.6778  26.812 0
1 90 31      53      52      60                                    .075 20
2                                          50     530     150     100
9 90     9.40132.2282  26.812 9.51501.6778  26.812 9.92662.0497  26.637 0
1 91 31      60      61      53                                    .075 20
2                                          50     530     150     100
9 91     9.92662.0497  26.637 9.79072.6234  26.637 9.40132.2282  26.812 0
1 92 31      54      53      61                                    .075 20
2                                          50     530     150     100
9 92     9.25592.7710  26.812 9.40132.2282  26.812 9.79072.6234  26.637 0
1 93 31      61      62      54                                    .075 20
2                                          50     530     150     100
9 93     9.79072.6234  26.637 9.62153.1882  26.637 9.25592.7710  26.812 0
1 94 31      55      54      62                                    .075 20
2                                          50     530     150     100
9 94     9.07913.3045  26.812 9.25592.7710  26.812 9.62153.1882  26.637 0
1 95 31      62      63      55                                    .075 20
2                                          50     530     150     100
9 95     9.62153.1882  26.637 9.52473.4667  26.637 9.07913.3045  26.812 0
1 96 31      57      56      64                                    .075 20
2                                          50     530     150     100
9 96    10.132 0.29475 26.63710.136           26.63710.6          26.456 0
1 97 31      64      65      57                                    .075 20
2                                          50     530     150     100
9 97    10.6           26.45610.582 0.61628 26.45610.132 0.29475 26.637 0
1 98 31      58      57      65                                    .075 20
2                                          50     530     150     100
9 98    10.097 0.88345 26.63710.132 0.29475 26.63710.582 0.61628 26.456 0
1 99 31      65      66      58                                    .075 20
```

```
2                                                    50    530    150    100
9 99   10.582 0.61628 26.45610.528 1.2306  26.45610.097 0.88345 26.637 0
1100 31     59     58     66                                          .075 20
2                                                    50    530    150    100
9100   10.029 1.4690  26.63710.097 0.88345 26.63710.528 1.2306  26.456 0
1101 31     66     67     59                                          .075 20
2                                                    50    530    150    100
9101   10.528 1.2306  26.45610.439 1.8407  26.45610.029 1.4690  26.637 0
1102 31     60     59     67                                          .075 20
2                                                    50    530    150    100
9102    9.92662.0497  26.63710.029 1.4690  26.63710.439 1.8407  26.456 0
1103 31     67     68     60                                          .075 20
2                                                    50    530    150    100
9103   10.439 1.8407  26.45610.314 2.4446  26.456 9.92662.0497  26.637 0
1104 31     61     60     68                                          .075 20
2                                                    50    530    150    100
9104    9.79072.6234  26.637 9.92662.0497  26.63710.314 2.4446  26.456 0
1105 31     68     69     61                                          .075 20
2                                                    50    530    150    100
9105   10.314 2.4446  26.45610.155 3.0401  26.456 9.79072.6234  26.637 0
1106 31     62     61     69                                          .075 20
2                                                    50    530    150    100
9106    9.6215 3.1882 26.637 9.7907 2.6234 26.63710.155  3.0401 26.456 0
1107 31     69     70     62                                          .075 20
2                                                    50    530    150    100
9107   10.155  3.0401 26.456 9.9607 3.6254 26.456 9.6215 3.1882 26.637 0
1108 31     63     62     70                                          .075 20
2                                                    50    530    150    100
9108    9.5247 3.4667 26.637 9.6215 3.1882 26.637 9.9607 3.6254 26.456 0
```

D. Matrix Data and Title Cards

VTC001	142		1	0				
11	11	1.0	12	12	1.0	13	13	1.0
14	14	1.0	15	15	1.0	16	16	1.0
21	21	1.0	22	22	1.0	23	23	1.0
24	24	1.0	25	25	1.0	26	26	1.0
31	31	0.940	32	31	0.342	31	32	-0.342
32	32	0.940	33	33	1.0	34	34	0.940
35	34	0.342	34	35	-0.342	35	35	0.940
36	36	1.0	41	41	1.0	42	42	1.0
43	43	1.0	44	44	1.0	45	45	1.0
46	46	1.0	51	51	1.0	52	52	1.0
53	53	1.0	54	54	1.0	55	55	1.0
56	56	1.0	61	61	0.940	62	61	0.342
61	62	-0.342	62	62	0.940	63	63	1.0
64	64	0.940	65	64	0.342	64	65	-0.342
65	65	0.940	66	66	1.0	71	71	1.0
72	72	1.0	73	73	1.0	74	74	1.0
75	75	1.0	76	76	1.0	81	81	1.0
82	82	1.0	83	83	1.0	84	84	1.0
85	85	1.0	86	86	1.0	91	91	0.940
92	91	0.342	91	92	-0.342	92	92	0.940
93	93	1.0	94	94	0.940	95	94	0.342
94	95	-0.342	95	95	0.940	96	96	1.0
101	101	1.0	102	102	1.0	103	103	1.0
104	104	1.0	105	105	1.0	106	106	1.0
111	111	1.0	112	112	1.0	113	113	1.0
114	114	1.0	115	115	1.0	116	116	1.0
121	121	1.0	122	122	1.0	123	123	1.0
124	124	1.0	125	125	1.0	126	126	1.0
131	131	1.0	132	132	1.0	133	133	1.0
134	134	1.0	135	135	1.0	136	136	1.0
141	141	0.940	142	141	0.342	141	142	-0.342
142	142	0.940	143	143	1.0	144	144	0.940
145	144	0.342	144	145	-0.342	145	145	0.940
146	146	1.0	151	151	1.0	152	152	1.0
153	153	1.0	154	154	1.0	155	155	1.0
156	156	1.0	161	161	1.0	162	162	1.0
163	163	1.0	164	164	1.0	165	165	1.0
166	166	1.0	171	171	1.0	172	172	1.0
173	173	1.0	174	174	1.0	175	175	1.0
176	176	1.0						
181	181	0.940	182	181	0.342	181	182	-0.342
182	182	0.940	183	183	1.0	184	184	0.940
185	184	0.342	184	185	-0.342	185	185	0.940
186	186	1.0	191	191	1.0	192	192	1.0
193	193	1.0	194	194	1.0	195	195	1.0
196	196	1.0	201	201	1.0	202	202	1.0
203	203	1.0	204	204	1.0	205	205	1.0
206	206	1.0	211	211	1.0	212	212	1.0
213	213	1.0	214	214	1.0	215	215	1.0
216	216	1.0	221	221	1.0	222	222	1.0
223	223	1.0	224	224	1.0	225	225	1.0
226	226	1.0	231	231	1.0	232	232	1.0
233	233	1.0	234	234	1.0	235	235	1.0
236	236	1.0	241	241	1.0	242	242	1.0
243	243	1.0	244	244	1.0	245	245	1.0
246	246	1.0	251	251	0.940	252	251	0.342
251	252	-0.342	252	252	0.940	253	253	1.0
254	254	0.940	255	254	0.342	254	255	-0.342

255	255	0.940	256	256	1.0	261	261	1.0
262	262	1.0	263	263	1.0	264	264	1.0
265	265	1.0	266	266	1.0	271	271	1.0
272	272	1.0	273	273	1.0	274	274	1.0
275	275	1.0	276	276	1.0	281	281	1.0
282	282	1.0	283	283	1.0	284	284	1.0
285	285	1.0	286	286	1.0	291	291	1.0
292	292	1.0	293	293	1.0	294	294	1.0
295	295	1.0	296	296	1.0	301	301	1.0
302	302	1.0	303	303	1.0	304	304	1.0
305	305	1.0	306	306	1.0	311	311	1.0
312	312	1.0	313	313	1.0	314	314	1.0
315	315	1.0	316	316	1.0	321	321	1.0
322	322	1.0	323	323	1.0	324	324	1.0
325	325	1.0	326	326	1.0	331	331	0.940
332	331	0.342	331	332	-0.342	332	332	0.940
333	333	1.0	334	334	0.940	335	334	0.342
334	335	-0.342	335	335	0.940	336	336	1.0
341	341	1.0	342	342	1.0	343	343	1.0
344	344	1.0	345	345	1.0	346	346	1.0
351	351	1.0	352	352	1.0	353	353	1.0
354	354	1.0	355	355	1.0	356	356	1.0
361	361	1.0	362	362	1.0	363	363	1.0
364	364	1.0	365	365	1.0	366	366	1.0
371	371	1.0	372	372	1.0	373	373	1.0
374	374	1.0	375	375	1.0	376	376	1.0
381	381	1.0	382	382	1.0	383	383	1.0
384	384	1.0	385	385	1.0	386	386	1.0
391	391	1.0	392	392	1.0	393	393	1.0
394	394	1.0	395	395	1.0	396	396	1.0
401	401	0.940	402	401	0.342	401	402	-0.342
402	402	0.940	403	403	1.0	404	404	0.940
405	404	0.342	404	405	-0.342	405	405	0.940
406	406	1.0	411	411	1.0	412	412	1.0
413	413	1.0	414	414	1.0	415	415	1.0
416	416	1.0	421	421	1.0	422	422	1.0
423	423	1.0	424	424	1.0	425	425	1.0
426	426	1.0	431	431	1.0	432	432	1.0
433	433	1.0	434	434	1.0	435	435	1.0
436	436	1.0	441	441	1.0	442	442	1.0
443	443	1.0	444	444	1.0	445	445	1.0
446	446	1.0	451	451	1.0	452	452	1.0
453	453	1.0	454	454	1.0	455	455	1.0
456	456	1.0	461	461	1.0	462	462	1.0
463	463	1.0	464	464	1.0	465	465	1.0
466	466	1.0	471	471	1.0	472	472	1.0
473	473	1.0	474	474	1.0	475	475	1.0
476	476	1.0	481	481	0.940	482	481	0.342
481	482	-0.342	482	482	0.940	483	483	1.0
484	484	0.940	485	484	0.342	484	485	-0.342
485	485	0.940	486	486	1.0	491	491	1.0
492	492	1.0	493	493	1.0	494	494	1.0
495	495	1.0	496	496	1.0	501	501	1.0
502	502	1.0	503	503	1.0	504	504	1.0
505	505	1.0	506	506	1.0	511	511	1.0
512	512	1.0	513	513	1.0	514	514	1.0
515	515	1.0	516	516	1.0	521	521	1.0
522	522	1.0	523	523	1.0	524	524	1.0
525	525	1.0	526	526	1.0	531	531	1.0

532	532	1.0	533	533	1.0	534	534	1.0
535	535	1.0	536	536	1.0	541	541	1.0
542	542	1.0	543	543	1.0	544	544	1.0
545	545	1.0	546	546	1.0	551	551	0.940
552	551	0.342	551	552	-0.342	552	552	0.940
553	553	1.0	554	554	0.940	555	554	0.342
554	555	-0.342	555	555	0.940	556	556	1.0
561	561	1.0	562	562	1.0	563	563	1.0
564	564	1.0	565	565	1.0	566	566	1.0
571	571	1.0	572	572	1.0	573	573	1.0
574	574	1.0	575	575	1.0	576	576	1.0
581	581	1.0	582	582	1.0	583	583	1.0
584	584	1.0	585	585	1.0	586	586	1.0
591	591	1.0	592	592	1.0	593	593	1.0
594	594	1.0	595	595	1.0	596	596	1.0
601	601	1.0	602	602	1.0	603	603	1.0
604	604	1.0	605	605	1.0	606	606	1.0
611	611	1.0	612	612	1.0	613	613	1.0
614	614	1.0	615	615	1.0	616	616	1.0
621	621	1.0	622	622	1.0	623	623	1.0
624	624	1.0	625	625	1.0	626	626	1.0
631	631	0.940	632	631	0.342	631	632	-0.342
632	632	0.940	633	633	1.0	634	634	0.940
635	634	0.342	634	635	-0.342	635	635	0.940
636	636	1.0						

WAR001	24		-1	0				
11	11	0	12	12	0	14	14	0
15	15	0	16	16	0	22	22	0
24	24	0	26	26	0	32	32	0
34	34	0	36	36	0	52	52	0
54	54	0	56	56	0	62	62	0
64	64	0	66	66	0	72	72	0
74	74	0	76	76	0	92	92	0
94	94	0	96	96	0	102	102	0
104	104	0	106	106	0	142	142	0
144	144	0	146	146	0	152	152	0
154	154	0	156	156	0	182	182	0
184	184	0	186	186	0	192	192	0
194	194	0	196	196	0	252	252	0
254	254	0	256	256	0	262	262	0
264	264	0	266	266	0	332	332	0
334	334	0	336	336	0	342	342	0
344	344	0	346	346	0	402	402	0
404	404	0	406	406	0	412	412	0
414	414	0	416	416	0	482	482	0
484	484	0	486	486	0	492	492	0
494	494	0	496	496	0	552	552	0
554	554	0	556	556	0	562	562	0
564	564	0	566	566	0	632	632	0
634	634	0	636	636	0			

```
                    G R I D P O I N T   D I S P L A C E M E N T S
                    G R I D P O I N T   R E A C T I O N   F O R C E S
ATC001      1                   1     0
      5     5        -1.0
                              E L E M E N T   S T R E S S E S
```

Appendix E. Input Data for Shallow Spherical Shell Dynamic Characteristics Problem

A. Pseudo Instructions

```
C SHALLOW SHELL PROBLEM. LOW FREQUENCY FLEXURAL MODES OF FREE SHELL.
C
C FORMATION OF THE STRUCTURE MASS AND STIFFNESS MATRICES.
C
     1.0   09001  KER001                        BILD                          5402
     1.5   10001  MER001                        CONT
     2.0   10001  MER001                        ADDS   11001  MAR001        5400
     3.0    9001  KER001                        ADDS   11002  KAR001        5400
C
C IMPOSITION OF SYMMETRY AND BOUNDARY CONDITIONS.
C
     4.0    9001  VTR001                        READ
     5.0    9001  VTR001                        COLS    9002  VTC001
     6.0    9002  VTC001                        FLIP    9003  VFR001
     7.0   11002  KAR001    9002  VTC001        MULT   10001  KVC001
     8.0   09003  VFR001   10001  KVC001        MULT   10002  KTC001
     9.0   10002  KTC001                        ROWS   11003  KTR001
    10.0   11001  MAR001    9002  VTC001        MULT   10001  MVC001
    11.0    9003  VFR001   10001  MVC001        MULT   10002  MTC001
C
C DECOMPOSITION OF THE MASS MATRIX.
C
    12.0   10002  MTC001                        ROWS   11004  MTR001
    13.0   11004  MTR001    9002  MRR001        CHIN   11005  MIR001
    14.0    9002  MRR001                        FLIP   10001  MFC001
C
C FORMATION OF THE DYNAMIC MATRIX.
C
    15.0   11003  KTR001   10001  MFC001        CHOL   10002  KBC001
    16.0    9002  MRR001   10002  KBC001        MULT   11006  DYC001
    17.0   11006  DYC001                        DECO   10001  DYD001
C
C DETERMINATION OF EIGENVALUES AND EIGENVECTORS.
C
    18.0   10001  DYD001   10002  EVD001        ROOT   10003  EID001        -100
    19.0   10002  EVD001                        CODE    9002  EVC001
C
C INVERSE TRANSFORMATION OF THE EIGENVECTORS.
C
    20.0   11005  MIR001    9002  EVC001        MULT   11007  ETC001
    21.0   11007  ETC001                        COLS   10004  ETC001
    22.0    9001  VTR001   10004  ETC001        MULT   11007  ETC001
C
C PRINTOUT OF RESULTS.
C
    23.0   10003  EID001                        INKS                            1
    24.0   11007  ETC001                        INKS                            1
    25.0                                        HALT
```

B. Material Table

```
  2014T6    530.0 12.5E-6 16.0E+6  8.0E+6 16.0E+6                        4.0E+6
          8.0E+6  8.0E+6          16.0E+6  4.0E+6          4.0E+6
0000000000000
```

C. Element Data

```
1  1 31      1       2       3                                    1.96E-5 0.075 20
9  1      0.0     0.0    28.50   1.800   0.0    28.44   1.273   1.273  28.44 0
1  2 31      1       3       4                                    1.96E-5 0.075 20
9  2      0.0     0.0    28.50   1.273   1.273  28.44   0.0     1.800  28.44 0
1  3 31      2       5       6                                    1.96E-5 0.075 20
9  3      1.800   0.0    28.44   3.500   0.0    28.28   3.233   1.339  28.28 0
1  4 31      6       3       2                                    1.96E-5 0.075 20
9  4      3.233   1.339  28.28   1.273   1.273  28.44   1.800   0.0    28.44 0
1  5 31      3       6       7                                    1.96E-5 0.075 20
9  5      1.273   1.273  28.44   3.233   1.339  28.28   2.475   2.475  28.28 0
1  6 31      3       7       8                                    1.96E-5 0.075 20
9  6      1.273   1.273  28.44   2.475   2.475  28.28   1.339   3.233  28.28 0
1  7 31      8       4       3                                    1.96E-5 0.075 20
9  7      1.339   3.233  28.28   0.0     1.800  28.44   1.273   1.273  28.44 0
1  8 31      4       8       9                                    1.96E-5 0.075 20
9  8      0.0     1.800  28.44   1.339   3.233  28.28   0.0     3.500  28.28 0
1  9 31      5      10      11                                    1.96E-5 0.075 20
9  9      3.500   0.0    28.28   5.200   0.0    28.02   5.100   1.014  28.02 0
1 10 31     11       6       5                                    1.96E-5 0.075 20
9 10      5.100   1.014  28.02   3.233   1.339  28.28   3.500   0.0    28.28 0
1 11 31      6      11      12                                    1.96E-5 0.075 20
9 11      3.233   1.339  28.28   5.100   1.014  28.02   4.326   2.889  28.02 0
1 12 31     12       7       6                                    1.96E-5 0.075 20
9 12      4.326   2.889  28.02   2.475   2.475  28.28   3.233   1.339  28.28 0
1 13 31      7      12      13                                    1.96E-5 0.075 20
9 13      2.475   2.475  28.28   4.326   2.889  28.02   2.889   4.326  28.02 0
1 14 31     13       8       7                                    1.96E-5 0.075 20
9 14      2.889   4.326  28.02   1.339   3.233  28.28   2.475   2.475  28.28 0
1 15 31      8      13      14                                    1.96E-5 0.075 20
9 15      1.339   3.233  28.28   2.889   4.326  28.02   1.014   5.100  28.02 0
1 16 31     14       9       8                                    1.96E-5 0.075 20
9 16      1.014   5.100  28.02   0.0     3.500  28.28   1.339   3.233  28.28 0
1 17 31      9      14      15                                    1.96E-5 0.075 20
9 17      0.0     3.500  28.28   1.014   5.100  28.02   0.0     5.200  28.02 0
1 18 31     16      11      10                                    1.96E-5 0.075 20
9 18      6.900   0.0    27.65   5.100   1.014  28.02   5.200   0.0    28.02 0
1 19 31     11      16      17                                    1.96E-5 0.075 20
9 19      5.100   1.014  28.02   6.900   0.0    27.65   6.375   2.640  27.65 0
1 20 31     17      12      11                                    1.96E-5 0.075 20
9 20      6.375   2.640  27.65   4.326   2.889  28.02   5.100   1.014  28.02 0
1 21 31     12      17      18                                    1.96E-5 0.075 20
9 21      4.326   2.889  28.02   6.375   2.640  27.65   4.879   4.879  27.65 0
1 22 31     18      13      12                                    1.96E-5 0.075 20
9 22      4.879   4.879  27.65   2.889   4.326  28.02   4.326   2.889  28.02 0
1 23 31     13      18      19                                    1.96E-5 0.075 20
9 23      2.889   4.326  28.02   4.879   4.879  27.65   2.640   6.375  27.65 0
1 24 31     19      14      13                                    1.96E-5 0.075 20
9 24      2.640   6.375  27.65   1.014   5.100  28.02   2.889   4.326  28.02 0
1 25 31     14      19      20                                    1.96E-5 0.075 20
9 25      1.014   5.100  28.02   2.640   6.375  27.65   0.0     6.900  27.65 0
1 26 31     20      15      14                                    1.96E-5 0.075 20
9 26      0.0     6.900  27.65   0.0     5.200  28.02   1.014   5.100  28.02 0
1 27 31     16      21      22                                    1.96E-5 0.075 20
9 27      6.900   0.0    27.65   8.700   0.0    27.14   8.533   1.697  27.14 0
1 28 31     22      17      16                                    1.96E-5 0.075 20
9 28      8.533   1.697  27.14   6.375   2.640  27.65   6.900   0.0    27.65 0
1 29 31     17      22      23                                    1.96E-5 0.075 20
```

```
9 29      6.375   2.640  27.65   8.533   1.697  27.14   8.038   3.329  27.14 0
1 30 31      17      23     24                                1.96E-5 0.075 20
9 30      6.375   2.640  27.65   8.038   3.329  27.14   7.234   4.833  27.14 0
1 31 31      24      18     17                                1.96E-5 0.075 20
9 31      7.234   4.833  27.14   4.879   4.879  27.65   6.375   2.640  27.65 0
1 32 31      18      24     25                                1.96E-5 0.075 20
9 32      4.879   4.879  27.65   7.234   4.833  27.14   6.152   6.152  27.14 0
1 33 31      18      25     26                                1.96E-5 0.075 20
9 33      4.879   4.879  27.65   6.152   6.152  27.14   4.833   7.234  27.14 0
1 34 31      26      19     18                                1.96E-5 0.075 20
9 34      4.833   7.234  27.14   2.640   6.375  27.65   4.879   4.879  27.65 0
1 35 31      19      26     27                                1.96E-5 0.075 20
9 35      2.640   6.375  27.65   4.833   7.234  27.14   3.329   8.038  27.14 0
1 36 31      19      27     28                                1.96E-5 0.075 20
9 36      2.640   6.375  27.65   3.329   8.038  27.14   1.697   8.533  27.14 0
1 37 31      28      20     19                                1.96E-5 0.075 20
9 37      1.697   8.533  27.14   0.0     6.900  27.65   2.640   6.375  27.65 0
1 38 31      20      28     29                                1.96E-5 0.075 20
9 38      0.0     6.900  27.65   1.697   8.533  27.14   0.0     8.700  27.14 0
1 39 31      21      30     31                                1.96E-5 0.075 20
9 39      8.700   0.0    27.14  10.60   0.0    26.46  10.40   2.068  26.46 0
1 40 31      31      22     21                                1.96E-5 0.075 20
9 40     10.40    2.068  26.46   8.533   1.697  27.14   8.700   0.0    27.14 0
1 41 31      31      23     22                                1.96E-5 0.075 20
9 41     10.40    2.068  26.46   8.038   3.329  27.14   8.533   1.697  27.14 0
1 42 31      23      31     32                                1.96E-5 0.075 20
9 42      8.038   3.329  27.14  10.40    2.068  26.46   9.793   4.056  26.46 0
1 43 31      23      32     33                                1.96E-5 0.075 20
9 43      8.038   3.329  27.14   9.793   4.056  26.46   8.814   5.889  26.46 0
1 44 31      33      24     23                                1.96E-5 0.075 20
9 44      8.814   5.889  26.46   7.234   4.833  27.14   8.038   3.329  27.14 0
1 45 31      33      25     24                                1.96E-5 0.075 20
9 45      8.814   5.889  26.46   6.152   6.152  27.14   7.234   4.833  27.14 0
1 46 31      25      33     34                                1.96E-5 0.075 20
9 46      6.152   6.152  27.14   8.814   5.889  26.46   7.495   7.495  26.46 0
1 47 31      25      34     35                                1.96E-5 0.075 20
9 47      6.152   6.152  27.14   7.495   7.495  26.46   5.889   8.814  26.46 0
1 48 31      35      26     25                                1.96E-5 0.075 20
9 48      5.889   8.814  26.46   4.833   7.234  27.14   6.152   6.152  27.14 0
1 49 31      35      27     26                                1.96E-5 0.075 20
9 49      5.889   8.814  26.46   3.329   8.038  27.14   4.833   7.234  27.14 0
1 50 31      27      35     36                                1.96E-5 0.075 20
9 50      3.329   8.038  27.14   5.889   8.814  26.46   4.056   9.793  26.46 0
1 51 31      27      36     37                                1.96E-5 0.075 20
9 51      3.329   8.038  27.14   4.056   9.793  26.46   2.068  10.40   26.46 0
1 52 31      37      28     27                                1.96E-5 0.075 20
9 52      2.068  10.40   26.46   1.697   8.533  27.14   3.329   8.038  27.14 0
1 53 31      37      29     28                                1.96E-5 0.075 20
9 53      2.068  10.40   26.46   0.0     8.700  27.14   1.697   8.533  27.14 0
1 54 31      29      37     38                                1.96E-5 0.075 20
9 54      0.0     8.700  27.14   2.068  10.40   26.46   0.0    10.60   26.46 0
```

D. Matrix Data and Title Cards (Symmetric Modes)

```
VTR001     83                    -1     0
    22     22   1.0              24    24   1.0              26    26   1.0
    31     31   1.0              32    32   1.0              33    22    .7738
    33     42    .7738           33    43  -0.7070           33    52    .6464
    33     62   1.527            33    63  -1.129            33    72   1.274
    33     73  -1.741            33    82   1.527            33    83  -2.728
    33     92    .6464           33    93  -1.250            33   102    .3005
    33    112   1.481            33   113  -0.9677           33   122   1.783
    33    123  -3.319            33   132   1.783            33   133  -4.969
    33    142   1.481            33   143  -4.867            33   152    .3005
    33    153  -1.006            33   162    .9575           33   172   1.927
    33    173  -4.298            33   182   1.927            33   183   7.945
    33    192   1.927            33   193 -10.38             33   202    .9575
    33    203  -5.580            33   212    .4026           33   222    .6942
    33    223  -1.741            33   232    .8049           33   233  -3.960
    33    242    .6942           33   243  -4.959            33   252    .8049
    33    253  -7.318            33   262    .6941           33   263  -7.421
    33    272    .8049           33   273  -9.563            33   282    .6942
    33    283  -8.755            33   292    .4026           33   293  -5.176
    33    313  -1.736            33   323  -1.868            33   333  -4.940
    33    343  -3.452            33   353  -7.394            33   363  -4.513
    33    373  -8.732            33   383  -2.442            34    34   1.0
    35     35   1.0              36    36   1.0              42    42   1.0
    43     43   1.0              44    44   1.0              46    46   1.0
    52     52   1.0              54    54   1.0              56    56   1.0
    61     61   1.0              62    62   1.0              63    63   1.0
    64     64   1.0              65    65   1.0              66    66   1.0
    71     71   1.0              72    72   1.0              73    73   1.0
    74     74   1.0              75    75   1.0              76    76   1.0
    81     81   1.0              82    82   1.0              83    83   1.0
    84     84   1.0              85    85   1.0              86    86   1.0
    92     92   1.0              93    93   1.0              94    94   1.0
    96     96   1.0             102   102   1.0             104   104   1.0
   106    106   1.0             111   111   1.0             112   112   1.0
   113    113   1.0             114   114   1.0             115   115   1.0
   116    116   1.0             121   121   1.0             122   122   1.0
   123    123   1.0             124   124   1.0             125   125   1.0
   126    126   1.0             131   131   1.0             132   132   1.0
   133    133   1.0             134   134   1.0             135   135   1.0
   136    136   1.0             141   141   1.0             142   142   1.0
   143    143   1.0             144   144   1.0             145   145   1.0
   146    146   1.0             152   152   1.0             153   153   1.0
   154    154   1.0             156   156   1.0             162   162   1.0
   164    164   1.0             166   166   1.0             171   171   1.0
   172    172   1.0             173   173   1.0             174   174   1.0
   175    175   1.0             176   176   1.0             181   181   1.0
   182    182   1.0             183   183   1.0             184   184   1.0
   185    185   1.0             186   186   1.0             191   191   1.0
   192    192   1.0             193   193   1.0             194   194   1.0
   195    195   1.0             196   196   1.0             202   202   1.0
   203    203   1.0             204   204   1.0             206   206   1.0
   212    212   1.0             214   214   1.0             216   216   1.0
   221    221   1.0             222   222   1.0             223   223   1.0
   224    224   1.0             225   225   1.0             226   226   1.0
   231    231   1.0             232   232   1.0             233   233   1.0
   234    234   1.0             235   235   1.0             236   236   1.0
   241    241   1.0             242   242   1.0             243   243   1.0
```

244	244	1.0	245	245	1.0	246	246	1.0
251	251	1.0	252	252	1.0	253	253	1.0
254	254	1.0	255	255	1.0	256	256	1.0
261	261	1.0	262	262	1.0	263	263	1.0
264	264	1.0	265	265	1.0	266	266	1.0
271	271	1.0	272	272	1.0	273	273	1.0
274	274	1.0	275	275	1.0	276	276	1.0
281	281	1.0	282	282	1.0	283	283	1.0
284	284	1.0	285	285	1.0	286	286	1.0
292	292	1.0	293	293	1.0	294	294	1.0
296	296	1.0	302	302	1.0	304	304	1.0
306	306	1.0	311	311	1.0	312	312	1.0
313	313	1.0	314	314	1.0	315	315	1.0
316	316	1.0	321	321	1.0	322	322	1.0
323	323	1.0	324	324	1.0	325	325	1.0
326	326	1.0	331	331	1.0	332	332	1.0
333	333	1.0	334	334	1.0	335	335	1.0
336	336	1.0	341	341	1.0	342	342	1.0
343	343	1.0	344	344	1.0	345	345	1.0
346	346	1.0	351	351	1.0	352	352	1.0
353	353	1.0	354	354	1.0	355	355	1.0
356	356	1.0	361	361	1.0	362	362	1.0
363	363	1.0	364	364	1.0	365	365	1.0
366	366	1.0	371	371	1.0	372	372	1.0
373	373	1.0	374	374	1.0	375	375	1.0
376	376	1.0	382	382	1.0	383	383	1.0
384	384	1.0	386	386	1.0			